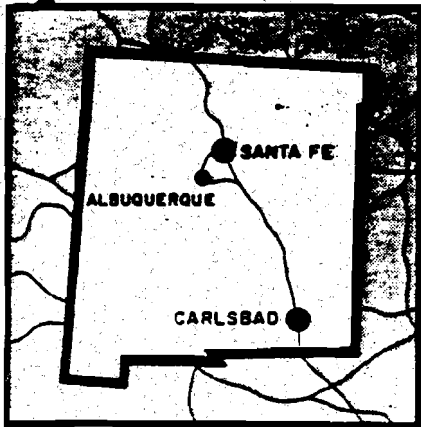# U.S. ATOMIC ENERGY COMMISSION
PLOWSHARE PROGRAM

Project
GNOME

CARLSBAD, NEW MEXICO
DECEMBER 10, 1961

Final Report

D. Rawson / C. Boardman / N. Jaffe-Chazan

LAWRENCE RADIATION LABORATORY

ISSUED: APRIL 20, 1965

Cavity produced by the Gnome explosion and subsequent collapse. Note figure right-center of rubble for scale. Cavity is 70 feet high and more than 150 feet across. Photograph by Lawrence Radiation Laboratory.

Geologic Studies
Project Gnome
Eddy County, New Mexico

By LEONARD M. GARD, JR.

UNITED STATES DEPARTMENT OF THE INTERIOR

STEWART. L. UDALL, *Secretary*

GEOLOGICAL SURVEY

William T. Pecora, *Director*

CONTENTS

ILLUSTRATIONS

CONTENTS

TABLES

GEOLOGIC STUDIES, PROJECT GNOME, EDDY COUNTY, NEW MEXICO

By Leonard M. Gard, Jr.

ABSTRACT

For Project Gnome, part of the Plowshare Program to develop peaceful uses for nuclear energy, a nuclear device was detonated December 10, 1961, underground in rock salt of the Permian Salado Formation southeast of Carlsbad, N. Mex.

The Geological Survey's investigations on behalf of the U.S. Atomic Energy Commission provided basic geologic and geophysical information needed to define preshot and postshot geologic and hydrologic conditions at and near the site. This report describes the geology of the site, some physical and chemical properties of the rocks, and the known effects of the nuclear detonation on the rocks of the site.

Geologic strata at the Gnome site consist of evaporite and clastic rocks of the Salado and Rustler Formations and Dewey Lake Redbeds, all of Late Permian age, the unconformably overlying Gatuna Formation of Pleistocene(?) age, and a cover of alluvial and eolian sands. All rocks, except where distorted by solution collapse, are nearly flat lying.

The evaporite deposits are easily dissolved and either are missing at the surface or only partially crop out in southeastern New Mexico; thus the sinking of a 1,200-foot shaft at Project Gnome provided an excellent opportunity to study these formations in detail. The strata were measured, sampled, and photographed while the shaft was being sunk.

The upper one-third of the Salado is exposed in the shaft and consists of 490 feet of bedded halite containing a few interstratified beds of clayey halite, anhydrite, polyhalite, and clay. The halite is overlain by a leached member comprised of 58 feet of clay, silt, gypsum, and anhydrite, much of which is a rubbly solution breccia.

The Rustler Formation disconformably overlies the Salado Formation. The five members of the Rustler are: lower member, 128 feet of silt and clay containing a few beds of gypsum; Culebra Dolomite Member, 28 feet of vesicular dolomite; Tamarisk Member, 113 feet mainly of beds of anhydrite partly hydrated to gypsum and a few thin beds of clay; Magenta Member, 21 feet of red-purple silty gypsiferous dolomite; and Fortyniner Member, 67 feet of anhydrite and gypsum.

The Dewey Lake Redbeds overlies the Rustler Formation with apparent conformity. These rocks are thinly laminated pale-reddish-brown siltstone displaying light-greenish-gray "reduction spots."

The Gatuna Formation of Pleistocene(?) age unconformably overlies the Dewey Lake Redbeds and consists of 49 feet of friable, poorly consolidated fine-grained sandstone and thin beds of clay, silt, and conglomerate. The Gatuna is in turn unconformably overlain by 43 feet of Recent alluvial bolson deposits, which are partly eolian and partly colluvial sand.

Mapping disclosed that deposition of the evaporite deposits was cyclical and resulted from repeated incursions of fresh sea water. Each cycle customarily begins with a bed of poly-halite, grades upward into pure halite, and ends with a clay-bearing halite at the base of the next higher polyhalite.

Comparison of preshot and postshot velocities in the salt near the shotpoint indicated that rock fracturing caused by the explosion was detectable from changes in elastic moduli, but compaction was not. No change in density of the rock could be detected.

The explosion formed a cavity about 70 feet high and more than 150 feet across. Postshot mining exploration revealed geologically interesting phenomena that resulted from the explosion. Intrusive breccia veins associated with complex thrust faulting were formed adjacent to the cavity. The breccia is composed of blocks of granulated and plastically deformed salt in a matrix of black melted salt. The black color of the matrix is due to the presence of laurionite, galena, and carbon. These materials, not present in the preshot rocks, were created by the shot. Lead from near the device combined with water and chlorine from salt to form laurionite and with sulfur from polyhalite to form galena. The carbon probably was derived from organic material present in the device chamber at shot time.

Lateral displacement of an instrument in a drill hole 100 feet from the shotpoint was about 16 feet. Strata 200 feet above the shotpoint were permanently displaced upward 5 feet, and a bed 55 feet below the shotpoint was displaced downward more than 10 feet.

INTRODUCTION

PURPOSE OF PROJECT GNOME

Project Gnome was a multiple-objective experiment conducted by the U.S. Atomic Energy Commission as part of the Plowshare Program to develop peaceful uses for nuclear explosives. Gnome was the first nuclear detonation within the continental limits of the United States outside of the Nevada Test Site since the Trinity shot in 1945.

The Project Gnome experiment consisted of the detonation of a nuclear device of about 3 kilotons equivalent TNT yield at a depth of about 1,200 feet below the surface in a thick salt deposit. The Gnome site is in the Nash Draw quadrangle in the approximate center of sec. 34, T. 23 S., R. 30 E., in Eddy County, and about 25 miles southeast of Carlsbad, N. Mex. (fig. 1).

The objectives of the experiment were fivefold (U.S. Atomic Energy Comm., 1961):

1. To explore the feasibility of converting the energy from a nuclear explosion into heat for the production of electric power.

1
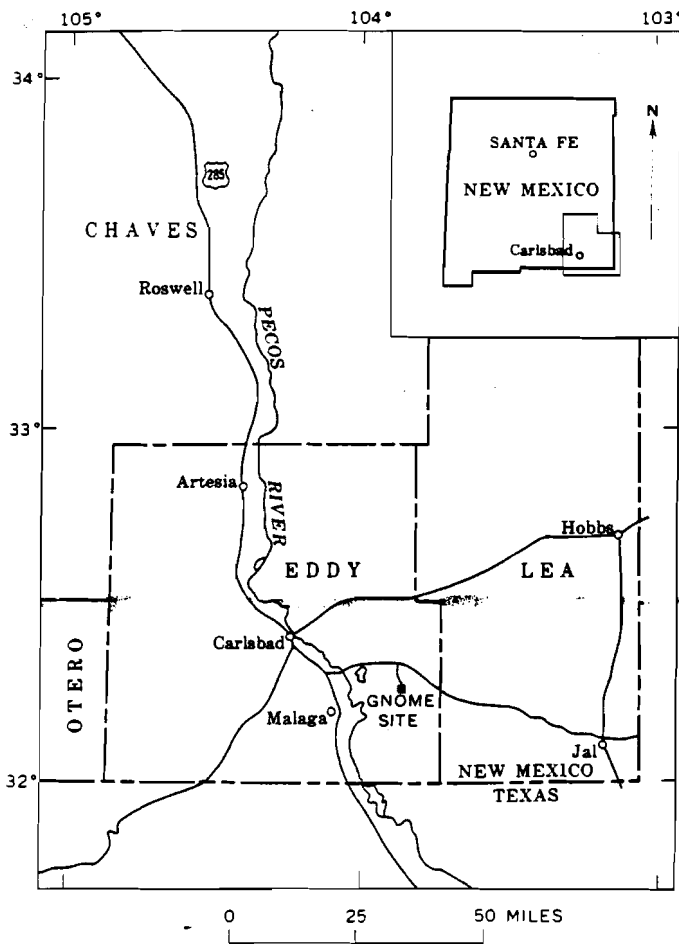
FIGURE 1.—Location of Project Gnome site, Eddy County, N. Mex.

2. To investigate the practicality of recovering useful radioisotopes for scientific and industrial applications.

3. To expand the data on characteristics of underground nuclear detonations to a new medium (salt), which differs markedly from the test media of the Nevada Test Site in which previous underground shots had been fired.

4. To make neutron cross-section measurements to contribute generally to scientific knowledge and to the reactor-development program.

5. To provide scientific and technical information on design principles useful in developing nuclear-explosive devices specifically for peaceful purposes.

HISTORICAL SUMMARY OF THE PROJECT

The Gnome shot was detonated on December 10, 1961. It was the culmination of planning and site selection that started in 1958 when a study was begun by the U.S. Geological Survey to locate a site that would satisfy both technical and public-safety requirements.

The required site was to have a deposit of relatively pure salt not more than 800 feet underground, to be within the continental United States, preferably on land controlled by the U.S. Government, and to be in an area having a low population density.

The Gnome site was selected after all possible sites in the United States had been thoroughly evaluated. Subsequently, a preliminary investigation of this area was undertaken by the Geological Survey. The surface and subsurface geology of the area was studied (Baltz, 1959; Moore, 1958a, b; Cooper, 1960, 1961, 1962; Jones, 1960; Vine, 1960, 1963); the regional ground-water conditions were appraised (Hale and Clebsch, 1959); the chemical and physical properties of salt were investigated (Morey, 1958; Harry Hughes, written commun., 1959; E. C. Robertson, A. R. Robie, and K. G. Books, written commun., 1958); the seismic properties of the salt were measured and compared with those of other rock types (Byerley and others, 1960; Roller and others, 1959); and a large-scale topographic map of the Gnome site was constructed.

This report describes the geology, hydrology, and physical, chemical, and optical properties of rocks at the site.

Shaft sinking began in July 1960 and was completed to a depth of 1,200 feet in May 1961. The Gnome shaft penetrates rocks of Permian and younger age. The shaft, circular in plan, has a finished diameter of 10 feet and is lined with reinforced concrete from the surface to a depth of 722 feet. The 1,000-foot drift was mined during the summer of 1961.

PARTICIPATION BY THE U.S. GEOLOGICAL SURVEY

The U.S. Geological Survey made scientific studies and investigations related to Project Gnome on behalf of the Atomic Energy Commission. The Survey acted as agency advisor and provided technical support, largely with respect to public-safety aspects. The broad objectives of the Geological Survey's program were (1) to provide the basic geologic and geophysical information needed to define the preshot and postshot geologic and physical properties of the salt and other rocks affected by the explosion, and (2) to provide geologic and hydrologic information on the preshot and postshot hydrologic conditions at the Gnome site and surrounding region.

This report does not attempt to describe all the geologic effects produced by the Gnome explosion. Other agencies have studied close-in surface effects (Hoy and Foose, 1962) and the environment created by the explosion (Rawson, 1963; Rawson and others, 1965).

This report describes the geology of the site, some physical and chemical properties of the rocks, and the effects, as far as they are known, of the nuclear detonation on the rocks at the site. It is based on studies that were carried out between July 1960 and June 1962.

ACKNOWLEDGMENTS

For their friendly cooperation and many kindnesses, the Geological Survey personnel on the Gnome Project thank the personnel, too numerous to mention individually, of the Atomic Energy Commission; Holmes and Narver, Inc.; Lawrence Radiation Laboratory; Reynolds Electrical and Engineering Co.; and Cementation Co. of America, Inc.

METHODS OF STUDY

The rocks in the shaft were measured, described (detailed measured section, p. 24), and sampled on a noninterference basis by L. M. Gard and W. A. Mourant during construction of the shaft. This was done as final mucking after each round was completed and before drilling for the next round began. Depending on the efficiency of the blasting, a round advanced the shaft 3–6 feet.

During this construction a section of the north wall was washed down and photographed in color. Unusual geologic features noted elsewhere in the shaft wall were also photographed and described. A complete photographic log in color is available for inspection at the Field Records and Photo Library, U.S. Geological Survey in Denver.

The geology of the preshot drift (pl. 1) was mapped by L. M. Gard and C. G. Bowles, using steel tape, at a scale of ¼ inch to 10 feet; vertical and horizontal control was established by Holmes and Narver, Inc. In the underground mapping, projections of both left and right ribs (walls) were used. (Left and right are identified as one faces the shotpoint.) The rib projections are rotated outward to the horizontal plane along the line that joins their bases to the sill (floor). The back (roof) was not mapped, because it displayed very few mappable geologic features.

The geology of the postshot workings (pl. 2) was mapped by L. M. Gard and W. L. Emerick, assisted by W. H. Laraway, M. L. Schroeder, and John Moreland, Jr. The method was the same as that used in preshot mapping except that near the cavity, to expedite the work because of time limitations, the ribs were mapped continuously. Thus, the nine walls of the drilling alcove and parts of the approaching drift are represented by a single straight projection, and the corners are indicated for clarity in map presentation. Although the preshot drift was intact after the shot, it was not remapped because of high levels of radiation.

Prior to mapping both the preshot, and the postshot workings, the ribs were washed with water. The cleaned wet rock displayed additional stratigraphic details.

Elastic properties of the salt were determined underground, both before and after the shot, by D. D. Dickey and D. R. Cunningham. Preshot calculations were made by R. D. Carroll and D. D. Dickey, and postshot calculations were made by D. D. Dickey.

From his knowledge of the minor-element content in evaporite rocks of southeastern New Mexico, C. G. Bowles suggested and later supervised the determination of the minor elements in the salt beds of the preshot drift. B. M. Madsen made the petrographic descriptions of the preshot samples, Julius Schlocker studied the insoluble clastic material from these samples, and Theodore Botinelly determined the composition of the intrusive breccia formed by the explosion.

GEOLOGY

REGIONAL SETTING

The Gnome site is on the Mescalero pediment on the east side of the Pecos Valley, a section of the Great Plains physiographic province (Fenneman, 1931, fig. 1). The Pecos River flows through the southwestern part of this section and divides it physiographically into the Mescalero pediment to the east and the alluvial plain north of Malaga and the Gypsum Hills south of Malaga to the west.

The Gnome site is in the northeastern part of the Deleware basin (Adams, 1944; King, 1948; Newell and others, 1953). This deep structural basin, which is about 135 miles long and 75 miles wide, lies in southeastern New Mexico and west Texas and is generally considered to be the area surrounded by the Capitan Limestone (a reef limestone of Late and Early Permian age). The Capitan reef is horseshoe shaped, opening southward, and extends in the subsurface from Carlsbad eastward nearly to Hobbs, N. Mex., and thence southeastward into Texas (fig. 2). West and southwest of Carlsbad the Capitan Limestone is exposed and forms El Capitan Peak and part of the Guadalupe Mountains. Large caverns—notably Carlsbad Caverns—were formed in the reef limestone through the solvent action of circulating ground water.

The Delaware basin was submerged in Permian time (230–280 million years ago, according to Kulp (1961)) and was filled with thousands of feet of sediment. Toward the end of Permian deposition in the basin, the
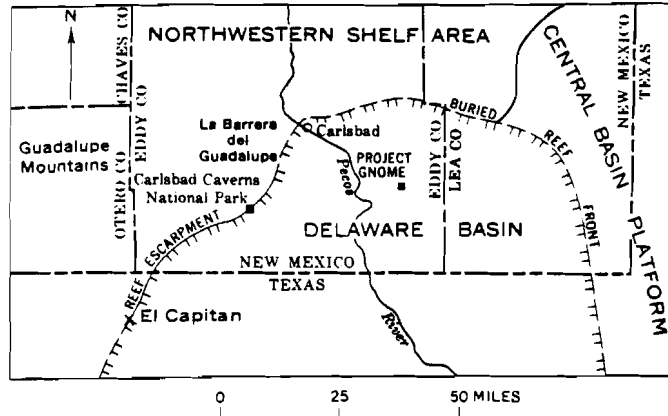
FIGURE 2.—Extent of the Delaware basin in New Mexico and adjacent structural and geographic features. Modified from King (1948) and Stipp and Haigler (1956).

reef growth around the basin was halted by increasing salinity of the sea water, and the evaporite rocks of the Castile, Salado, and Rustler Formations were deposited.

The Salado Formation, almost wholly salt, was deposited in a sea that extended from the Delaware basin across the Capitan reef zone many miles onto the shelf to the north. The southern end of this sea apparently had a restricted opening, and the consequent reduced circulation and outflow allowed evaporation to concentrate the sea water therein until salt was precipitated on the floor of the basin in southeastern New Mexico. The concentrated brine undoubtedly was replenished periodically by normal sea water; otherwise, the process would soon have ceased as the basin dried up. The salt beds of the Salado Formation grade southward into calcium sulfate and then into calcium carbonate facies, suggesting that the source of normal sea water lay in that direction and that the water became more concentrated as it moved northward.

After deposition of the evaporite rocks ceased, deposition of fine-grained terrestrial clastic sediment (Dewey Lake Redbeds) marked the close of the Permian. Terrestrial deposition continued during parts of Triassic time (181–230 million years ago), although subsequent erosion has removed Triassic beds from the Gnome area. Additional thin sediments accumulated in Quaternary time.

The evaporite rocks in the Delaware basin contain extensive deposits of potash minerals, which are mined at many localities. Many wells produce oil from the reef limestone in southeastern New Mexico and west Texas. Oil and gas are produced also from some of the deeper formations in the Delaware basin.

GNOME AREA

The Gnome area referred to in this report is the square mile of sec. 34, T. 23 S., R. 30 E. (fig. 3). The land surface at the area is covered with as much as 43 feet of alluvial and windblown sand and caliche. More than 18,000 feet of sedimentary material ranging in age from Ordovician to recent underlies the Gnome site. Beneath the surface lie, in descending order, the Gatuna Formation of Pleistocene(?) age, the Dewey Lake Redbeds, and the Rustler and Salado Formations of Late Permian age. Beneath the Salado are thousands of feet of Paleozoic rocks which are not discussed in this report. All these formations are concealed by alluvium in the Gnome area, but all except the Salado crop out nearby (Vine, 1963).

Solution by ground water of salt at the top of the Salado Formation and of anhydrite within the Rustler Formation has removed thick sections of these rocks. A subsequent lowering of the land surface and differential collapse of the Rustler have formed many sinkholes and created a karst topography over much of this part of southeastern New Mexico. Nash Draw, about 6 miles to the northwest, is one of the largest depressions. Within Nash Draw are several smaller depressions, the largest of which is Laguna Grande de la Sal (Salt Lake).

The rocks dip gently to the east and southeast, and progressively younger formations are exposed in that

FIGURE 3.—Location of shaft, ground zero, and U.S. Geological Survey test holes at Project Gnome site.

FIGURE 4.—Geologic section between Carlsbad Caverns National Park and Project Gnome site. Modified from Cooper (1960).

TABLE 1.—*Generalized stratigraphic section of rocks exposed in the Gnome shaft*

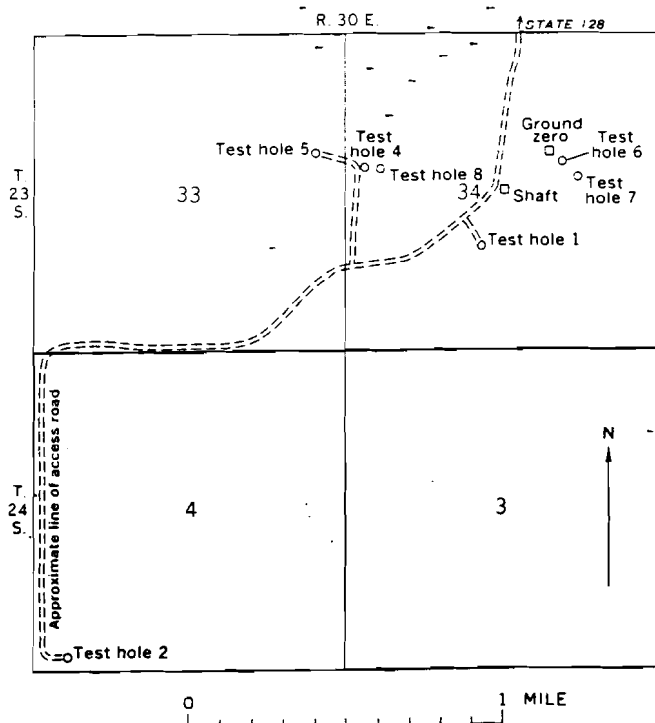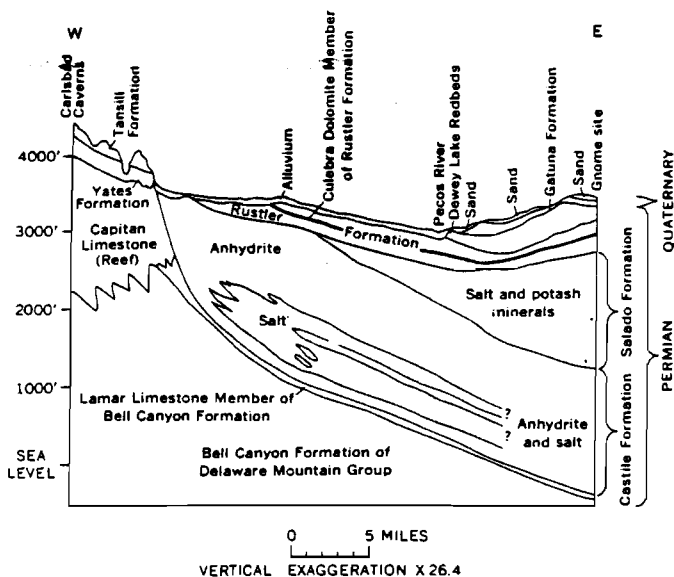| Age	Unit	Lithology	Depth below surface (ft)	Thickness (ft)
Recent...........	Alluvial bolson deposits.	Unconsolidated sand.	0 – 43	43.0
Pleistocene(?)...	Gatuna Formation.	Friable sandstone and conglomerate.	43 – 91.9	48.9
Late Permian...	Dewey Lake Redbeds.	Thin-bedded siltstone.	91.9–294	202.1
	Rustler Formation; Forty-niner Member.	Chiefly gypsum and anhydrite.	294 –361.3	67.3
	Magenta Member.	Silty dolomite.....	361.3–382.2	20.9
	Tamarisk Member.	Chiefly anhydrite and gypsum.	382.2–495.5	113.3
	Culebra Dolomite Member.	Dolomite..........	495.5–523.5	28.0
	Lower member.	Chiefly clay and silt, with some gypsum and anhydrite.	523.5–651.2	127.7
	Salado Formation: Leached member.	Chiefly claystone and siltstone.	651.2–709.3	58.1
	Unleached part.	Chiefly impure halite rock, with some anhydrite, polyhalite, and siltstone.	709.3–1,202	492.7

(Bottom of shaft.)

direction (fig. 4). Although the Salado Formation underlies an extensive area in southeastern New Mexico, no outcrops of it are known.

In many places the salt of the Salado Formation has been wholly or partially removed by solution. West of the Pecos River, very little salt remains; to the northwest over the buried Capitan reef, no salt is present; and south of the Gnome site, the Saldo salt is thin or absent over an area of nearly 100 square miles (Cooper, 1962). As much as 800 feet of salt has been removed. Within Nash Draw, solution has removed, and is presently removing, salt from the upper part of the Salado Formation.

The Rustler Formation crops out in numerous places west and northwest of the Gnome area and south of Malaga, a small town about 10 miles west of the area. The Dewey Lake Redbeds is exposed at several localities north and west of the Gnome area, especially along the margin of Nash Draw, and also crops out in a narrow discontinuous north-south belt a few miles east of the Pecos River. Triassic rocks are represented by the Santa Rosa Sandstone north of Nash Draw and southeast of the area; the Santa Rosa is not present, however, at the Gnome site. Unconsolidated Tertiary rocks crop out east of the area.

Quaternary rocks include the Gatuna Formation of Pleistocene(?) age, and alluvium, windblown sand, caliche, and playa lake deposits of Recent age. Alluvium occurs chiefly near the Pecos River north of Malaga. A recent report by Vine (1963) includes a geologic map of the Nash Draw quadrangle and stratigraphic sections of exposed rocks. The following generalized strati-

graphic section (table 1) describes the rocks exposed in the Gnome shaft (fig. 5).

Structural deformation of the rocks is limited mainly to a gentle monocline in the Permian rocks and to collapse structures in the evaporite sections of the Permian rocks. No deeply buried faults are known. Locally, there are structural features related to the hydration of anhydrite to gypsum. This hydration considerably increased the volume of the affected rocks and caused them to be deformed, and in many places domed, where they are exposed at the surface (Vine, 1960).

STRATIGRAPHY AT THE SITE

The following stratigraphic descriptions are supplemented by the detailed measured section at the end of the report (p. 24).

SALADO FORMATION

At the Gnome site the Salado Formation is about 1,550 feet thick. More than 75 percent of the thickness of the Salado is salt, except where solution has thinned the formation. The remainder of the formation consists of potassium minerals and minor amounts of sandstone, siltstone, shale, anhydrite, and gypsum.

The bulk of the Salado is not known to contain ground water, although the leached member at the top of the formation is a brine aquifer locally. No free water has been reported to occur within the formation in the potash mines nor in the many drill holes throughout the
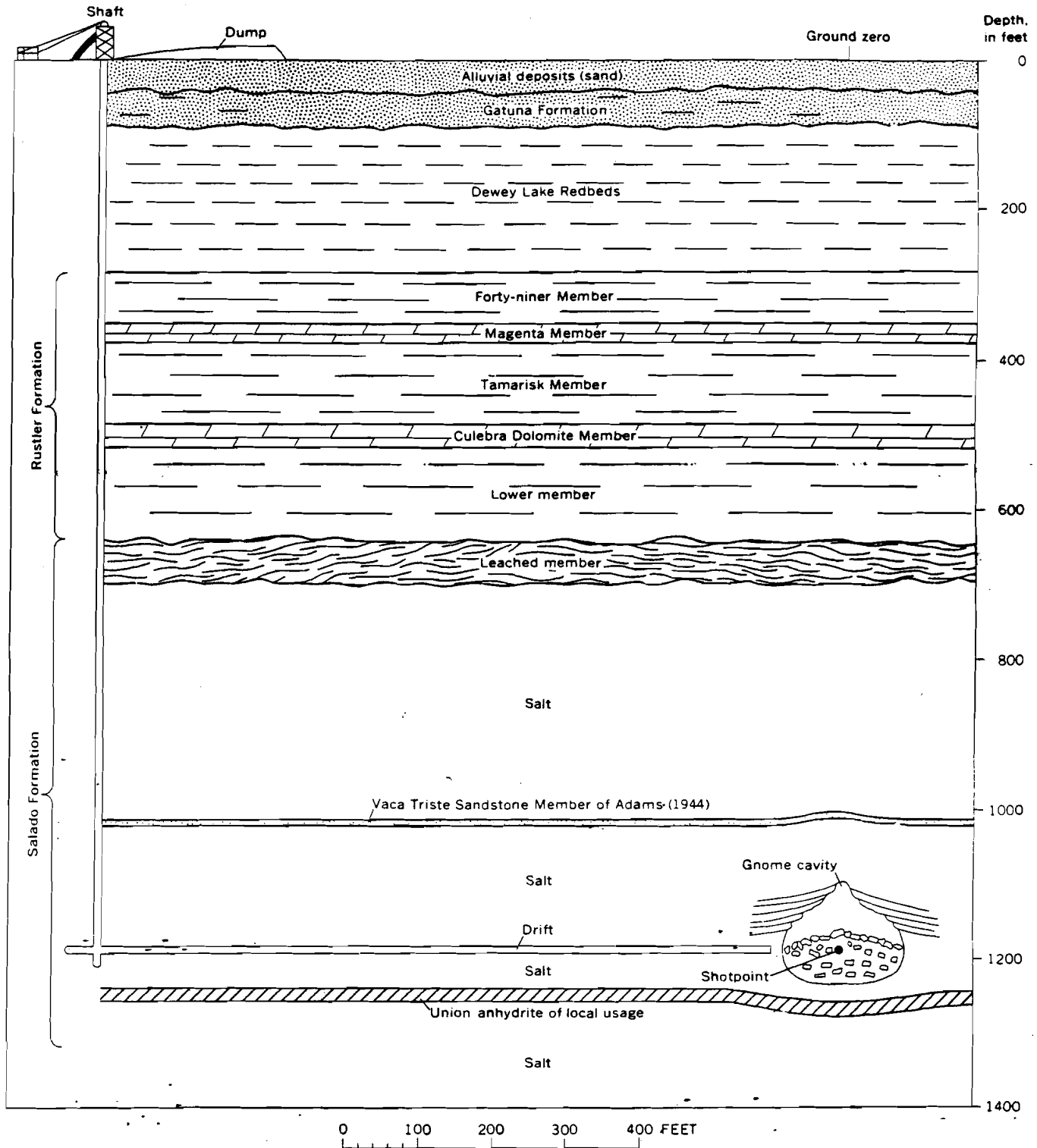
FIGURE 5.—Geologic cross section between shaft and cavity, Project Gnome site.

area. The halite rock is virtually impermeable because recrystallization of the salt restricts migrating fluids and prevents the formation of open spaces.

The shaft penetrated more than 490 feet of bedded halite that contains minor interstratified beds of clayey halite, anhydrite, polyhalite, and clay. The halite beds range in color from transparent colorless through white to reddish orange. The intensity of the orange color depends upon the amount of disseminated iron and polyhalite impurities present. The clayey halite beds range in color from reddish brown to greenish gray. The reddish-brown polyhalite beds, locally used as marker beds, average about 1 foot thick. They commonly have a thin bed of greenish-gray clay at the base. From 1,024.3 to 1,029 feet the shaft cut the Vaca Triste Sandstone Member of Adams (1944), a pale-reddish-brown clayey siltstone that forms a well-known marker unit.

The total thickness of the Salado Formation at the Gnome site has not been determined accurately, but data from nearby oil tests indicate that as much as 1,550 feet of the formation may be present (fig. 4).

The uppermost 58 feet of the Salado Formation consists of reddish-brown to gray clay and silt with a few interstratified gypsum and anhydrite beds. These strata represent, at least in part, an insoluble residue left after the removal of halite by ground water. This leached member or zone is estimated to be roughly one-third to one-tenth the thickness of the original halite rock that was present. The thickest unit of this leached zone is a solution breccia 36 feet thick. It is a heterogeneous rubbly mixture composed of siltstone, gypsum, and polyhalite blocks as much as 3 feet long set in a matrix of plastic grayish-red clay. In the shaft the leached zone did not contain water, although a small amount of water was detected in this zone in an observation well drilled about three-fourths mile west of ground zero (Gard and others, 1962, p. 121). Vine (1963, p. 8) reported that locally the leached zone is a prolific aquifer.

The top of the Salado Formation is considered by many geologists to be at the top of the uppermost halite bed, and the leached member is assigned to the Rustler Formation. This assignment is based partly on the fact that the Rustler Formation is reported to contain some salt beds to the southeast, and partly on the fact that the leached member cannot be distinguished from the lower member of the Rustler in either drill cuttings or geophysical logs. However, because the leached member was recognized as a distinct unit in the Gnome shaft and because it has a disconformable upper contact and contains several collapse breccia beds that are distinctly different from the lower member of the Rustler, it has been assigned in this report to the Salado Formation.

RUSTLER FORMATION

The Rustler Formation of Late Permian age unconformably overlies the Salado Formation and is composed mainly of evaporite deposits of anhydrite (commonly altered to gypsum) and dolomite and contains some siltstone and clay in the lower part. The thickness of the Rustler at the shaft is 357.2 feet, although in nearby areas the thickness ranges from 90 to more than 500 feet.

The Rustler is divided into five members, all present in the Gnome shaft. The upper four members crop out near Nash Draw to the north and near the Pecos River to the west.

The lower, unnamed member of the Rustler Formation lies disconformably on the leached top of the Salado Formation. It is 127.7 feet thick and consists principally of poorly consolidated silt and clay and contains a few interstratified beds of gypsum.

The Culebra Dolomite Member overlies the lower member and consists of 28 feet of yellowish-gray generally microcrystalline dolomite. It contains some massive zones, as well as as brecciated zones, that are recemented with pale-yellowish-brown dolomite. A characteristic feature of the Culebra is the presence of numerous small nearly spherical cavities that range from 1 to 20 mm in diameter. Some cavities are partly filled with secondary gypsum and calcite, but most are open. They do not appear to be interconnected. These cavities are thought to have originated either by solution of a highly soluble mineral aggregate or by the inclusion of gas or liquid when the sediment was soft (Vine, 1963, p. 14).

The Culebra Member is an artesian aquifer at the shaft, where it has a head of about 75 feet. The water appears to be contained in fractures and is confined above by the anhydrite and gypsum of the Tamarisk Member and below by clay of the lower member.

The Culebra is an excellent subsurface marker, because its lithology is unique in southeastern New Mexico. It is widespread in the Delaware basin and has been identified in many hundreds of drill holes. It is the principal aquifer at the Gnome site and yields water to wells in the western half of the project area. The depth to the top of the Culebra ranges from zero in the Nash Draw–Pecos River area to at least 1,200 feet in the eastern part of the State. The configuration of the top of the Culebra is similar to that of the top of the salt in the Salado Formation. Apparently, as salt in the Salado was removed by solution, the overlying beds settled and assumed, in general, the shape of the surface of the remaining salt.

The overlying Tamarisk Member is 113.3 feet thick and is composed mainly of beds of anhydrite partly

hydrated to gypsum, but it contains some thin beds of clay.

The overlying Magenta Member is a red-purple (magenta) silty gypsiferous dolomite 20.9 feet thick. Although an aquifer in some places, it contains no water at the shaft.

The Forty-niner Member, like the Tamarisk Member, is composed mainly of anhydrite and gypsum. It is 67.3 feet thick in the shaft, but is missing in U.S. Geological Survey hydrologic test holes 4 and 5 about one-half mile west of the shaft (fig. 3). Whether removal of the Forty-niner Member was by erosion prior to deposition of the Dewey Lake Redbeds or by leaching subsequent to deposition is not known, although leaching is considered to be more likely.

The structure of the Rustler Formation is mildly undulating where these beds are 200-300 feet below the ground surface. Locally, however, solution and collapse have affected the formation where it is deeply buried. Generally the carbonate members—the Culebra and the Magenta—are the least affected by solution and are present throughout most of the area. At the Gnome site they are separated by more than 100 feet of the Tamarisk Member. In the Nash Draw area, solution and collapse have locally removed the entire Tamarisk, and the Magenta rests directly upon the Culebra.

DEWEY LAKE REDBEDS

The Dewey Lake Redbeds of Late Permian age overlies the Rustler Formation with apparent conformity. The contact is marked by the abrupt color change from the white of the gypsum of the Forty-niner Member of the Rustler Formation to the red of the Dewey Lake.

The Dewey Lake is mainly made up of pale-reddish-brown siltstone that displays a polka-dot appearance, owing to the presence of light-greenish-gray reduction spots (round spots about 0.5 cm across where ferric iron has been reduced to ferrous iron). The formation is 202.1 feet thick in the shaft and is composed mainly of subangular to subrounded clear quartz grains and chert and feldspar grains in a clay matrix. Muscovite, biotite, rock fragments, and opaque minerals make up less than 10 percent of the mineral grains. Bedding consists of thin (0.5-1.5 mm) laminae and, less commonly, very small scale cross-laminations. Red clay forms 15-25 percent of the rock and is the principal cement, although calcite and gypsum are common. The Dewey Lake represents the beginning of detrital sedimentation following the long period of chiefly evaporite deposition in the Delaware basin and adjacent shelf areas in southeastern New Mexico.

GATUNA FORMATION

The Gatuna Formation of Pleistocene(?) age unconformably overlies the Dewey Lake Redbeds and is pale-red to moderate-brown friable fine-grained sandstone, 48.9 feet thick in the shaft, that contains a few thin beds of clay and silt and many thin beds of conglomerate. The sand- and silt-sized material is mainly made up of quartz grains, and the pebbles are quartzite, limestone, and chert. The grains are weakly to moderately cemented with calcium carbonate. The presence, in several beds, of reworked fragments from the underlying Dewey Lake suggests that the Gatuna was deposited on a surface of considerable relief.

Elsewhere in the Nash Draw quadrangle (Vine, 1963), the Santa Rosa Sandstone of Triassic age lies between the Dewey Lake Redbeds and the Gatuna Formation, but it is missing at the Gnome site.

ALLUVIAL BOLSON DEPOSITS

Alluvial bolson deposits of Recent age unconformably overlie the Gatuna Formation and are chiefly made up of unconsolidated moderate-brown fine-to medium-grained quartz sand. The upper 9 feet of these deposits is dune sand, but the lower 34 feet is partly eolian and partly colluvial. The sand has been derived from the Gatuna Formation and perhaps in part from the Ogallala Formation of Pliocene age, which may once have covered the area (Vine, 1963, p. 36). The top 3 feet of the lower 34 feet is weakly cemented by caliche, a near-surface accumulation of calcareous material, that was precipitated by subsurface evaporation of moisture in this semiarid region.

STRUCTURE

The rocks penetrated by the shaft are nearly flat lying, although locally in the shaft the Rustler Formation dips steeply. The regional structure is a small homoclinal dip to the east (Vine, 1963, p. 37). In the shaft the Dewey Lake rocks strike N. 45° E. and dip about 5° NW. Bedding in the Salado Formation observed in the drift strikes N. 89° E. and dips 0°20′ N. The attitude of the bedding in the Salado Formation is locally variable. Information from a drill hole 500 feet south of ground zero suggests that the same beds may be as much as 10 feet higher in the drill hole than in the drift. Whether this difference is due to a local flexure or to an error in drilling observations is not known.

Fairly steep dips were observed in some beds of the Rustler Formation, especially in gypsum and anhydrite. Dips as high as 42° NW. were noted in a gypsum bed in the lower member of the Rustler. These anomalous attitudes are believed to be associated with vol-

ume changes that take place when anhydrite changes to gypsum or when solution differentially telescopes the rocks. The northwest dip observed in the Dewey Lake Redbeds may result from thinning of the underlying Rustler Formation to the west or northwest. As previously noted, the Forty-niner Member of the Rustler is completely missing in test holes drilled about half a mile west of the shaft.

GEOLOGY OF THE PRESHOT GNOME DRIFT

The nuclear device was placed in a small chamber at the end of a drift (pl. 1) driven N. 50° E. from the bottom of the shaft. The drift was 1,223 feet long and included a curved section near the shaft. The end of the drift curved around a "buttonhook," doubling back on itself and ending at the device chamber. The device chamber was about 1,000 feet horizontally from the bottom of the shaft and slightly less than 1,200 feet below the ground surface. Thus, the rock cover over the detonation point consisted of about 500 feet of massive salt beds and about 700 feet of other sedimentary rocks. Below the detonation point was probably an additional 1,000 feet of bedded salt.

Only the Salado Formation is exposed in the drift; bedding strikes N. 89° E. and dips 0°20′ N. Owing to the low dips, the ribs (walls) of the drift were mapped to show geologic features that could not be included on an ordinary map (pl. 1). Mapping, done during July 1961, was on a scale of 1 inch to 10 feet to show the depositional features in the salt strata in some detail.

Eight mappable beds of halite rock containing varying amounts of clay and polyhalite and one mappable bed of polyhalite were transected by the drift. The nine beds were arbitrarily numbered in descending order from 10 to 18. Because the drift intersects the bedding at an angle of about 40° to the strike, the beds have a component of dip toward the device chamber; thus, the lowest beds are exposed near the shaft, and successively higher beds are exposed toward the device chamber. Total thickness of the exposed beds is about 22 feet. The following stratigraphic section (table 2) describes the beds in the Gnome drift.

Deposition of the Salado Formation was often cyclic, as indicated by the strata exposed in the drift. Ideally, a cycle begins with a polyhalite bed at the base, grades upward into halite containing polyhalite, and terminates with clay-bearing halite at the top. A cycle represents an incursion of fresh sea water that temporarily decreased the salinity of the brine and caused deposition of calcium sulfate. Concentration of the fresher sea water subsequently caused the precipitation of sodium chloride.

TABLE 2.—*Detailed stratigraphic section of Salado Formation along drift from device chamber to shaft*

Unit	Description	Thickness (ft)
120	Polyhalite rock (marker bed 120), reddish-brown, microcrystalline; varies in thickness because upper contact gradational into overlying halite. (Exposed in postshot workings.)	0. 5–1. 5
10	Halite rock, colorless to pale-orange; grain size 10–20 mm; bands 0.25–0.3 ft thick of colorless to milky halite alternate with 0.1- to 0.2-ft-thick bands of pale-orange halite containing disseminated orange polyhalite; 0.18-ft thick discontinuous band of orange polyhalite 1.2 ft below top of unit; polyhalite more concentrated in lower 1.5 ft; dark-gray clay layer 5.4 ft above base (clay seam in fig. 12); lower 0.8 ft contains 4 percent gray clay in thin horizontal streaks and bands; device set at base of this unit. (Only lower 4.3 ft exposed in preshot drift.)	8. 0
11	Halite rock, clear, gray, rarely brown, gray clay seam 0.05 ft thick at top; contains a few discontinuous bands of halite with disseminated polyhalite; displays ripple-mark casts where back of drift breaks to base of unit.	. 2–1. 0
12	Halite rock, light-gray to light-brown; clay content 10–50 percent; clay generally brown but some gray; base of unit a brown clay seam which at places truncates upturned beds of underlying unit.	. 2–1. 0
13	Halite rock; contains inclusions of brown clay; upper 2 ft contains irregular layers of brown clayey halite alternating with pale-orange to grayish-white halite; contains vertical mudcracks filled with clay, polyhalite, and secondary halite; layers between mudcracks near top of unit are concave upward; lower 1.5 ft light-brown halite with 20–25 percent inclusions and vertical streaks of brown clay; clay content decreases downward; contact with underlying unit gradational.	3. 5
14	Halite rock, pale-orange to white; contains blebs and disseminated particles of orange polyhalite forming indistinct layers which are most noticeable in lower half.	3. 5–4. 0
15	Polyhalite rock (marker bed 121), moderate-reddish-brown, microcrystalline; variable thickness usually due to irregularity of upper contract, which may be gradational; lower contact sharp.	. 5–1. 0
16	Halite rock, colorless to gray-green to pale-orange; 0.1 ft greenish-gray clay at top; upper 1.6 ft contains 20 percent gray-green clay and 3 percent polyhalite; clay content decreases downward; upper part contains pods and downward-tapering wedges of secondary halite containing gray-green clay and polyhalite.	4. 8
17	Halite rock, colorless to light brown; 10 percent streaks and inclusions of brown clay. (Exposed only in blast-door alcove.)	. 5
18	Halite rock, colorless to light-brown; contains 2 percent brown clay and 2 percent polyhalite. (Exposed only in blast-door alcove.) Base not exposed.	3+
	Total exposed thickness.	22+

One complete cycle of deposition and parts of two others are represented in the drift. The complete cycle began with the deposition of unit 15, the polyhalite bed, and ceased with the deposition of unit 13. Units 16–18 are part of the previous cycle, and units 10–12 are part of the subsequent cycle.

Polyhalite probably was not deposited from the original brine but was altered from gypsum or anhydrite
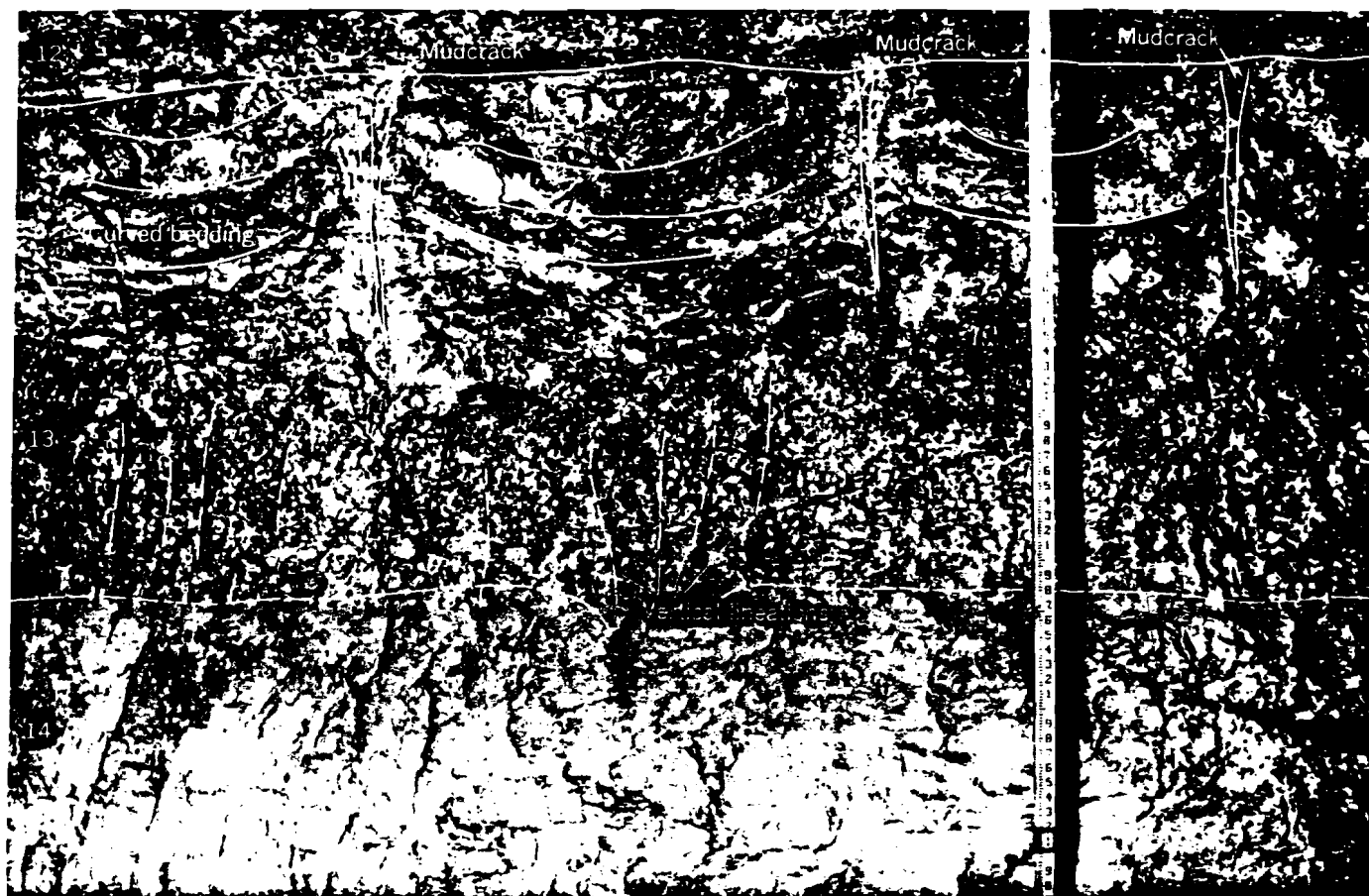
FIGURE 6.—Units 12, 13, and 14 exposed in preshot drift. Note mudcracks in unit 13
with curved bedding between, and vertical lineations at base of unit 13.

by the later addition of potassium and magnesium (Moore, 1958b, p. 14).

The polyhalite bed (unit 15), known locally as marker bed 121, is present in the Salado Formation over a wide area. Its sharp regular lower contact is underlain by a thin layer of greenish-gray clay. Thin clay layers underlie many of the polyhalite beds in the Salado Formation and are thought to have been concentrated by the re-solution of impure salt when the brine was freshened.

In places along the drift the polyhalite is underlain by pods of abnormally large halite crystals which contain disseminated gray clay and polyhalite. Whenever the pods are present, the underclay is absent. The gross halite crystals in these pods are thought to have resulted from secondary recrystallization.

Continued concentration of the brine by evaporation resulted in deposition of unit 14, which contains little or no clay but contains polyhalite blebs. Unit 14 is gradational upward into unit 13, which contains as much as 25 percent clay. Further evaporation, perhaps even to dryness, produced desiccation cracks in unit 13 (fig. 6). These cracks are filled with clay, halite, and polyhalite.

In the upper part of this unit, bedding between the desiccation cracks is concave upward and resembles the cross section of curved polygonal plates that commonly develop between desiccation cracks. Most of these features were seen only in cross section; one polygonal structure, however, is well exposed in the back of the drift at station 4+35 and exhibits a typical 120° junction of three mud-filled cracks, one of which is traceable down the right rib. Another such junction is well exposed in the No. 12 lateral in the reentry drift. Probably this part of the basin either was evaporated to dryness or was locally uplifted to above sea level at this time. Desiccation cracks observed at several places in the shaft and in the core from a hole drilled at ground zero indicate recurrent complete evaporation during deposition of the Salado Formation. These cracks could, however, represent a time of local upwarp and subaerial exposure of a limited area rather than evaporation to dryness of the entire basin.

The clay in unit 13, which decreases downward, displays faint vertical brown clayey lineations, which may have been caused by downward percolation of rain water, if salt strata were exposed by local upwarp, or by

sea water when the area was again submerged. This vertical lineation is clearly visible in figure 6.

Units 11 and 12 are very thin, aggregating generally less than a foot in thickness, and are separable only by the difference in color of their contained clay. Unit 11 is generally gray, and unit 12 is generally brown. The top of unit 12 and the bottom of unit 11 display current ripple marks in the back of the drift near station 5+45 where the underside of unit 12 is exposed in the back of the drift. The contact between units 12 and 13 is very sharp, and some of the upturned beds at the top of unit 13 appear to have been truncated by unit 12.

Precipitation of salt began again with the formation of unit 12; the brine was apparently concentrated enough so that sodium chloride was the first mineral deposited. In unit 10 alternating layers of colorless halite and orange halite (colored from the iron in disseminated polyhalite) suggest rhythmical freshening of the brine. The top bed of this cycle seen in the postshot workings and cavity walls is a polyhalite bed (marker bed 120) that lies only a few feet above unit 10 and indicates the beginning of a new depositional cycle.

PROPERTIES OF THE ROCKS

To define the rocks surrounding and overlying the device chamber various properties were determined, both before and after the shot. Certain physical properties were determined both in the laboratory and in situ. Semiquantitative spectrographic analyses were made, and the petrography of the rocks exposed in the drift was studied.

These preshot determinations were made to provide a basis for postshot comparisons. It was found, however, that the shot had little effect on the bulk of the geologic medium, and, accordingly, detailed postshot analyses were made only in specific places on rocks close to the cavity.

PHYSICAL PROPERTIES

Various physical properties were determined by the Geological Survey laboratories for 32 samples (tables 3, 4) collected from the Gnome shaft during construction. These samples are considered to be representative of the rocks overlying the device chamber.

Porosity, grain density, and dry-bulk density of the insoluble samples were determined by the water-saturation, mercury-displacement, and powder-grain methods. For water-soluble samples, kerosene was substituted for water, and the proper density corrections were made (table 3).

Dynamic elastic moduli were determined from calculations using torsional and flexural resonant frequencies of specimens (table 3). Static elastic moduli and compressive strength were measured on cores 1 inch in diameter and 2 inches long (table 4).

TABLE 3.—*Physical properties of rock samples from Gnome shaft*

[Analysts: D. R. Cunningham, John Moreland, Jr., and E. F. Monk. Asterisk (*) indicates 10⁵ psi (pounds per square inch); nd, not determined; .., not determined owing to insufficient sample]

Geologic unit	Lithology	Depth (ft)	Porosity (percent)	Grain density (g per cc)	Dry-bulk density (g per cc)	Magnetic suscepti- bility (10⁻⁶ cgs units) air dried	Sonic method				
							Young's modulus (10⁶ psi)	Modulus rigidity (10⁶ psi)	Poisson's ratio	Longitu- dinal velocity (ft per sec)	Trans- verse velocity (ft per sec)
Gatuna Formation	Sandstone	50– 70	31.9	2.66	1.81	36.9	*5.38	*2.64	0.0189	6,072	3,552
Dewey Lake Redbeds	Siltstone	95– 100	21.6	2.68	2.19	7.8	nd	nd	nd	nd	nd
	do	250	11.8	2.68	2.36	10.8	nd	nd	nd	nd	nd
Rustler Formation: Forty-niner Member.	Anhydrite	298	7.9	2.50	2.31	5.3	2.56	1.09	.1743	10,825	6,816
	do	320	12.2	2.82	2.48	6.0	3.19	1.30	.2269	10,223	6,076
	Siltstone	331	24.9	2.66	2.00	14.9	1.18	*5.34	.1028	6,836	4,548
	Gypsum	343	8.7	2.43	2.22	6.7	2.66	1.27	.0472	10,715	7,386
	Gypsum and anhydrite	350	3.5	2.37	2.29	3.6	2.52	1.00	.2600	11,275	6,421
Magenta Member	Dolomite	365	34.7	2.92	1.91	4.8	*7.10	*2.85	.2456	5,587	3,244
	Dolomitic siltstone	370	22.7	2.81	2.17	7.9	nd	nd	nd	nd	nd
	Dolomite	380	19.1	2.91	2.35	4.1	nd	nd	nd	nd	nd
Tamarisk Member	Gypsum and anhydrite	400	2.5	2.39	2.33	4.3	5.41	2.89	.1812	15,205	9,487
	Claystone	482	22.1	2.68	2.08	6.2	*9.39	*3.71	.2655	6,546	3,713
Culebra Dolomite Member.	Dolomite	505	12.5	2.85	2.49	5.8	nd	nd	nd	nd	nd
	do	515	12.3	2.83	2.48	2.1	2.96	1.28	.1563	9,809	6,261
Lower member	Claystone	527	29.6	2.71	1.91	10.5	nd	nd	nd	nd	nd
	Gypsum and anhydrite	535	3.1	2.37	2.3	4.6	2.93	1.13	.2965	12,706	6,834
	Claystone	552	25.1	2.68	2.01	8.2	*8.41	*3.40	.2368	6,201	3,642
	Siltstone	590	21.3	2.71	2.13	19.1	1.34	*5.98	.1167	7,044	4,640
	do	620	19.3	2.70	2.17	7.7	nd	nd	nd	nd	nd
Salado Formation	Claystone breccia (residuum).	653	26.2	2.69	1.98	17.2	nd	nd	nd	nd	nd
	Siltstone (residuum)	693	1.1	2.15	2.13	5.8	1.40	*6.67	.0526	7,367	5,062
	Anhydrite (residuum)	700	2.7	2.52	2.45	4.6	1.86	*7.04	.3210	9,064	4,653
	Halite	715	2.7	2.16	2.11	3.2					
	do	720– 725	1.1	2.49	2.46	4.3					
	do	1,013–1,015	5.1	2.24	2.13	3.7					
	do	1,019–1,023	1.2	2.27	2.24	6.7					
	do	1,120–1,123	7.1	2.33	2.17	12.1					
	do	1,130	1.7	2.18	2.14	9.5					
	do	1,147–1,152	.8	2.18	2.16	7.8					
	do	1,173–1,178	3.2	2.15	2.09	6.3					
	do	1,177–1,181	2.7	2.38	2.31	5.4					

TABLE 4.—*Physical properties of rock samples from Gnome shaft, as determined by static method*

[Analysts: T. C. Nichols, J. C. Thomas, and R. A. Speirer]

Lab. No. P1-	Depth (ft)	Lithology of sample	Condition of sample	Description	Unconfined compressive strength (psi)	Secant Young's modulus (psi)	Secant range (psi)	Poisson's ratio	Shore hardness	Remarks
102	320	Anhydrite..	Good....	Lineation of gypsum-filled fractures approximately 70° to platens. Length, 3.0 in.; diameter, 1.470 in.; parallelism, .0012 in. Oven dried.	3,900	2.86×10⁶	500-1400	0.19	24	Loading: Longitudinal strain, first cycle; latitudinal strain, second cycle. Failure occurred along fracture planes.
104	343	Gypsum....	..do.......	Both ends slightly chipped. No lineation. Length, 2.078 in.; diameter, 1.0 in.; parallelism, <.001 in. Oven dried.	3,180	3.18×10⁵	300-1300	.10	12	Loading: Longitudinal strain, first cycle; latitudinal strain, second cycle; compressive strength, third cycle.
109a	400	Anhydrite and gypsum.	Fair......	No fractures. One end of core chipped. Length, 2.716 in.; diameter, 1.438 in.; parallelism, .0009 in. Oven dried.	2,400	2.2 ×10⁵	500-1400	.23	....	Loading: Longitudinal strain, first cycle; latitudinal strain, second cycle.
109b	400	...do.........	Poor.....	Many gypsum-filled fractures normal to platens. Length, 2.078 in.; diameter, 1.0 in.; parallelism, <.001 in. Oven dried.	8,900	1.14×10⁶	300-1600	.10	7	Loading: Longitudinal strain, first cycle; latitudinal strain, second cycle. Both extension and shear fractures occurred along gypsum planes during failure.
112	515	Dolomite....	Good....	A few weathered holes. No lineation. Length, 2.031 in.; diameter, 1.0 in.; parallelism, <.001 in. Oven dried.	12,700	4.31×10⁶	300-2500	.27	17	Loading: Longitudinal strain, first cycle; latitudinal strain, second cycle; compressive strength, third cycle.
119	693	Siltstone....	Fair......	Several fractures. One end chipped. No lineation. Length, 4.063 in.; diameter, 2.109 in.; parallelism, .0048 in. Oven dried.	6,200	1.14×10⁶	600-2300	.31	13	Only one cycle of loading.
120	700	Andydrite..	Good....	A small chip on one end. Lineation approximately parallel to platens. Length, 4.10 in.; diameter, 2.109 in.; parallelism, .0019 in. Oven dried.	3,200	2.97×10⁶	600-1700	.42	19	Only one cycle of loading. Failure occurred along planes normal to lineation.

The hardness of the rocks (table 4) was measured on a Shore scleroscope. This instrument utilized a diamond-tipped hammer, which is raised to a standard height above the rock specimen and then dropped onto it. The height of the rebound is proportional to hardness and is recorded on a scale of 0 to 120.

Porosity of rocks above the salt ranges from as high as 34.7 percent for the Magenta Member of the Rustler Formation to as low as 1.1 percent for siltstone residuum at the top of the Salado Formation. Porosity of halite from the Salado ranges from 7.1 percent to 0.8 percent. Grain density ranges from 2.92 g per cc (grams per cubic centimeter) for the Magenta to 2.15 g per cc for the same siltstone residuum at the top of the Salado. Grain density of the halite ranges from 2.49 to 2.15 g per cc. Dry-bulk density ranges from a high of 2.49 g per cc in the Culebra Member of the Rustler Formation to a low of 1.81 g per cc in the Gatuna Formation. Dry-bulk density of the halite in the Salado ranges from 2.46 to 2.09 g per cc.

Sonic velocities were determined in the laboratory for rocks overlying the Salado Formation. Longitudinal velocities range from 15,205 fps (feet per second) for gypsum and anhydrite of the Tamarisk Member of

TABLE 5.—*Measured velocities and calculated elastic moduli for rock salt near the position of the Gnome explosion*

[From Dickey (1964, p. b109). All arrival times determined from comparison of two or more records from each line of measurement except those for line J-O. Only one acceptable record was obtained from line J-O. Line Y-Z, the preexplosion line of measurement, is 5.5 feet higher stratigraphically than the other lines. Measurements by D. D. Dickey and D. R. Cunningham]

Line of measurement (fig. 9)	Distance from explosion point (ft)	Length of line (ft)	Traveltime of first arrival (milliseconds)		Velocity (fps)		Poisson's ratio	Young's modulus (10⁶ psi)	Shear modulus (10⁶ psi)	Bulk modulus (10⁶ psi)
			Compressional	Shear	Compressional	Shear				
				Postshot measurements						
A-C.....	80-110	34.99	2.9	6.05	12,100	5,800	0.35	2.6	0.95	2.9
B-C.....	80-110	32.15	2.7	5.6	11,900	5,750	.35	2.5	.93	2.8
G-E.....	140-205	66.80	5.6	10.4	11,900	6,400	.30	3.0	1.1	2.5
G-F.....	140-205	67.09	5.7	10.4	11,800	6,450	.29	3.0	1.2	2.4
J-O.....	235-350	114.74	8.8	14.9	13,000	7,700	.23	4.1	1.7	2.6
J-K....	235-325	90.52	7.0	13.1	12,900	6,900	.30	3.5	1.4	2.9
U-W....	600-785	186.22	13.4	24.4	13,900	7,650	.29	4.2	1.6	3.3
				Preshot measurements						
Y-Z.....	5-85	81.37	6.05	11.5	13,500	7,100	.31	3.5	1.4	3.1

the Rustler Formation to 5,072 fps for sandstone of the Gatuna Formation. Transverse velocities range from 9,487 fps for the same gypsum and anhydrite sample to 3,244 fps for the Magenta Member of the Rustler.

CHANGES IN PHYSICAL PROPERTIES

The dynamic properties of the rock salt in the underground workings at Project Gnome were calculated from preshot and postshot in situ measurements of the compressional and shear velocities of acoustic waves. This work was described by Dickey (1964). Figure 9 shows the plan of the preshot and postshot workings and location of the sonic-velocity stations. Velocities and calculated elastic moduli are shown in table 5.

Dickey (1964, p. B111) concluded that:

* * * the results of this study showed that (1) although fracturing of this rock is detectable by the acoustic method used, compaction is not, and (2) the elastic moduli are changed for reasons other than compaction. Furthermore, the amount of fracturing is semiquantitatively estimable by acoustic means. Compaction is not shown by the changes in elastic moduli caused by the explosion, because of the larger changes in elastic moduli not related to compaction. These changes, however, may indicate the amount and position of changes in stress of the rock surrounding an explosion.

Density changes were not detected in laboratory measurements (table 6), and, therefore, compaction was less than 1 percent on any sample tested.

TABLE 6.—*Physical properties of samples of halite from unit 10, Salado Formation*

[Analysts: John Moreland, Jr., and E. F. Monk. Salt-saturated kerosene density: 0.8098 at 19.8°C]

Lab. No. P2–	Location in drift	Rock type	Effective porosity (percent)	Grain density	Dry-bulk density, mercury displacement	Saturated-bulk density (in salt-saturated kerosene)	Total porosity (percent)
1198	Sta. 6+94.	Preshot halite.	1.0	2.17	2.14	2.15	1.2
1012	105 ft from shot-point.	Postshot halite.	1.02	2.18	2.11	....	3.65
1199	....do....	....do......	.9	2.18	2.14	2.15	1.7
1200	....do....	Postshot vein halite.	.9	2.17	2.13	2.13	1.9

MINOR ELEMENTS IN SALADO FORMATION IN THE GNOME DRIFT

The Gnome drift, whose rocks show a sequence of cyclic deposition, provided a rare opportunity to study the distribution and association of minor elements of evaporite rocks in a nonmineralized part of the Salado Formation.

Semiquantitative spectrograph analyses were made on samples from seven stratigraphic units exposed in the Gnome drift and from four replacement zones in these units. In addition, analyses for minor elements were made for comparative purposes on samples of the langbeinite and sylvite ore zones from the 800- and 900-

foot levels of the International Minerals and Chemical Corp. mine, 12 miles northwest of the Gnome site, and on samples of selenite crystals precipitated in Salt Lake, 8 miles west of the site. These analyses were by Gard, Cooper, and others (1962, tables 9, 11). Samples from the Gnome drift are described in table 7 of the present report, and the semiquantitative spectrographic analyses of these samples are summarized in table 8.

Many elements either compose the clay minerals or are closely associated with the clays. These elements are, in order of decreasing abundance: potassium, magnesium, calcium, silica, aluminum, iron, titanium, lithium, boron, barium, manganese, vanadium, zirconium, chromium, molybdenum, copper, nickel, yttrium, gallium, cobalt, scandium and ytterbium. Several elements that are associated with the clays also form parts of one

TABLE 7.—*Description and stratigraphic position of samples of Salado Formation analyzed by semiquantitative spectrographic methods*

[All samples from Gnome drift]

Sample	Stratigraphic unit within Salado Formation	Description
30	10 (upper part).	Halite rock, colorless.
31	....do.......	Halite rock, orange, translucent; contains trace of disseminated orange polyhalite.
33	....do.......	Halite rock; composite sample.
34	10 (lower part).	Halite rock; contains some polyhalite.
35	....do........	Halite rock; contains some gray clay and trace of polyhalite.
37	11.............	Halite rock; contains gray clay and streaks of polyhalite.
39	12.............	Halite rock; contains gray and brown clay.
41	13 (upper part).	Halite rock, orange; shows streaks of orange polyhalite and brown clay; contains trace of gray clay.
42	....do.........	Halite rock, colorless; contains some brown clay and trace of orange polyhalite.
43	13 (lower part).	Halite rock; contains some brown clay and polyhalite.
46	14.............	Halite rock; contains blebs of orange polyhalite.
47	15 (upper part).	Polyhalite rock, moderate-reddish-brown; contains trace of halite.
48	15 (middle part).	Polyhalite rock, moderate-reddish-brown; contains trace of halite.
49	15 (lower part).	Same; contains inclusions of gray clay.
50	15.............	Underclay, gray; contains some halite and trace of polyhalite.
51	16.............	Halite rock; 0.3- to 0.5-in.-square crystals; contains some gray clay and orange polyhalite.
52	16.............	Halite rock; 0.3- to 1.0-in.-square crystals; contains some brown clay.
53	16.............	Halite rock, colorless; contains some blebs of orange polyhalite.

TABLE 8.—*Summary of semiquantitative spectrographic analyses of evaporite rocks (Salado Formation) from Gnome drift, in percent*

[Samples described in table 7. Analyst: J. C. Hamilton. M, major constituent (greater than 10 percent); L, looked for but not detected. Average: where results are reported as 0 or <, with a number, the half-value of the threshhold of detection was used in determining the average. Other elements looked for but not detected: phosphorus, silver, arsenic, gold, beryllium, bismuth, cadmium, germanium, hafnium, mercury, indium, lanthanum, nickel, palladium, platinum, rhenium, antimony, tin, tantalum, tellurium, thorium, thallium, uranium, tungsten, zinc, and cerium]

Unit in Salado Formation	10	11	12	13	14	15		16
Sample Nos	30, 31, 33–35	37	39	41–43	46	47–49	50	51–53
Si	0.007 -0.15	0.3	1.5	0.3 -0.7	0.007	0.03 -0.3	M	0.003 -0.3
Al	.015 - .15	.3	.7	.3	.007	.015 - .3	1.5	<.005 - .15
Fe	.007 - .03	.05	.3	.1 - .2	.002	.07 - .3	.7	0 - .03
Mg	.15 -2	.7	3	.7 -2	5		7	.15 - .5
Ca	.07 -7	.5	.07	.07 -5	1.5	M	.7	.1 - .5
Na	M	M	M	M	M	1	7	M
K	0-5	1	1.5	0-5	2	M	7	0-1
Ti	.0007- .003	.005	.03	.01 - .015	<.0005	.0015- .015	.15	<.0005- .007
Mn	0- .0003	.0007	.005	.001 - .0015	L	.0005- .003	.015	0- .0007
B	L	L	.005	L	L	L	.05	L
Ba	<.0002- .0015	.007	.005	.0005- .003	<.0002	.005 - .007	.015	<.0002- .0005
Co	L	L	L	L	L	L	.0007	L
Cr	0- .0002	.0005	.002	.0003- .0005	L	0- .005	.005	L
Cu	.0001- .001	.0001	.0002	.0002- .0003	.00015	.0002- .0015	.002	0- .0007
Ga	L	L	L	L	L	L	.0015	L
Li	L	L	.03	L	L	L	.1	L
Mo	L	L	L	L	L	L	.003	L
Ni	L	L	L	L	L	L	.002	L
Sc	L	L	L	L	L	L	.0007	L
Sr	.003 - .3	.05	.005	.005 - .3	.07	.15 - .3	.015	.005 - .05
V	L	L	.002	0- .001	L	.001 - .0015	.007	L
Y	L	L	L	L	L	L	.002	L
Yb	L	L	L	L	L	L	.00015	L
Zr	L	L	.0015	L	L	L	.007	L

or more minerals. Potassium and magnesium form an integral part of the polyhalite lattice, and calcium is also a major constituent of polyhalite. Included iron, which is also concentrated in the clays, imparts the characteristic reddish-orange color to polyhalite. Barium is more abundant in the clay concentrates and in the sulfate mineral polyhalite than in the halite.

Boron is commonly associated with the clays but was not found in the halite or polyhalite. Strontium is relatively abundant in polyhalite but is less abundant in halite rocks containing accessory polyhalite as blebs, streaks, or disseminated particles.

Elements reported by Moore (1958b, tables 4, 5) in anhydrite, polyhalite, and halite rocks of the Salado Formation, but not determined by the semiquantitative spectrographic method, are: chlorine, sulfur, oxygen, hydrogen, bromine, carbon, fluorine, iodine, and selenium. Thorium and zinc were also reported by Moore but are not present in the Gnome samples in amounts detectable by this method. Six elements not previously reported were detected by the spectrographic method: chromium, lithium, scandium, yttrium, ytterbium, and gallium.

MINERALOGY AND PETROGRAPHY OF THE SALADO FORMATION NEAR THE DEVICE CHAMBER

A petrographic study was made by B. M. Madsen of the evaporite rocks near the device chamber, and the insoluble clastic material from these rocks was studied by Julius Schlocker. Seventeen thin sections from a 100-foot section of the recovery-hole core and four thin sections from rock samples collected in the drift were studied and described. The 100-foot section of the core extended from 50 feet above to 50 feet below the device chamber. The predominant mineral is halite, and lesser amounts of polyhalite and clay are present. The other minerals present are magnesite, quartz, chlorite, mica, and anhydrite, which generally occur in amounts of 1 percent or less.

HALITE

Halite makes up more than 90 percent of the 100-foot section of the recovery-hole core. The halite rock is hypidiomorphic-granular and shows no strain birefringence or schistosity in thin section. The grains range in size from 0.75 to 50.8 mm, but most are between 7.62 and 17.8 mm. A plot of the crystal size of the halite on a strip log showing lithology and depth shows a slight tendency for the size of the halite crystals to decrease as the disseminated-clay content increases. More than half the halite crystals contain negative crystals (crystal-shaped voids) filled with a liquid and gas. These negative crystals are both cubic and rectangular, but they always maintain right-angle corners, and they are as much as 0.05 mm in diameter. Generally the negative crystals occur in zones three or four crystals wide and parallel to the cleavage of the host halite crystal, but in some the zones of negative crystals are at a 45° angle

ing zones or in small irregular masses of several hundred crystals.

POLYHALITE

The second most abundant mineral in the 100-foot section of core is polyhalite, which ranges in color from white and gray to brick red. In thin section the polyhalite exhibits a variety of textures, which are divided into four types (Schaller and Henderson, 1932, p. 51). These types may occur singly, intimately mixed, or grading from one to the other.

The first texture is fine grained, the crystal size ranging from 0.001 to 0.02 mm, and is allotriomorphic-granular. The fine-grained texture generally characterizes the more massive forms of polyhalite.

The second texture is coarse grained, the crystal size ranging from 0.02 to 0.5 mm. Crystals range from anhedral to euhedral, but are mainly subhedral and twinned.

The third texture is euhedral twinned and includes two distinct forms, both of which show laminar and sector twinning, are colorless, and range in crystal size from 0.2 to 6.0 mm. One form of the euhedral-twinned group is spear shaped (fig. 7A), and the length is no greater than twice the width. The second form of the euhedral-twinned variety is the lath (fig. 7B). The length of the euhedral-lath twins is generally at least 10 times the width; normally this form occurs as inclusions in halite crystals or as projections into a halite crystal. The lathlike crystals range in width from 0.01 to 0.5 mm and in length from 0.2 to 5.0 mm.

The fourth texture is fibrous and is characterized by crystals that range in width from 0.001 to 0.004 mm and in length from 0.1 to 0.9 mm. The fibrous and fine-grained granular textures are gradational and commonly occur together. Individual fibrous crystals are common in the halite. The fibrous form shows all gradations from almost perfect spherulites to faint wisps of fibers.

Color.—Polyhalite imparts a light-orange or reddish-brown color to the rock and is the most conspicuous megascopic mineral. The color depends on the amount of
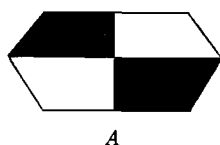
A

B

FIGURE 7.—Twinned polyhalite crystal forms: *A*, spear shaped; *B*, lath shaped.

included hematite in the polyhalite. Hematite occurs as an extremely fine dust disseminated through the fine-grained and fibrous forms of polyhalite but is absent in the euhedral forms, which are colorless. Hematite also occurs in the brown clay and along some cleavage planes in the halite immediately adjacent to the brown clay inclusions. Mottling observed at the top of the Union anhydrite, a locally used name, in the Salado Formation is due to a mixture of hematitic fine-grained to fibrous polyhalite and colorless coarse-grained polyhalite.

Structure.—Polyhalite occurs as blebs, growths, streaks, seams, beds, bands, and disseminated crystals or particles. The terms "bed," "band," and "seam" are applied to horizontal laminae of polyhalite which may be brick red, orange, or white and range in thickness in this part of the section from a few hundredths of a foot to 1.5 feet. In texture these laminae are mostly fine grained or fine grained to fibrous. At the contact of a polyhalite band with halite, long euhedral-twinned laths of polyhalite usually project into the halite. Rounded masses of coarse-grained polyhalite and remnants of large euhedral-twinned crystals of polyhalite are also present in some bands.

Polyhalite is nearly ubiquitous in the halite as small masses that make up 1–10 percent of the rock. Where these masses are roughly equidimensional, they are called blebs or growths; if they are at least three times longer than they are wide, they are called streaks. These small masses average 1–5 mm in width, are orange, and occur in or between halite crystals. Generally they have a center of fine-grained polyhalite, and long fibrous or euhedral laths make up an outer rim that projects into the surrounding halite. The laths projecting into the halite are so evenly developed that they look like the teeth of a comb or the spokes of a wheel. The centers of some blebs are mixtures of coarse- and fine-grained polyhalite or of fine-grained and fibrous polyhalite. A few blebs are composed of a mat of fibrous crystals and contain no fine-grained polyhalite.

ANHYDRITE

Anhydrite was found in only two thin sections, where it amounted to 1 percent or less. One thin section is from a sample taken 1.5 feet below marker bed 121 and shows anhydrite crystals at least 5.5 mm long that have been badly corroded by halite. The other section is from a sample taken from the top of marker bed 120 and shows a single perfectly euhedral anhydrite crystal in halite. This crystal is 0.21 mm long and 0.07 mm wide.

CLASTIC MATERIAL

The presence of clastic material in the Salado Formation is an anomaly. This material was probably not brought in from the open sea to the south, and a postu-

lated landmass to the northwest must have been many miles away. The clastic material is mainly clay and silt size (table 9), has minor amounts of sand-sized material, and could have been carried in suspension by streams from such a landmass; possibly some of this material was airborne. According to Julius Schlocker (written commun., 1961), the sand-sized material consists of doubly terminated quartz crystals that attain a maximum diameter of 0.6 mm. Cores of some of these euhedral crystals show ghosts of well-rounded quartz grains, which indicate that the crystals were much smaller when deposited and that they acquired overgrowths of quartz after deposition. Clasts of other minerals, which are sparse and mostly very fine grained, include microcline, plagioclase (mostly oligoclase), and quartz with biotite inclusions.

TABLE 9.—*Approximate size and heavy-mineral composition of clastic material in units 11–13 of the Salado Formation in Gnome drift*

[Julius Schlocker, written commun., 1961]

Unit	Percentage of material of given size			Heavy minerals (percent)
	Less than 2 microns	Silt	Sand	
11		15.0	10.0	0.17
12		14.5	7.2	.22
13	73.2	19.3	7.5	.13

The heavy-mineral assemblage, according to Schlocker (written commun., 1961), is approximately the same in all units and is as follows.

Abundant: ilmenite; leucoxene; magnetite with drusy surfaces; biotite, green and brown; muscovite.

Common: hornblende, blue-green to yellow-green, palebrown to brown, green to brown; monazite; epidote; chlorite; tourmaline, yellowish-red-brown to colorless, greenish-brown to colorless, dark-green to palebrown.

Scarce: zircon; rutile; apatite; sphene; clinozoisite; garnet, pale-brown, colorless, and rutilated; iron sulfides.

Rare: oxyhornblende; anatase; anhydrite; actinolite-tremolite; sillimanite in quartz; hypersthene, etched.

Clay.—The term "clay" is here used for the water-insoluble minerals of clay and silt size. Clay-sized particles make up more than 75 percent of this material. This clay-silt mixture occurs as irregular streaks, inclusions, and partings in the Salado Formation. The partings vary in thickness from a featheredge to 19 mm. The silt-sized material was examined with the petrographic microscope, and the clay-sized fraction was analyzed by X-ray diffraction by Julius Schlocker of the Geological Survey.

The silt-sized material is made up largely of quartz, magnesite, chlorite, and mica. All clay-sized samples that were examined are of similar composition, according to Schlocker (written commun., 1962), and contain about equal proportions of (1) interstratified chlorite and montmorillonite having both regular 1:1 alternations and random alternations; (2) mica, both trioctahedral (biotite: phlogopite type) and dioctahedral (muscovite type); and (3) chlorite. A trace of magnesite is present in the clay-sized material. In the halite rock the proportion of clay- and silt-sized grains ranges from 0 to 40 percent, but averages 1–3 percent. Talc, which commonly occurs in halite rock, was not found. The color of the clay ranges from gray to gray green to reddish brown. The reason for the color difference was not determined. The colors persist even in the less than 2-micron-sized fraction and in the clay minerals themselves.

EFFECTS OF THE NUCLEAR EXPLOSION

The Gnome shot was fired at noon on December 10, 1961, and produced a yield of about 3 kilotons (equivalent to 3,000 tons TNT). At shot time the ground surface above the detonation point rose about 5 feet and then dropped (Hoy and Foose, 1962). Shortly thereafter, observers 5 miles away felt a strong ground roll.

The ground surface was permanently domed upward for more than 400 feet radially around ground zero, the maximum rise being 1.9 feet. An irregular pattern of radial and concentric fractures with slight displacement was formed in the stabilized caliche pad and adjacent dune sand. Most of the concentric fractures had the outer side upthrown (Hoy and Foose, 1962).

One interesting surface effect was the appearance shortly after the shot of a large number of freshly dug or recently cleaned-out animal burrows in the vicinity of ground zero (Hoy and Foose, 1962).

The explosion melted approximately 3.2×10^6 kilograms of salt and produced a standing cavity with a volume of about 27,200 cubic meters (Rawson and others, 1965). The shock of the explosion opened radial fractures and produced some thrust faults in the adjacent rock that were filled with melted salt and rock fragments. Fractures as much as 130 feet from the cavity were injected with radioactive gases, as shown by blue coloration of the salt.

A few moments after firing, the shot vented into the drift and up the shaft, having breached the salt in the vicinity of the line-of-sight neutron-tube hole and having blown a rupture disk out of a ventilation hole in the blast door. Stemming at the bypass section near the blast door prevented any ultrahigh-pressure gases or particles from escaping through the vent. For more than a day

~~clouds of steam laden with short-lived radioactive gases~~ drifted gently from the shaft and ventilation pipes. Air and surface contamination were closely monitored, and traffic near the site was stopped for a short time to ensure public safety. Because of the radiation, reentry to the main station was delayed for nearly a week.

The shot was completely contained by the rocks directly over the shot, and there has been no indication that any radioactivity leaked into the ground water in the Culebra Dolomite Member of the Rustler Formation.

EFFECT ON THE SHAFT

Damage to the shaft was very limited. At 75 feet and 90 feet below the collar, the reinforced-concrete shaft lining displayed horizontal fractures, with minor lateral movement, around its entire circumference. The concrete liner above each fracture had moved radially away from ground zero relative to the part below. Neither fracture had a displacement of more than one-fourth inch. The differential movement at these two positions was probably localized by two contacts: at 90 feet by the contact of the Dewey Lake Redbeds with the less consolidated overlying Gatuna Formation, and at 75 feet by a contact between conglomerate and less consolidated sandstone in the Gatuna.

The concrete lining contained several minor horizontal fractures, with showed no visible displacement, at depths of 160 and 480 feet. The lower of these, about 15 feet above the top of the water-bearing Culebra Dolomite Member, produced a slight water seep. However, no large amount of water seeped from the Culebra into the shaft or the cavity (J. B. Cooper, U.S. Geol. Survey, oral commun., 1962). Below the concrete lining there was small-scale spalling of salt and clayey beds from the shaft wall.

EFFECT AT THE MAIN STATION

At the main station (junction of the shaft and drift) damage from the shot consisted of large-scale spalling from the ribs, especially at exterior corners, and of slabbing from the back of about 3–4 feet of units 13 and 14, which parted at the contact with the clayey units 11 and 12. Where roof bolts, netting, and a monorail were affixed in the back, large slabs of units 13 and 14 were hanging free, and this loose rock had to be removed during cleanup operations.

The marker bed 121 polyhalite (unit 15) was bleached to a depth of a few millimeters, probably by the steam that leaked from the cavity. The 16-foot-deep sump at the bottom of the shaft was filled with water condensed from the steam, and, for a few weeks after the explosion, ankle-deep water was present on the sill (floor) at the main station.

Because radiation levels were high in the original drift, a reentry drift was driven parallel to and about 30 feet south of the original drift. The reentry drift was constructed to allow close-in sample-recovery drilling and recovery of instruments buried before the shot.

The reentry drift and appurtenant exploratory laterals were mapped in June 1962, 6 months after the shot was fired (pl. 2). Unlike the original drift, which was horizontal, the reentry drift was sloped slightly downward, following the bedding, to take advantage of the parting between beds 11 and 12. This provided a smooth strong back which did not require any bolting. The reentry drift, thus, exposed the same beds for its entire length.

Seeps.—Explosion effects, such as faults, fractures, and irradiated salt, were not seen in the reentry drift beyond 250 feet from the shotpoint. The most obvious difference observed between the salt exposed in the reentry drift and that exposed in the preshot drift was the presence of water seeps along the reentry drift. Several seeps were visible at the base of unit 15 (from the clay underlying the polyhalite) and from the thin clayey units 11 and 12. This water must have been derived from the steam created by the blast. If it had merely been moisture squeezed out of the clays by the blast, it would have been more widely distributed and should have been more abundant where the clays were thicker. Seeps also were associated with the grout-filled instrument holes intercepted by the drift. Some of this water could have been introduced by the grouting operation.

VENTING

Venting occurred because the larger-than-anticipated cavity and spalling from the cavity walls resulting from the explosion reduced the separation between the cavity and the end of the straight part of the drift. Radial fracturing from the cavity provided avenues of escape for the high-pressure steam, and, once open, these fractures became enlarged by solution and erosion. Salt along the path of the steam was dissolved and sculptured in potholelike cusps (fig. 8). At the drift elevation, the thin, potentially weaker, clayey halite beds—units 11 and 12—probably contributed by providing a lubricated zone of weakness.

THE CAVITY

An open cavity about 70 feet high and more than 150 feet across resulted from the detonation and postshot collapse (fig. 5). In plan, the cavity is roughly oval and is elongated in the same direction as the drift (fig. 9). Postshot drilling indicated that strata 200 feet above the shotpoint were permanently displaced 5 feet

FIGURE 8.—Steam-eroded potholes in unit 10 where shot vented into preshot drift. Corner of preshot drift shows at lower left.

upward (Lawrence Radiation Lab., written commun., 1962), and that the Union anhydrite, a locally used name, in the Salado Formation, which lay 55 feet below the shotpoint, was displaced downward more than 10 feet (T. S. Sterrett, U.S. Geol. Survey, oral commun., 1962).

The bottom of the cavity contains a heap of rubble composed of large angular blocks of salt which have fallen from the vault and sides (frontispiece). Bowed-up ends of strata crop out in the walls of the cavity, and the walls exhibit no evidence of melting. Colors in the cavity are spectacular and include red, brown, white, orange, yellow, and blue. The yellow and blue

colors are caused by radiation damage to the salt. Radial fractures are seen in the vault of the cavity; these fractures narrow radially from the center of the vault. They are filled with white salt evidently redeposited from solution, and thin white salt stalactites hang from the vault and sides (frontispiece).

EXPLOSION-INDUCED STRUCTURE

Detailed geologic mapping of the reentry drift disclosed that the detonation had surprisingly little effect on the strata lying at the same altitude as the shotpoint. Evidence for this is, of course, confined to what could be seen in the limited postshot mine workings. Undoubtedly, blast effects will be found in salt beds above and below the drift level if exploration is carried out at other levels. A belt of salt about 30 feet high in the cavity wall at about device level seems to have been moved radially outward as a unit, and the beds above it are bent upward. The contact between beds showing these different types of movement lies about at marker bed 119 (detailed measured section, p. 24), and it is postulated, therefore, that structures similar to those exposed in the postshot workings will be found at least to that level. Beds logged in the recovery hole and shaft can be identified clearly in the cavity walls.

Major lateral blast-induced effects were largely confined to a radial distance of about 140 feet from the shotpoint, although curving vertical faults, concave toward the preshot drift and showing slight horizontal movement, are found as far as 250 feet away from the
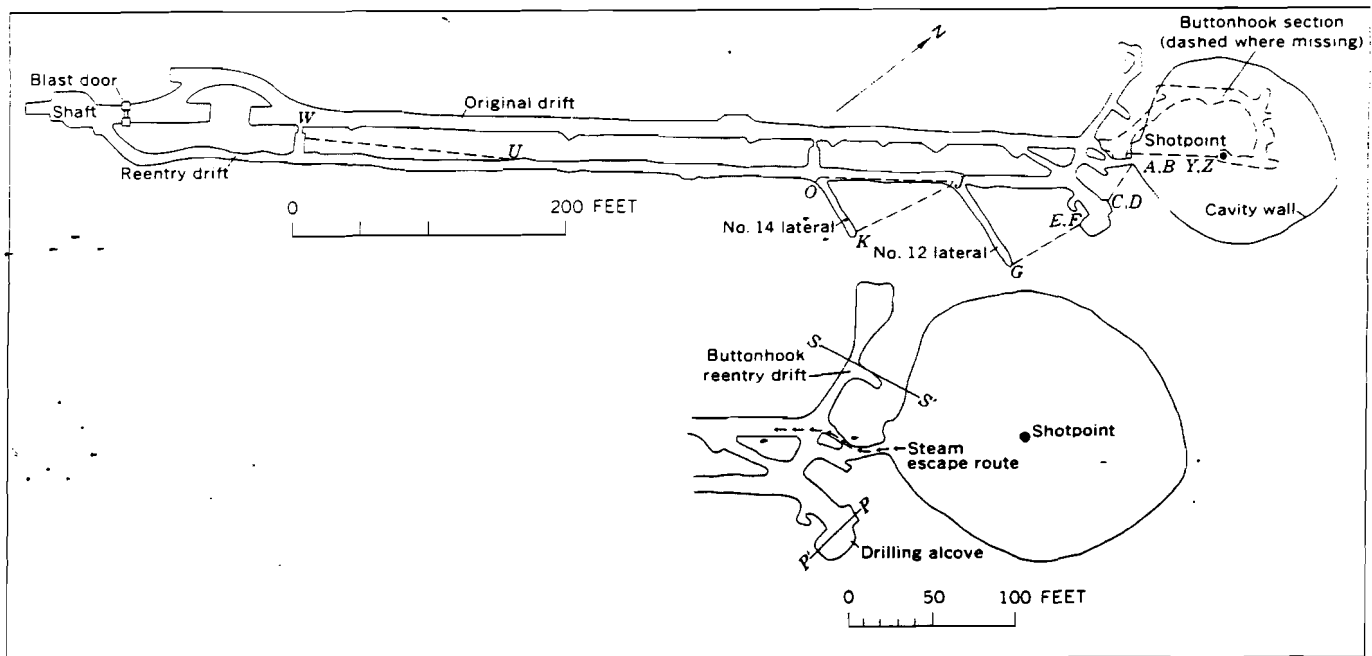

FIGURE 9.—Map of underground workings and cavity. Sonic velocity stations are indicated by italic letters, and lines of sonic measurement, by dashed lines; from Dickey (1964). Enlargement shows location of geologic cross sections (figs. 10, 12). Arrows show route of venting.

shotpoint. These faults probably were formed because of the relief effect of the preshot drift, although they may be tear faults representing the ends of thrust faults that lie concealed above the mine workings.

The contact between the thin clayey halite beds that form units 11 and 12 forms the back of the reentry drift. In many places the bottom of unit 11 displays the cast of ripple marks that were present on the upper surface of unit 12. These ripple marks were destroyed by differential movement along this contact and are commonly replaced by slickensides to about 230 feet from the shotpoint. Beyond there the ripple marks are intact. In most places the slickensides trend N. 35° E., roughly radically from the shotpoint; but at station 8+58, near the junction of the reentry drift and the lateral IH-8, a set of slickensides trends N. 80° E., indicating that some motion was not radial.

STRUCTURE IN CONFINED SALT

Except for the radial fractures seen in the vault of the cavity and a few others exposed in the buttonhook reentry drift, blast-produced faults in the confined salt appear to be restricted to a 10-foot section of salt (units 13–15) bounded above by the clayey layers (units 11 and 12) and below by the clay at the base of the polyhalite. These fractures are mainly thrust faults that dip both toward and away from the cavity and die out in the clay layers. Overthrusts are more common than underthrusts. The thrust faults end laterally by curving downward into vertical tear faults that die out in the salt beds.

Typical examples of these faults are seen in the drilling alcove (section A–A', pl. 2) where two thrust faults that dip toward the cavity are well exposed. The one exposed in the east wall has 2 feet of throw, which can be measured from the offset of the contact between units 13 and 14 in the alcove wall. A 2-foot-square hole dug in the wall revealed that, although unit 15 is offset, the fault dies out in the underclay and does not offset unit 16. The north end of this fault dies out in a tear fault in unit 13. The other fault has only one-half foot of throw and can be traced in the south, west, and north walls of the alcove. The lower end of the fault originates in the clay under unit 15 and offsets the polyhalite slightly, but the upper end is not exposed (fig. 11A). Figure 10 is an interpretation of these two faults.

In the No. 12 lateral, which was driven to recover an instrument, unit 14 displays horizontal hairline fractures along the wall nearest the cavity that are similar in appearance to the fault just described. The offset on these fractures could not be determined, nor is the direction of dip known, but any movement along them must have been very slight. The gouge in these fractures
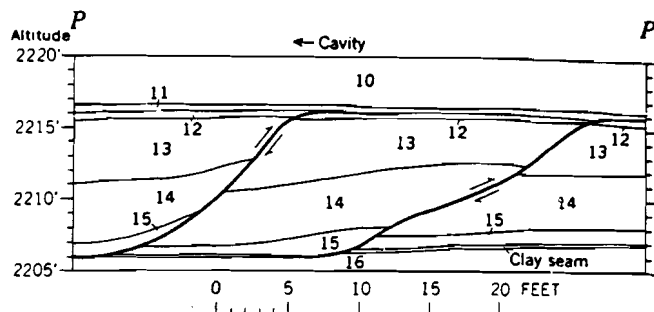
FIGURE 10.—Geologic cross section P-P' of drilling alcove, showing thrust faults. Right fault shown in figure 11A. See table 2 for description of numbered stratigraphic units.

is blue in places, indicating that radiation leaked this far along the fractures. There is no indication in this lateral of any offset of the polyhalite bed.

Adjacent to the cavity, faulting is more common and more complex, although no faults were seen that had more than a few feet of displacement. On many faults at least some component of movement could be measured, from offset either of beds or of mudcracks in unit 13.

According to a resurvey of grout-filled instrument holes, total lateral displacement 100 feet from the shotpoint was 16 feet. An instrument 127 feet from the shotpoint had been moved away 8 feet. Bags of salt in the alcove at the end of the straight section of the preshot drift that initially were about 90 feet from the shotpoint were about 120 feet away and had been lithified into well-compacted salt breccia (fig. 11B). Outlines of individual bags with cloth fragments between are still discernible.
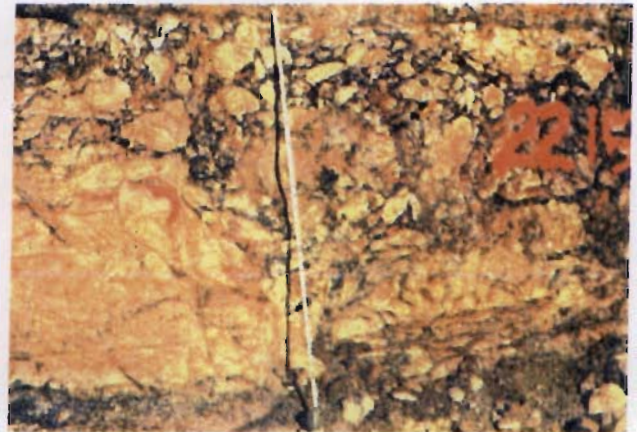
STRUCTURE IN UNCONFINED SALT

On the west side of the shotpoint, the buttonhook drift remained open up to shot time. It was designed to be blown shut when the shot went off, and in this it was eminently successful—material that had been left in the open drift was blown 35 feet from its original position and sealed tightly in a well-lithified intrusive breccia of salt. Complex thrust faulting accompanied by intrusive breccia is found as far as 110 feet from the shotpoint on this side of the cavity.

Faulting.—The rocks observed in the buttonhook reentry drift were complexly faulted. Several thrust faults can be seen along the right rib, and many of them contain melt. The section exposed in the left rib is unfaulted, but the beds lie about 4 feet above their preshot altitude. The thrust faults generally die out laterally in downcurving tear faults. The main rock unit involved in the faulting is unit 10, which has been thrust under itself. A small lateral driven toward the cavity revealed details of one of these faults (figs. 11C, 12).
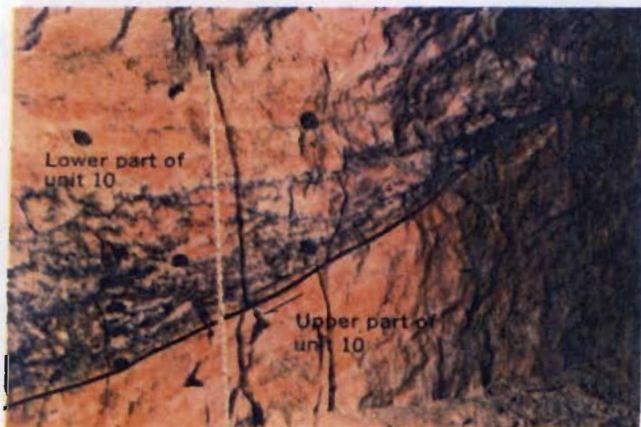
A

D

B

C

E

and cloth fragments near "2" on rule. (See pl. 2, section B-B', left rib.) C, Underthrust fault in unit 10 in buttonhook reentry drift. Fault parallels bedding of lower plate, following a thin clay seam that normally lies 5.5 feet above basal clayey halite at left. Cavity to right. Scale is 3 feet long. (See pl. 2, section E-E', left rib.) D, Intrusive breccia in buttonhook recovery drift. Blocks are composed of intensely granulated halite crystals, mainly from unit 10. Black matrix is chilled salt melt containing disseminated opaque black carbon and the blast-produced minerals laurionite and galena. (See pl. 2, section D-D'.) E, Intrusive breccia vein in rib of buttonhook recovery drift. Rule is 30 inches long. (See pl. 2, section D-D'.)

FIGURE 11.—Thrust faults, lithification, and brecciation resulting from the Gnome explosion. A, Thrust fault offsetting unit 15 (polyhalite) in drilling alcove. Fault originates in thin clay at base of polyhalite (left of hammer) and does not offset unit 16 (below hammer). B, Lithified salt bags. Note outline of bag shape top center indicated by arrows
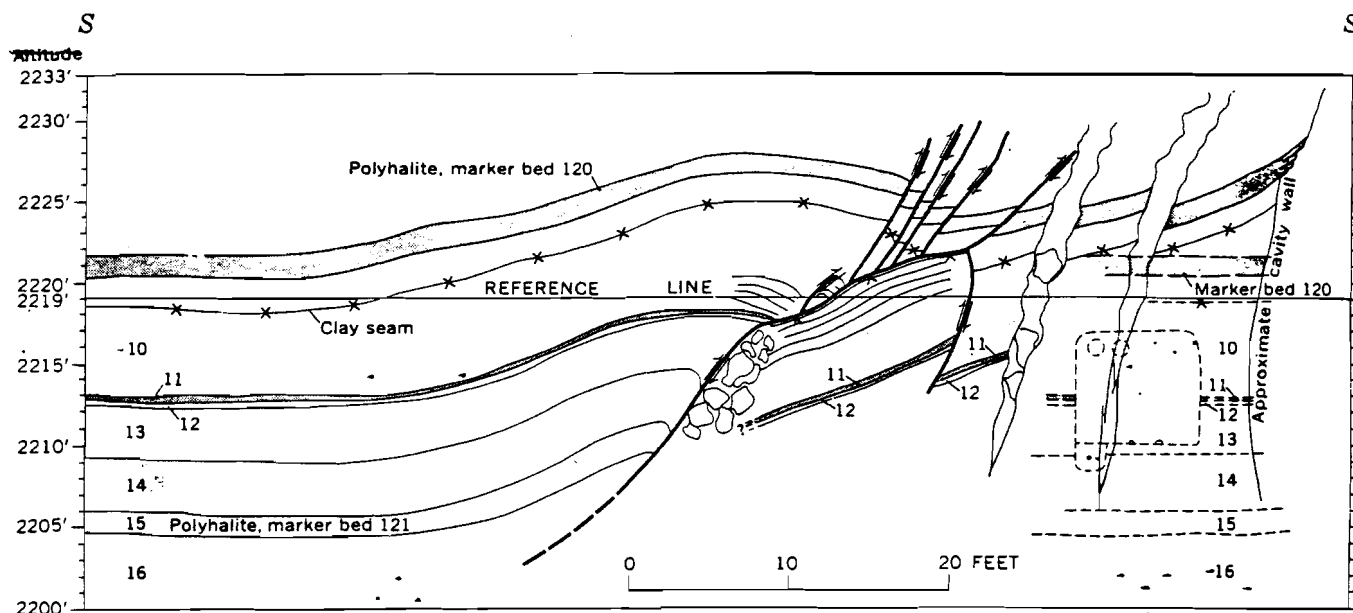
FIGURE 12.—Geologic cross section S-S' through buttonhook reentry drift. See table 2 for description of numbered stratigraphic units. Dashed lines indicate original position of buttonhook drift and strata.

The determination of the details of the structure from the limited exposures available was facilitated by the presence of several thin distinctive beds in unit 10.

Intrusive breccia.—Intrusive breccia is associated with the faulting along the right rib of the buttonhook reentry drift. The breccia consists of fragments that are largely composed of salt from unit 10 and range in diameter from a few millimeters to several tens of feet. These brecciated salt fragments occur in a matrix of black salt melt (fig. 11D). The black color is imparted by two blast-produced lead minerals—laurionite and galena—and disseminated carbon. The breccia contains twisted fragments of mine rail, steel ventilation pipe, wire, aluminum conduit, and cable covering and a few slightly scorched fragments of wood that had been left in the buttonhook drift. These fragments now lie about 35 feet from their original position. Salt in the blocks was granulated by the shock but not melted. Halite crystals in unit 10 ranged from 10 to 20 mm in diameter before the shot (fig. 13) but were shattered by the explosion and reduced to angular fragments measuring a millimeter or less (fig. 14A). This granulation must have resulted from the amount of free movement in these blocks, because it is not seen elsewhere, even in the cavity walls. Halite crystals in the cavity walls are fractured, but their outlines are plainly visible. Bedding planes in the larger fault blocks are distinct and still roughly horizontal, although the smaller blocks in the breccia are randomly oriented. Bedding planes are not disrupted within the larger blocks, although they may display drag against faults.
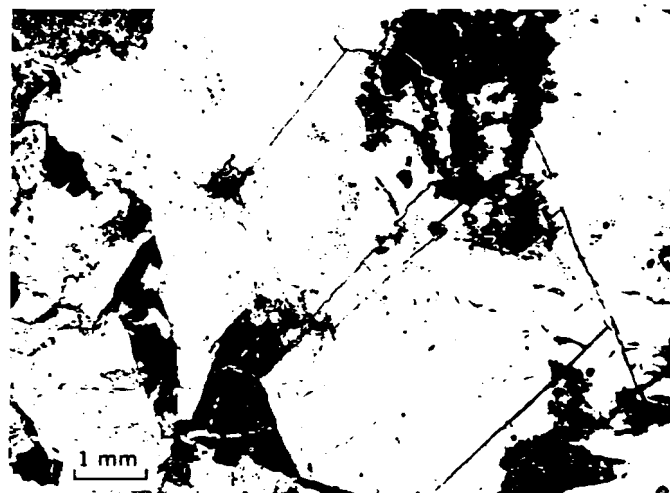
FIGURE 13.—Photomicrograph of preshot salt. Dark areas are polyhalite and clay. Note cleavage planes.

The density and porosity of samples of the granulated halite from the breccia and some of the vein material were determined in the laboratory (table 6) and compared with the results obtained on preshot sample (tables 3, 4). If any change in the density occurred, it was less than the limit of error due to sampling a slightly variable unit. Total porosity appears to have increased slightly, probably owing to the increased number of grain boundaries.

NEW MINERALS FORMED

Associated with the blocks of granulated salt are black veins of intrusive breccia containing the manmade
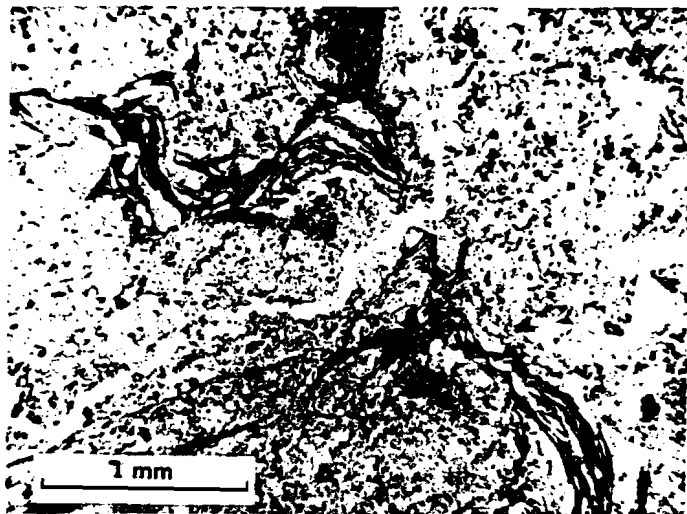
A

B
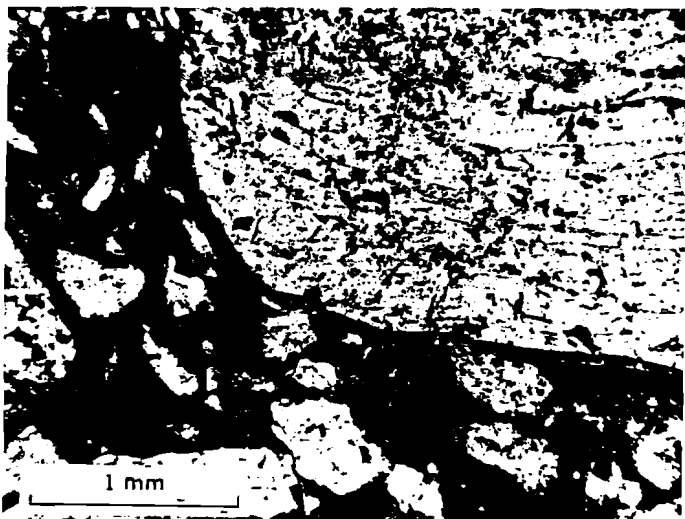
C

FIGURE 14.—Photomicrographs of intrusive breccia resulting from Gnome explosion. A, Swirl pattern of fragments in intrusive breccia veinlet; black areas are carbon, laurionite, and galena. B, Plastically deformed salt fragment in intrusive breccia. C, Chilled border of melt against fragment; chilled border contains fewer opaque minerals.

fragments reminiscent of that commonly seen in welded tuffs (fig. 14A). Minute fragments of copper and steel wire are not uncommon constituents.

Thin sections of the veins show that the melt has narrow chilled borders where it is in contact with many of the larger fragments and wallrock. The chilled borders are relatively free of lead minerals, but those minerals occur in the interior of the veins in the form of dust lying between the tiny crystals of melted salt (fig. 14C).

A mixed grab sample of black salt that was thought to be representative of the melt was collected from several places along the buttonhook recovery drift and submitted to the laboratory for analyses. Theodore Botinelly (written commun., 1962) reported as follows:

A part of the sample was leached with distilled water in the ultrasonic agitator. The X-ray diffractometer pattern of the black (dark blue-gray) residue showed laurionite (Pb(OH) Cl), galena (PbS), and a mica. One fragment of vein material was cleaned of salt and leached with water. The residue amounted to approximately 15 percent of the weight of the original material. Slight effervescence with acid indicates some carbonate is present. (Magnesite is present in the preshot clays.) Microscopic examination showed, in addition, doubly terminated quartz crystals with a small 2V. Quartz from a preshot sample of fairly pure salt showed no 2V. Also present in the residue from the preshot salt were flakes of muscovite.

Synthetic laurionite was prepared from lead acetate and sodium chloride solutions. Dehydrated at 150°C. for 12 hours it broke down to a mixture of lead oxides and lead chlorides. The mixture did not revert to laurionite in 48 hours. After 64 hours

minerals laurionite[1] and galena (Gard, 1963). These veins are not radioactive. The veins, which are seldom more than a few inches wide and are generally radial to the shotpoint (figs. 11E, 15), display sharp contacts with the host rock and are intruded along faults and fractures. The black veins and breccia matrix consist of melted and recrystallized salt and contain minute opaque black minerals disseminated between the salt crystals and sharp-bordered fragments of clear unmelted plastically deformed salt. Some of the unmelted salt fragments have a very thin selvage suggesting partial melting, and many of the fragments show warping and bending of bedding and cleavage suggesting plastic deformation (fig. 14B). In one thin section a tiny vein displays flow textures with warping and swirling of

[1] Laurionite was first found at Laurium, Greece, where it is formed by the action of sea water on slags from lead mines that were operated during the time of Pericles (4th century B.C.).

FIGURE 15.—Hand specimen showing vein of intrusive breccia. Unmelted salt fragments set in matrix of black melted salt. Black color is caused by presence of carbon and of lead minerals laurionite and galena, which were formed by heat and pressure of the shot.

in an atmosphere saturated with water, the mixture showed a laurionite X-ray pattern.

Induction-furnace determinations, by I. C. Frost, showed total carbon content of the insoluble residue of two samples to be 5.64 and 6.74 percent.

ELEMENTS INTRODUCED

Comparison of the semiquantitative spectrographic analysis of the insoluble residue from the black veins (table 10) with analyses of the rock units exposed in the preshot drift (table 8) shows that silver, bismuth, lead, tin, zinc, and carbon are new elements that must have been introduced by the explosion. There are two potential sources for these elements: first, the nuclear device and material placed around the device, and, second, material left in the buttonhook drift after excavation.

At the time of the explosion, large quantities of lead, iron, and paraffin were present in the shielding block used in the device-performance measurements. Substantial amounts of wood and aluminum also were present.

The postshot presence of silver, bismuth, and zinc, which were not detected in preshot samples, is readily accounted for, as they are common minor impurities in

TABLE 10.—*Semiquantitative spectrographic analysis of insoluble residues of vein material resulting from the Gnome explosion*

[Asterisk indicates slight increase or decrease from amount present in preshot samples (table 8), probably due to analytical error. M, major constituent (greater than 10 percent)]

Element	Percent	Element	Percent
Si	M	Cr	0.005
Al	1.5	Cu	.7
Fe	1.5	Ga	.0015
Mg	M	Li	*0
Ca	.5	Mo	*0
Na	*1.5	Ni	.007
K	*1.0	Pb	M
Ti	.15	Sc	.0005
Mn	.015	Sn	.007
Ag	.003	Sr	.01
B	.05	V	*.005
Ba	.01	Y	.002
Bi	.005	Yb	*.0002
Ce	0	Zn	.07
Co	*.002	Zr	.0007

lead from western smelters. The additional copper could have come either from the vicinity of the device or from a wire fragment left in the buttonhook drift that was unnoticed in the sample. The presence of zinc is harder to explain, but both the zinc and the copper could have been derived from brass fittings around the device. Carbon could have come from vaporized paraffin or wood near the device.

Rawson (1963, p. 133) suggested that the lead was derived from a small number of lead bricks that were placed at one point in the buttonhook drift, and that the carbon was derived from the burning of wood left in the buttonhook drift. Yet it hardly seems possible that the small amount of lead left in the buttonhook drift could have had such wide circumferential distribution from a point source. Wood fragments recovered from the breccia were only slightly scorched—not charred—and much of the wire found in the breccia still had uncharred insulation around it. Bags of salt that were only 90 feet from the shotpoint were found with fragments of the cloth still intact (fig. 11B), and the cloth showed no evidence of charring. Because of the foregoing evidence, it seems unlikely that materials left in the buttonhook drift could have been the source of the lead and carbon.

There are two possible sources for the melted salt in the vein material. The first of these, of course, is salt directly melted by the heat from the blast. The second is salt produced by shock-induced melting from the free-moving salt near the buttonhook drift. The first source seems more plausible because of the presence of elements that must have come from the device chamber. Moreover, the fact that the lead combined with sulfur and chlorine suggests that those elements were provided by vaporized halite and polyhalite near the device, and, as noted above, the organic materials in the breccia do not

appear to have been subjected to heat intense enough to destroy them.

It is postulated, therefore, that the melted salt, as well as the introduced elements, was derived from the vicinity of the device and was injected through fractures that were sealed before any radioactive elements were able to escape. There was no increase in iron content in the postshot rocks. Presumably the iron did not vaporize as early as the other elements[2] and thus was unable to escape.

The lead combined with chlorine from the sodium chloride and with water to form laurionite and with sulfur derived from the sulfate mineral polyhalite to form galena. The presence of the OH radical in the laurionite suggests that the mineral was formed at a temperature less than 142°C, because above that point laurionite breaks down into lead chlorides and lead oxides. Thus, it must have formed approximately in place during retrograde temperature change.

DETAILED DESCRIPTION OF ROCKS IN THE GNOME SHAFT

Section measured in 1961 (preexplosion) by L. M. Gard, Jr., and W. A. Mourant. Color designations are from the Rock-Color Chart (Goddard and others, 1948)

Description	Thickness (ft)	Depth (ft)
Concrete collar	0.8	0.0 – 0.8
Fill (caliche material used to stabilize area)	.5	.8 – 1.3
Alluvial bolson deposits (Quaternary):		
Sand, moderate-brown (5YR 4.5/5), unconsolidated (dune sand); made up of fine to medium subrounded to well-rounded clear and dark-stained quartz grains; contains some quartz crystals with subrounded faces	7.6	1.3 – 8.9
Caliche, white, poorly indurated; contains white calcium carbonate cementing sand like that described above	3.3	8.9 – 12.2
Sand, moderate-brown (5YR 4.5/5), unconsolidated; made up of fine to coarse subrounded to well-rounded clear and stained quartz grains; some quartz crystals have subrounded faces; contains some small grains of calcareous cementing material	30.8	12.2 – 43.0
Total thickness of alluvial bolson deposits	43.0	

[2] See the following table:

	Melting point (°C)	Boiling point (°C)
Iron	1,535	3,000
Tin	231.9	2,270
Silver	960	1,950
Lead	327	1,620
Bismuth	271	1,560±5
Salt	801	1,413
Zinc	419	907

Description	Thickness (ft)	Depth (ft)
Gatuna Formation (Pleistocene(?)):		
Sandstone, moderate-brown (5YR 4.5/5), very fine grained to medium-grained with pebbles as large as 4 mm, partly indurated; made up of subrounded to well-rounded clear and dark-stained quartz grains; has calcareous cement	2.0	43.0 – 45.0
Conglomerate, pale-red (10R 6/2), well-indurated; made up of 20 percent fine to medium sand, 50 percent coarse-grained sand, 30 percent very fine to coarse pebbles of quartzite, limestone, siltstone; has calcareous cement	1.0	45.0 – 46.0
Sandstone, as in 43.0–45.0 ft; contains thin lenses of conglomerate as above	1.7	46.0 – 47.7
Conglomerate, as in 45.0–46.0 ft	.5	47.7 – 48.2
Sandstone, as in 43.0–45.0 ft	.4	48.2 – 48.6
Conglomerate, as in 45.0–46.0 ft	1.3	48.6 – 49.9
Sandstone, as in 43.0–45.0 ft	.6	49.9 – 50.5
Conglomerate, as in 45.0–46.0 ft	.4	50.5 – 50.9
Sandstone, as in 43.0–45.0 ft; contains three lenses (each about 0.05 ft thick) of conglomerate as in 45.0–46.0 ft	2.6	50.9 – 53.5
Conglomerate, as in 45.0–46.0 ft	.6	53.5 – 54.1
Sandstone, as in 43.0–45.0 ft	.6	54.1 – 54.7
Conglomerate, as in 45.0–46.0 ft	.1	54.7 – 54.8
Sandstone, as in 43.0–45.0 ft	.2	54.8 – 55.0
Conglomerate, as in 45.0–46.0 ft	.5	55.0 – 55.5
Sandstone, as in 43.0–45.0 ft	.3	55.5 – 55.8
Conglomerate, as in 45.0–46.0 ft	2.4	55.8 – 58.2
Sandstone, as in 43.0–45.0 ft	2.3	58.2 – 60.5
Conglomerate, as in 45.0–46.0 ft	.8	60.5 – 61.3
Sandstone, as in 43.0–45.0 ft	2.3	61.3 – 63.6
Conglomerate, as in 45.0–46.0 ft	.1	63.6 – 63.7
Sandstone, as in 43.0–45.0 ft	1.8	63.7 – 65.5
Conglomerate, as in 45.0–46.0 ft	.2	65.5 – 65.7
Sandstone, as in 43.0–45.0 ft	.6	65.7 – 66.3
Conglomerate, as in 45.0–46.0 ft	1.8	66.3 – 68.1
Sandstone, as in 43.0–45.0 ft	.7	68.1 – 68.8
Conglomerate, as in 45.0–46.0 ft	.2	68.8 – 69.0
Sandstone, as in 43.0–45.0 ft	3.1	69.0 – 72.1
Conglomerate, as in 45.0–46.0 ft	.1	72.1 – 72.2
Sandstone, as in 43.0–45.0 ft	.6	72.2 – 72.8
Conglomerate, as in 45.0–46.0 ft	.1	72.8 – 72.9
Sandstone, as in 43.0–45.0 ft	.6	72.9 – 73.5
Conglomerate, as in 45.0–46.0 ft	1.3	73.5 – 74.8
Sandstone, as in 43.0–45.0 ft	.5	74.8 – 75.3
Conglomerate, as in 45.0–46.0 ft; contains reworked fragments of red and gray siltstone from Dewey Lake Redbeds	1.0	75.3 – 76.3

Description	Thickness (ft)	Depth (ft)
Gatuna Formation (Pleistocene (?))—Continued		
Sandstone, as in 43.0–45.0 ft; contains reworked fragments of red and gray siltstone from Dewey Lake Redbeds_____	.4	76. 3 – 76. 7
Conglomerate, as in 45.0–46.0 ft; contains reworked fragments of red and gray siltstone from Dewey Lake Redbeds_____	1.7	76. 7 – 78. 4
Clay, pale-reddish-brown (10R 5/4), very hard, dense; contains interwoven black carbonaceous material_____	.1	78. 4 – 78. 5
Sandstone, as in 43.0–45.0 ft__	1.0	78. 5 – 79. 5
Clay, as in 78.4–78.5 ft_____	.1	79. 5 – 79. 6
Sandstone, as in 43.0–45.0 ft__	1.0	79. 6 – 80. 6
Clay, as in 78.4–78.5 ft_____	.05	80. 6 – 80. 65
Sandstone, as in 43.0–45.0 ft__	.75	80. 65– 81. 4
Sandstone, as in 43.0–45.0 ft; contains many thin lenses of clay (about 0.01 ft. thick) as described in 78.4–78.5 ft____	4.1	81. 4 – 85. 5
Sand, pale-reddish-brown (10R 5/4), very fine grained to coarse-grained, sub-rounded to well-rounded, unconsolidated; contains a few large yellow-green quartz pebbles and clear and stained quartz grains, a few quartz crystals with sub-rounded faces, some small grains of calcareous cementing material, and reworked fragments of Dewey Lake Redbeds_____	6.4	85. 5 – 91. 9
Total thickness of Gatuna Formation_____	48. 9	
Unconformity.		
Dewey Lake Redbeds (Upper Permian):		
Siltstone, sandy, pale-reddish-brown (10R 5/4), well-indurated; contains light-greenish-gray (5GY 8/1), reduction spots and fine silt; calcite crystals and clusters dispersed throughout rock; has calcareous cement_____	1.7	91. 9 – 93. 6
Siltstone, as above except contains some clayey layers_____	3.7	93. 6 – 97. 3
Clay, pale-reddish-brown (10R 5/4), very dense; contains interspresed black carbon spots, and silty streaks containing reduction spots__	.1	97. 3 – 97. 4
Siltstone, as in 91.9–93.6 ft____	4.6	97. 4 – 102. 0
Siltstone, light-greenish-gray (5GY 8/1), fine-grained, well-indurated; contains calcite crystals in clusters and interspersed throughout rock; has calcareous cement_	.4	102. 0 – 102. 4
Siltstone, as in 91.9–93.6 ft____	3.6	102. 4 – 106. 0
Siltstone, as above but darker and finer grained; contains lenses of white very fine grained sandstone_____	.7	106. 0 – 106. 7
Siltstone, as in 91.9–93.6 ft____	4.3	106. 7 – 111. 0
Siltstone, as in 91.9–93.6 ft. but contains thin wavy bands of gray siltstone which extend around shaft_____	1.1	111. 0 – 112. 1

Description	Thickness (ft)	Depth (ft)
Dewey Lake Redbeds (Upper Permian)—Continued		
Siltstone, pale-reddish-brown (10R 5/4), well-indurated, mostly thin-bedded; contains light-greenish-gray (5GY 8/1) reduction spots; calcite crystals in clusters dispersed throughout rock and fill joints; contains thin bands of clay or clayey material and black spots of manganese or oil(?) in joints and porous strata; has calcareous cement_____	10. 5	112. 1 – 122. 6
Siltstone, same as above but contains thin lenses of sandstone_____	8. 1	122. 6 – 130. 7
Siltstone, as in 102.0–102.4 ft__	.4	130. 7 – 131. 1
Siltstone, as in 122.6–130.7 ft; contains 0.5-ft-thick layers of siltstone as in 102.0–102.4 ft_____	13. 9	131. 1 – 145. 0
Siltstone, same as above; contains 1-mm-thick bands of selenite crystals_____	8. 0	145. 0 – 153. 0
Siltstone, sandy, pale-reddish-brown (10R 5/4), well-indurated to very friable; contains light-greenish-gray (5GY 8/1) reduction spots and thin layers; sand grains well rounded; has calcareous cement_____	16. 0–	153. 0 – 169. 0
Siltstone, as in 112.1–122.6 ft; jointing in interval 169–133 ft, as follows: Strike N. 70° W., dip 75° N.; strike N. 20° W., dip approximately 85° E.; bedding strikes N. 45° E., dips 4° NW; reduction spots in vertical zone tapering from 8 to 0 in.; apparently following fractures; from 175 to 178 ft, some reduction spots 1 ft in diameter; joints at 200 ft strike N. 30° W., dip 70° NE.; joints at 216 ft strike N. 90° E., dip 75° N.; calcite fills veins; joints at 278–284 ft strike N. 30° W., dip 50° N. to vertical_____	125. 0	169. 0 – 294. 0
Total thickness of Dewey Lake Redbeds_____	202. 1	
Unconformity.		
Rustler Formation (Upper Permian):		
Forty-niner Member:		
Gypsum rock, white (N 9) to olive-gray (5Y 5/1); crystals 1–5 mm long; upper contact, with the Dewey Lake Redbeds at 294 ft, undulating and marked by green clay seam about 0.5 in. thick underlain by gray clay layer about 0.06 in. thick between red beds and white gypsum; gypsum grades into anhydrite from 298 to 300 ft with no definite contact, either laterally or vertically_____	6. 0	294. 0 – 300. 0

Description	Thickness (ft)	Depth (ft)
Rustler Formation (Upper Permian)—Continued		
Forty-niner Member—Continued		
Anhydrite rock, olive-gray (5Y 5/1), massive, crystalline; contains some gypsum crystals; grades into gypsum above and below; white and pink fibrous gypsum and many fractures present at 315 ft; slickensides present at 316 ft	22.0	300.0 – 322.0
Gypsum rock, white (N 9) to olive-gray (5Y 5/1), massive, crystalline; contains white and pink fibrous gypsum at 325 ft and white and gray bands throughout	6.5	322.0 – 328.4
Siltstone, greenish-gray (5GY 7/1); well-indurated; has calcareous cement	.2	328.4 – 328.6
Siltstone, sandy, pale-reddish-brown (10R 5/4), well-indurated to friable; contains some brecciated layers, fragments of gypsum, and light-greenish-gray reduction spots; has mostly calcareous cement; some clay lenses	11.0	328.6 – 339.6
Gypsum, breccia, grayish-red (10R 4/2) well-indurated; contains 1- to 2-cm long fragments of clear, red, and gray gypsum and fragments of gray and red siltstone; has calcareous cement	1.0	339.6 – 340.6
Gypsum rock, banded, pinkish-gray (5YR 8/1) and pale-red (10R 6/2), massive, crystalline; gradational with breccia above; red bands appear to be stylolitic; some patches of anhydrite grade into gypsum in lower 10 ft; lower 6 ft has 1-cm-thick fibrous veins of white gypsum approximately parallel to the bedding and about 5 cm apart; gypsum breccia at 359 ft	20.7	340.6 – 361.3
Total thickness of Forty-niner Member	67.3	
Magenta Member:		
Dolomite rock, red-purple (magenta) (5RP 5/2), massive; contains white 1-mm-thick bands of selenite about 1 cm apart and scattered crystals of selenite in dolomite; cement dolomitic or calcareous; has fractures 1–5 cm wide filled with selenite	6.8	361.3 – 368.1
Siltstone, light-brownish-gray (5YR 6/1) to moderate-red (5Y 5/4); layers of siltstone alternate with irregular bands of selenite; has dolomitic or calcareous cement; beds range from paper thin to 0.5 ft thick	3.6	368.1 – 371.7
Rustler Formation (Upper Permian)—Continued		
Magenta Member—Continued		
Dolomite rock, silty, gypsiferous, pale-red (5R 6/2) to light-gray (N 7), thin-bedded; contains 1-mm to 1-cm-thick wavy bands of fibrous gypsum parallel to bedding; has wavy botryoidal bedding in lower 6 ft; joints strike N. 90° E., dip 84° N., and strike N. 10° E., dip 84° W.; bedding strikes north, dips 7° E; cluster of black manganese(?) in red and colorless fibrous gypsum at 379 ft	10.5	371.7 – 382.2
Total thickness of Magenta Member	20.9	
Tamarisk Member:		
Anhydrite rock and gypsum rock, pale-red (10R 6/2) to light-olive-gray (5Y 6/1); contains 1-cm-thick bands of fibrous gypsum parallel to bedding; anhydrite grades into gypsum; some small irregular masses of gypsum throughout massive anhydrite rock microcrystalline; 1-cm-thick red clay layer at 403.5 ft in north wall of shaft; joint sets at 410–416 ft: strike N. 5° W., dip 75° W.; strike N. 25° E., dip 55° SE.; strike N. 90° E., dip 65° N.; strike N. 25° E., dip 55° NW.; joints cemented with selenite; joints at 432–438 ft strike N. 20° W. and dip 45° NE	66.3	382.2 – 448.5
Clay, brownish-black (5YR 2/1); plastic, slickensided; contains irregular fragments of fibrous gypsum; thickness ranges from 0.01 to 0.2 ft; dips 36° N. in shaft; this layer is at 440.5 ft in south wall	.1	448.5 – 448.6
Anhydrite rock and gypsum rock, light-olive-gray (5Y 6/1); anhydrite and gypsum intergrade; massive anhydrite rock microcrystalline; contains large masses of fibrous and tabular gypsum; joint system strikes N. 55° E., dips 70° N.; folds in gypsum at 472–477 ft; a few thin gray plastic clay seams in gypsum at 477–480 ft	31.4	448.6 – 480.0
Clay, plastic, grayish-red (10R 4/2); interbedded gypsum fragments and crystals; selenite veins fill joints and occur along bedding; some cement grout in with selenite and clay; a few gray plastic clay seams at 484 ft; ground water seeps through wall, that has no visible openings	5.0	480.0 – 485.0

Description	Thickness (ft)	Depth (ft)
Rustler Formation (Upper Permian)—Continued		
Tamarisk Member—Continued		
Anhydrite rock and gypsum rock, light-olive-gray (5Y 6/1), banded; 2-in.-thick gray clay seam at 489 ft; contains thin bands of selenite	10.5	485.0 – 495.5
Total thickness of Tamarisk Member	113.3	
Culebra Dolomite Member:		
Dolomite rock, dark-yellowish-brown (10YR 4/2), vesicular and vuggy, well-indurated; openings contain calcite crystals	.5	495.5 – 496.0
Dolomite rock, yellowish-gray (5Y 8/1), microcrystalline, highly fractured, few vugs, poorly indurated	3.3	496.0 – 499.3
Dolomite rock, yellowish-gray (5Y 8/1), microcrystalline; contains brecciated zones, some of which fill vertical fractures; breccia recemented with pale-yellowish-brown (10YR 6/2) dolomite, mostly well indurated; contains zones of vesicular or "worm-eaten" dolomite, some of which are highly fractured; cement and chemical grout fill some openings; most vesicles spherical and range in diameter from a pinhead to about 1 inch; most openings not interconnected; some massive zones do not contain any openings	24.2	499.3 – 523.5
Total thickness of Culebra Dolomite Member	28.0	
Lower member:		
Siltstone, medium-dark-gray (N 4), clayey, semiplastic; contains dolomite fragments from overlying unit	1.7	523.5 – 525.2
Clay, grayish-red (10R 4/2), very plastic; contains fragments and large breccia blocks from overlying units and grout; gypsum fragments mixed through the clay, and this mixture fills many openings in the dolomite; selenite band 0.5 in. thick at 527–530 ft	9.3	525.2 – 534.5
Gypsum rock and anhydrite rock, light-olive-gray (5Y 6/1), crystalline, massive; contains a few silty layers; some platy gypsum; beds strike N. 60° E., dip 16° NW.; joints strike N. 30° W., dip 86° S. at 541 ft; gray clay on south wall at 547 ft; beds strike N. 45° E., dip 10° NW. at 541–549 ft	13.1	534.5 – 547.6
Rustler Formation (Upper Permian)—Continued		
Lower member—Continued		
Claystone, grayish-red (10R 4/2) and light-gray (N 7), plastic; contains alternating layers of red and gray and gypsum bands and gypsum nodules; gray claystone very plastic and in irregular bands in red claystone; has some reduction zones; claystone absorbs water readily	11.5	547.6 – 559.1
Gypsum rock and anhydrite rock, as in 534.5–547.6 ft	3.9	559.1 – 563.0
Claystone, silty, moderate-reddish-brown (10R 4/6), poorly indurated; contact irregular, dips NW	3.0	563.0 – 565.0
Siltstone, clayey, sandy, grayish-red (10R 4/2); contains alternate discontinuous bands of light-olive-gray (5Y 6/1) gypsum; siltstone contains small selenite crystals and blebs of gypsum; no jointing obvious, bedding dips about 10° NW.; lens of gypsum and anhydrite 4 ft long and 1 ft thick at 564 ft in northwest wall	6.0	565.0 – 571.0
Gypsum rock, olive-gray (5Y 4/1), massive, crystalline, banded; beds dip about 10°–15° NW. in most of shaft but dip as much as 42° NW. in northwest wall	1.0	571.0 – 572.0
Siltstone, clayey, dark-reddish-brown (10R 3/4) and greenish-gray (5GY 5/1), laminated, noncalcareous; contains alternating layers of brown and gray; unconsolidated except for some partly consolidated lenses about 0.5 ft thick; more plastic from 577 to 579 ft; bedding dips northwest; sides of shaft spall off	20.0	572.0 – 592.0
Siltstone, clayey, sandy, olive-gray (5Y 5/1), very fine grained, poorly indurated, friable; contains blebs of gypsum crystals; shows crenulated wavy bedding, tends to spall off wall in some zones; a few zones fairly well indurated; rock predominantly angular to subrounded silt-size quartz but contains about 1 percent mafic minerals; rock disaggregates with effervescence in dilute HCl; bottom 2 ft of this unit fairly well indurated	59.2	592.0 – 651.2
Total thickness of lower member	127.7	
Total thickness of Rustler Formation	357.2	

Description	Thickness (ft)	Depth (ft)
Salado Formation (Upper Permian): Contact with Rustler Formation unconformable and very irregular. Top of Salado at 647.5 ft at southeast wall of shaft and at 660.0 ft at west wall of shaft.		
Claystone breccia, grayish-red (10R 4/2 to 5/2); contains angular and subrounded fragments and blocks of gray siltstone, gypsum, and polyhalite ranging from sand size to 3 ft; contains discontinuous beds of gypsum and veins of fibrous gypsum; has zones of plastic red clay at 680–684 ft that taste salty	36.0	651.2 – 687.2
Claystone, medium-gray (N 5), plastic; contains abundant fragments and veins of colorless crystalline gypsum or selenite	.4	687.2 – 687.6
Polyhalite rock, dark-reddish-brown (10R 3/4), crystalline, massive, platy; strikes N. 50° E., dip 18° NW	.9	687.6 – 688.5
Siltstone, clayey, sandy, grayish-red (10R 4/2), calcareous; contains fragments of colorless crystalline gypsum	.3	688.5 – 688.8
Claystone, plastic, poorly indurated; consists of very thin bands of dark-gray and grayish-red claystone containing veins and fragments of colorless crystalline gypsum	.4	688.8 – 689.2
Siltstone, clayey, grayish-red (10R 5/2), calcareous; contains small amount of tiny fragments of clear gypsum and fragments of polyhalite	4.3	689.2 – 693.5
Gypsum rock, very pale orange (10YR 8/2) to light-brown (5YR 6/4), massive, microcrystalline; shows irregular stains of light-brown clay	.5	693.5 – 694.0
Anhydrite rock, olive-gray (5Y 5/1), microcrystalline, massive	12.0	694.0 – 706.0
Claystone, medium-dark-gray (N 4), plastic; contains poorly indurated blocks of anhydrite	2.0	706.0 – 708.0
Anhydrite rock, olive-gray (5Y 4/1), massive microcrystalline; shows conchoidal fracture; bedding dips 5° NW	1.2	708.0 – 709.2
Claystone, light-gray (N 7), banded, well-indurated; probably alteration product of anhydrite above; interbedded with halite below	.1	709.2 – 709.3
Halite rock, colorless to white; contains small blebs of moderate-reddish-orange (10R 6/7) halite and less than 1 percent gray clay	1.7	709.3 – 711.0
Halite rock, colorless to white; contains less than 1 percent small blebs of moderate-red (5R 4/6) clay	4.5	711.0 – 715.5
Claystone, pale-reddish-brown (10R 5/4) and light-gray (N 7); dips west at less than 1°; contains about 25 percent halite	.5	715.5 – 716.0
Salado Formation (Upper Permian)—Continued		
Halite rock; contains about 50 percent dark-reddish-brown (10R 3/4) clay	3.5	716.0 – 719.5
Halite rock; contains about 10 percent medium-light-gray (N 6) clay	1.5	719.5 – 721.0
Halite rock, colorless to white	1.7	721.0 – 722.7
Halite rock; contains about 5 percent medium-light-gray (N 6) clay; has irregular band of dark-reddish-brown (10R 3/4) clay at top which ranges from 0 to 1 ft thick	2.5	722.7 – 725.2
Claystone, plastic, dark-reddish-brown (10R 4/4) and medium-gray (N 5)	.4	725.2 – 725.6
Halite rock, colorless; contains about 5 percent medium-gray (N 5) clay	1.9	725.6 – 727.5
Halite rock, colorless; contains blebs and spots of reddish-orange (10R 6/7) halite; contains less than 2 percent medium-gray (N 5) clay	3.8	727.5 – 731.3
Claystone, medium-dark-gray (N 4); irregular in thickness	.2	731.3 – 731.5
Halite, colorless to white; contains some blebs of reddish-orange halite; thin discontinuous clay layer in lower 1 ft; clay content less than 1 percent	9.7	731.5 – 741.2
Polyhalite rock, orange	.7	741.2 – 741.9
Halite rock, reddish-orange (10R 6/7) to transparent white; at 742.6 ft contains 1.2-ft-thick reddish-brown clay layer	6.0	741.9 – 747.9
Halite rock, 5–10 percent reddish-brown clay; upper 2 ft contains 50 percent brown clay; unit contains several thin discontinuous clay seams and stringers and blebs of moderate-reddish-orange (10R 5/6) polyhalite	13.1	747.9 – 761.0
Halite rock; contains medium-gray clay band 0.1 ft thick at 762.0 ft, and dark-reddish-brown clay band 0.3 ft thick at 763.3 ft; above gray clay band is a double band of polyhalite separated by transparent colorless halite 0.2 ft thick (marker horizon(?))	5.0	761.0 – 766.0
Halite rock, transparent colorless; contains three bands of thin moderate-orange-pink (10R 7/4) polyhalite	.9	766.0 – 766.9
Halite rock, colorless transparent to white; contains blebs of moderate-orange-pink halite	2.3	766.9 – 769.2
Polyhalite rock, moderate-orange-pink (10R 7/4); contains 0.2-in.-thick band of halite in middle	.3	769.2 – 769.5
Halite rock, white; contains less than 1 percent moderate-gray clay; some polyhalite blebs and stringers scattered throughout lower half	4.1	769.5 – 773.6
Claystone, dark-reddish-brown (10R 3/4), plastic; contains scattered crystals of halite; 0.5-in.-thick gray layer at top	1.2	773.6 – 774.8

Description	Thickness (ft)	Depth (ft)
Salado Formation (Upper Permian)—Continued		
Halite rock; contains about 20 percent dark-reddish-brown clay; grades into overlying unit; irregular and discontinuous polyhalite band at 776.6 ft that averages 0.2 ft thick	6.3	774.8 – 781.1
Claystone, dark-reddish-brown (10R 3/4); dips less than 1° NW	.1	781.1 – 781.2
Halite rock; contains about 35 percent dark-reddish-brown clay in blebs and discontinuous bands; contains about 2 percent polyhalite in blebs	4.4	781.2 – 785.6
Polyhalite rock about 0.1 ft thick overlying 0.1 ft of gray anhydrite rock	.2	785.6 – 785.8
Halite rock; contains about 10–20 percent polyhalite in blebs and stringers and about 5 percent gray clay	9.7	785.8 – 795.5
Polyhalite rock; moderate-orange-pink (10R 7,4); contains 1-mm-thick discontinuous dark-gray clay band in middle	1.4	795.5 – 796.9
Claystone, medium-light-gray (N 6); contains about 20 percent halite	.3	796.9 – 797.2
Halite rock, moderate-reddish-orange (10R 6 6); contains about 20 percent gray clay	.8	797.2 – 798.0
Claystone, dark-reddish-brown; contains about 50 percent halite	6.0	798.0 – 804.0
Halite rock; upper 5 ft contains about 10–20 percent gray clay in blebs; lower 6 ft contains about 2 percent polyhalite in discontinuous stringers and blebs	9.3	804.0 – 813.3
Halite rock; contains about 20 percent polyhalite in blebs, stringers, and irregular masses	5.2	813.3 – 818.5
Claystone, medium-dark-gray (N 4) to medium-light-gray (N 6); contains about 25 percent halite	2.1	818.5 – 820.6
Claystone, same as next higher unit but contains about 10 percent polyhalite	2.0	820.6 – 822.6
Anhydrite rock, yellowish-gray (5Y 8/1), banded, vuggy; contains about 5 percent halite; some polyhalite blebs at top	2.4	822.6 – 825.0
Anhydrite rock, banded with gypsum and halite; gypsum and halite are dusky yellow (5Y 6/4); anhydrite is light gray (N 7); in other walls of shaft, more than 1 ft of polyhalite underlies this unit, but it pinches out and is absent from north wall	2.5	825.0 – 827.5
Claystone, medium-gray (N 5), plastic	.5	827.5 – 828.0
Halite rock, transparent, colorless; contains about 5 percent gray clay in blebs and about 2 percent polyhalite	3.3	828.0 – 831.3
Anhydrite rock, light-gray (N 7)	.2	831.3 – 831.5
Halite rock; contains about 20 percent polyhalite that occurs in discontinuous bands	1.5	831.5 – 833.0

Description	Thickness (ft)	Depth (ft)
Salado Formation (Upper Permian)—Continued		
Anhydrite rock, very light gray (N 8); banded upper foot contains some halite and polyhalite in discontinuous bands 0.8 ft thick	2.5	833.0 – 835.5
Halite rock, colorless to white; contains about 1 percent polyhalite in blebs and one band of anhydrite 1 in. thick	1.3	835.5 – 836.8
Anhydrite rock, very light gray (N 8), microcrystalline	.4	836.8 – 837.2
Halite rock; contains a 1-mm-thick band of anhydrite and more than 1 percent gray clay in blebs	.8	837.2 – 838.0
Anhydrite rock, very light gray (N 8), laminated; at 839.2–838.4 ft, contains breccia layer consisting of anhydrite fragments in clay matrix; at 839.8–840.1 ft, contains band of moderate-orange-pink (10R 7/4) to white halite; basal 0.3 ft contains gray clay and orange-pink halite	6.3	838.0 – 844.3
Halite, rock transparent, colorless; contains about 1 percent gray clay blebs	6.9	844.3 – 851.2
Claystone, medium-dark-gray (N 4); contains 2-mm-thick discontinuous bands of halite	.7	851.2 – 851.9
Halite rock, transparent, colorless to moderate-orange-pink; contains about 20 percent medium-gray (N 5) and dark-reddish-brown (10R 3/4) clay in blebs and 5 percent moderate-orange-pink (10R 7/4) polyhalite	1.1	851.9 – 853.0
Halite rock, transparent, colorless to white; contains about 5 percent polyhalite in blebs	1.9	853.0 – 854.9
Halite rock; contains about 30–50 percent dark-reddish-brown (10R 3/4) clay	1.5	854.9 – 856.4
Halite rock, transparent, colorless to white; contains about 10 percent greenish-gray (5GY 6/1) clay in blebs and 1 percent polyhalite in blebs	5.3	856.4 – 861.7
Halite rock, transparent, colorless to white; contains about 2 percent medium-gray (N 5) clay and less than 1 percent polyhalite, both in blebs; separated from overlying unit by distinct change in amount of clay	5.6	861.7 – 867.3
Halite rock, white; contains about 5 percent medium-gray (N 5) clay and about 1 percent polyhalite in blebs; drill holes in sump at 874 ft have gas bubbling up	9.4	867.3 – 876.7
Polyhalite rock, moderate-reddish-orange (10R 6/6); contains about 25 percent halite	1.8	876.7 – 878.5
Claystone, light-gray (N 7); contains about 50 percent halite	1.5	878.5 – 880.0
Claystone, dark-reddish-brown (10R 3/4); contains about 25 percent halite	1.5	880.0 – 881.5

Description	Thickness (ft)	Depth (ft)
Salado Formation (Upper Permian)—Continued		
Halite rock, colorless to orange; contains about 40 percent clay, both grayish red (10R 4/2) and greenish gray (5GY 6/1), and about 5 percent polyhalite in blebs	5.0	881.5 – 886.5
Polyhalite rock, moderate-reddish-orange (10R 6/6)	1.0	886.5 – 887.5
Halite rock, white to moderate-orange; upper foot contains about 5 percent light-gray (N 7) clay; remainder contains less than 1 percent clay; a discontinuous polyhalite bed at 895.5 ft averages 2 in. thick	10.0	887.5 – 897.5
Polyhalite rock, grayish-orange-pink (10R 8/2)	.3	897.5 – 897.8
Halite rock, white; contains about 10 percent medium-gray (N 5) clay	.7	897.8 – 898.5
Halite rock, moderate-reddish-orange (10R 6/6); contains 1 percent polyhalite in blebs near base	2.3	898.5 – 900.8
Halite rock, moderate-reddish-orange (10R 6/6); contains about 25 percent medium-gray (N 5) clay in bands; has 2-in.-thick band of dark-reddish-brown (10R 3/4) clay at base	1.5	900.8 – 902.3
Halite rock, transparent, colorless; contains about 30 percent dark-reddish-brown (10R 3/4) clay	1.7	902.3 – 904.0
Halite rock, white; contains about 10 percent greenish-gray (5GY 6/1) clay in blebs and bands; contains about 1 percent polyhalite in blebs	8.1	904.0 – 912.1
Halite rock, clear; contains about 25 percent medium-light-gray (N 6) clay	.6	912.1 – 912.7
Halite rock, transparent, colorless to moderate-orange-pink (10R 7/4); contains discontinuous 1-in.-thick bands of polyhalite	2.0	912.7 – 914.7
Polyhalite rock, moderate-reddish-orange (10R 6/6); contains irregular discontinuous bands of transparent, colorless halite	.7	914.7 – 915.4
Claystone, medium-light-gray (N 6); thickness ranges from featheredge to 0.2 ft	.2	915.4 – 915.6
Halite rock; contains about 2 percent gray clay and about 1 percent polyhalite in blebs	4.2	915.6 – 919.8
Halite rock; contains about 20 percent of both gray and reddish-brown clay and about 10 percent polyhalite; 0.2-ft-thick bed of polyhalite present at 920 ft	1.2	919.8 – 921.0
Halite rock; contains about 5 percent gray clay in blebs and about 2 percent polyhalite in blebs	6.6	921.0 – 927.6
Halite rock; contains about 10 percent polyhalite in blebs and bands; bottom 1 foot contains about 50 percent polyhalite in alternating bands with halite	3.9	927.6 – 931.5
Salado Formation (Upper Permian)—Continued		
Claystone, dark-reddish-brown (10R 3/4); contains about 40 percent halite	1.5	931.5 – 933.0
Halite rock; contains about 10 percent medium-gray (N 5) clay and about 5 percent polyhalite in blebs and discontinuous layers	10.2	933.0 – 943.2
Polyhalite rock in layers 0.1–0.3 ft thick alternating with halite	1.8	943.2 – 945.0
Halite rock, white; contains less than 1 percent polyhalite in blebs	2.5	945.0 – 947.5
Halite rock, moderate-reddish-orange (10R 6/6); appears to be layered in about 0.5-ft-thick layers owing to variations in color; contains thin (1 mm) bands of white opaque halite; becomes darker orange near base	8.0	947.5 – 955.5
Polyhalite rock; lower half contains thin (2 mm) bands of clay	1.0	955.5 – 956.5
Halite rock; contains about 1 percent polyhalite in blebs; contains about 5 percent gray clay from 960 to 960.7 ft	2.5	956.5 – 959.0
Claystone, medium-dark-gray (N 4); contains about 50 percent halite	1.0	959.0 – 960.0
Claystone, dark-reddish-brown (10R 3/4); contains about 50 percent halite	3.0	960.0 – 963.0
Halite rock; contains about 20 percent dark-reddish-brown (10R 3/4) clay and about 5 percent polyhalite in blebs	1.0	963.0 – 964.0
Halite rock; contains about 25 percent polyhalite	1.5	964.0 – 965.5
Anhydrite rock, yellowish-gray (5Y 8/1), dense, fine-grained; contains crystalline grayish-orange (10YR 7/4) anhydrite	1.5	965.0 – 967.0
Halite rock, transparent, colorless to white; contains 0.1- to 0.2-ft-thick bands of polyhalite separated by 0.2- to 1-ft-thick layers of halite	5.7	967.0 – 972.7
Polyhalite rock, moderate-reddish-orange (10R 6/6)	.4	972.7 – 973.1
Anhydrite rock, yellowish-gray (5Y 8/1), banded in 0.5-in.-thick layers	.9	973.1 – 974.0
Halite rock, colorless to white; contains about 10–20 percent polyhalite in blebs and thin layers, and about 2 percent gray clay in blebs; 0.2-ft-thick discontinuous layer of polyhalite present at 981.5 ft	11.2	974.0 – 985.2
Halite rock; contains about 10 percent medium-dark-gray (N 4) clay and 1 percent polyhalite; has 0.2-ft-thick bed of medium-dark-gray clay at base	1.4	985.2 – 986.6
Halite rock; contains about 50 percent dark-reddish-brown (10R 4/6) clay	3.4	986.6 – 990.0
Halite rock; contains thin bands of polyhalite	2.8	990.0 – 992.8

Description	Thickness (ft)	Depth (ft)
Salado Formation (Upper Permian)—Continued		
Polyhalite rock, moderate-red (5R 5/4)	0.1	992.8 – 992.9
Halite rock, transparent, colorless; contains about 10–15 percent greenish-gray (5G 6/1) clay in irregular layers and about 2 percent polyhalite in blebs; halite coarsely crystalline, occurring as 1-in. crystals	7.6	992.9 –1,000.5
Halite rock, white to colorless, transparent; contains less than 1 percent polyhalite in thin irregular streaks	2.5	1,000.5 –1,003.0
Polyhalite rock, grayish-orange-pink (YR 7/2), banded; from 1,003 to 1,004 ft consists mainly of polyhalite and halite with some anhydrite bands; anhydrite is microcrystalline and spalls and shatters when struck. One joint set strikes N. 50° E., dips 65° NW.; another set is normal to this; joints spaced about 0.5 ft apart	4.0	1,003.0 –1,007.0
Anhydrite rock, light-olive-gray (5Y 6/1), banded in ¼-in.-thick bands; basal 0.5 ft contains medium-gray clay (N 5) and gypsum	2.2	1,007.0 –1,009.2
Halite rock, transparent, colorless to moderate-reddish-orange; contains about 2 percent polyhalite in blebs	3.1	1,009.2 –1,012.3
Polyhalite rock, pale-reddish-brown (10R 5/4); contains several thin gray clay seams	1.7	1,012.3 –1,014.0
Halite rock, medium-light-gray (N 6); contains about 10 percent clay	.9	1,014.0 –1,014.9
Halite rock; in alternating white and pale-yellowish-orange (10YR 8/6) bands 0.2–0.3 ft thick	5.9	1,014.9 –1,020.8
Halite rock; alternates with irregular bands of silty dark-reddish-brown (10R 3/4) clay; contains about 50 percent clay; contains 2 percent polyhalite in blebs near top of unit	3.5	1,020.8 –1,024.3
Siltstone, clayey, pale-reddish-brown (10R 5/4); contains light-gray (N 7) clay blebs. (With subjacent unit is Vaca Triste Sandstone Member of Adams (1944).)	2.0	1,024.3 –1,026.3
Siltstone, clayey, pale-reddish-brown (10R 5/4); contains about 50 percent halite	2.7	1,026.3 –1,029.0
Halite rock; top 3 ft contains about 40 percent dark-reddish-brown (10R 3/4) clay; basal 2 ft contains about 5 percent polyhalite in blebs and stringers	5.7	1,029.0 –1,034.7
Halite rock; contains about 20 percent light-gray (N 7) clay	1.4	1,034.7 –1,036.1
Halite rock, transparent, colorless; contains about 10 percent polyhalite in irregular layers and blebs	3.5	1,036.1 –1,039.6
Salado Formation (Upper Permian)—Continued		
Halite rock; contains about 10 percent light-gray (N 7) clay in irregular thin bands and blebs	0.9	1,039.6 –1,040.5
Halite rock, transparent, colorless; contains about 5 percent polyhalite in irregular horizontal stringers and blebs; contains 1-cm-thick band of light-gray (N 7) clay at 1,043.3 ft	4.0	1,040.5 –1,044.5
Claystone, light-gray (N 7); contains about 50 percent halite; has 0.1-ft-thick layer of dark-reddish-brown (10R 3/4) clay at base	2.1	1,044.5 –1,046.6
Halite rock, white to colorless, transparent; contains about 10 percent polyhalite in blebs; irregular clayey zone present at 1,057 ft; interval 1,053–1,057 ft contains about 2 percent polyhalite in discontinuous layers; irregular band of gray clay at base averages 0.05 ft thick	10.4	1,046.6 –1,057.0
Claystone, dark-reddish-brown (10R 3/4); contains about 30–40 percent halite; discontinuous gray clay layers at top	2.0	1,057.0 –1,059.0
Halite rock, white to colorless; contains about 1 percent polyhalite in blebs and thin bands and about 10–20 percent of both red and gray clay in irregular bands and disseminated blebs; layer at 1,061–1,063 ft contains about 40 percent clay; unit contains gas under pressure	5.3	1,059.0 –1,064.3
Polyhalite rock; underlain by 0.5 in. light-gray (N 7) clay	.2	1,064.3 –1,064.5
Halite rock; contains about 5 percent polyhalite in stringers and blebs	2.8	1,064.5 –1,067.3
Claystone, pale-red (10R 6/2); top 0.2 ft light-gray (N 7) clay; unit contains about 5 percent halite; gas present in this unit	3.7	1,067.3 –1,071.0
Halite rock, white to colorless; contains less than 1 percent polyhalite in blebs and less than 1 percent red clay in blebs	3.5	1,071.0 –1,074.5
Halite rock, transparent, colorless; contains about 5 percent polyhalite in irregular discontinuous bands; contains a few 2-mm-thick layers of brown clay at 1,078–1,083.4 ft	9.0	1,074.5 –1,083.5
Halite rock; contains about 25 percent medium-light-gray (N 6) clay	.9	1,083.5 –1,084.4
Halite rock; contains about 40 percent pale-reddish-brown (10R 5/4) clay; basal contact irregular	4.6	1,084.4 –1,089.0
Halite rock; contains about 10 percent polyhalite in irregular horizontal bands about 1 in. thick; upper part of unit contains vertical stringers of medium-gray (N 5) clay	7.0	1,089.0 –1,096.0

| Description	Thickness (ft)	Depth (ft)
Salado Formation (Upper Permian—Continued)		
Polyhalite rock; upper half contains about 10 percent halite in blebs	1.0	1,096.0 –1,097.0
Polyhalite rock, banded; 0.2-ft-thick medium-gray (N 5) clay layer at base	1.6	1,097.0 –1,098.6
Halite rock, colorless to white; contains less than 1 percent polyhalite in blebs and less than 1 percent gray clay in blebs	11.7	1,098.6 –1,110.3
Halite rock; contains about 30–50 percent pale-reddish-brown (10R 5/4) clay, and contains about 1 percent polyhalite in blebs near top; clay in top and bottom 1 foot is gray	5.2	1,110.3 –1,115.5
Halite rock, colorless to white; contains 10–20 percent stringers and blebs of polyhalite; 0.1-ft-thick layer of polyhalite underlain by 0.05-ft-thick layer of gray clay at base	1.9	1,115.5 –1,117.4
Halite rock; contains about 25 percent medium-light-gray (N 6) clay in upper part; basal 2 ft contains no clay	2.9	1,117.4 –1,120.3
Anhydrite rock; in alternating grayish-orange (10YR 7/4) and very light gray (N 8) bands; contains scattered blebs and lenses of polyhalite and halite; 0.2-ft-thick gray clay layer at base	3.9	1,120.3 –1,124.2
Halite rock, colorless to moderate-reddish-orange (10R 6/6); contains a band of grayish-orange-pink (5YR 7/2) anhydrite from 1,125.5 to 1,125.8 ft; contains gas	3.1	1,124.2 –1,127.3
Polyhalite rock, banded, grayish-orange-pink (5YR 7/2); 0.05 ft of gray clay at base	.5	1,127.3 –1,127.8
Halite rock, in alternating white and moderate-reddish-orange (10R 6/6) bands; contains discontinuous clayey zones near top and base	3.0	1,127.8 –1,130.8
Claystone, grayish-red (10R 4/2); contains about 30 percent halite; 0.05-ft-thick layer of gray clay at top; contains irregular bands of polyhalite and halite in interval 1,131.2–1,131.8 ft	4.0	1,130.8 –1,134.8
Halite rock; contains about 50 percent polyhalite and about 10 percent gray clay	1.0	1,134.8 –1,135.8
Claystone, greenish-gray (5GY 6/1); contains about 50 percent halite, and inclusions of grayish-red (10R 4/2) clay; lower contact gradational	2.0	1,135.8 –1,137.8
Halite rock, transparent colorless; contains vaguely defined bands of moderate-reddish-orange (10R 6/5) halite and 2- to 4-mm-thick bands of anhydrite in the lower half	18.2	1,137.8 –1,156.0
Salado Formation (Upper Permian—Continued)		
Polyhalite rock, moderate-reddish-brown (10R 4/6); contains several plastic medium-gray (N 5) clay layers 2–5 mm thick; contains lenses of halite. (Marker bed 119)	1.0	1,156.0 –1,157.0
Claystone, medium-gray (N 5); irregular in thickness	.7	1,157.0 –1,157.7
Halite rock, moderate-reddish-orange (10R 6/5); contains about 10 percent polyhalite in blebs, and about 5 percent gray clay in layers	2.3	1,157.7 –1,160.0
Claystone, medium-gray (N 5); contains about 30–50 percent halite and about 2 percent polyhalite near base	8.0	1,160.0 –1,168.0
Halite rock, transparent, colorless; contains about 2 percent gray clay in blebs and 2 percent polyhalite in blebs; at 1,170.0 ft is moderate reddish orange (10R 6/6)	8.5	1,168.0 –1,176.5
Polyhalite rock; contains discontinuous lenses of halite; grades into overlying unit. (Marker bed 120)	1.5	1,176.5 –1,178.0
Halite rock, moderate-reddish-orange (10R 6/6)	.7	1,178.0 –1,178.7
Halite rock; contains about 25 percent gray clay; top 0.2 ft is medium-gray (N 5) clay layer	.7	1,178.7 –1,179.4
Halite rock, banded white and moderate-reddish-orange (10R 6/6); contains about 5 percent polyhalite in blebs and lenses	4.6	1,179.4 –1,184.0
Halite rock; contains about 2 percent polyhalite in blebs and 2 percent gray clay in blebs	1.0	1,184.0 –1,185.0
Halite rock, colorless; contains about 25–30 percent clay both reddish brown and gray in blebs; grades downward into underlying unit	6.0	1,185.0 –1,191.0
Halite rock; contains about 10 percent polyhalite in blebs	2.7	1,191.0 –1,193.7
Polyhalite rock; 0.1-ft-thick bed of gray clay at base. (Marker bed 121)	.9	1,193.7 –1,194.6
Halite rock; contains about 2 percent gray clay and 2 percent polyhalite in blebs	7.4	1,194.6 –1,202.0
Total partial thickness of Salado Formation	550.8	

Bottom of shaft.

REFERENCES

Adams, J. E., 1944, Upper Permian Ochoa series of Delaware Basin, West Texas and southeastern New Mexico: Am. Assoc. Petroleum Geologists Bull., v. 28, no. 11, p. 1596–1625.

Baltz, E. H., 1959, Provisional diagram showing relations of Permian rocks in part of Eddy County, New Mexico: U.S. Geol. Survey TEM-1035 [1960].

Byerly, P. E., Stewart, S. W., and Roller, J. C., 1960, Seismic measurements by the U.S. Geological Survey during the pre-Gnome high-explosives tests near Carlsbad, New Mexico —Final report: U.S. Geol. Survey TEI–761, 40 p., 9 figs., issued by U.S. Atomic Energy Comm. Tech. Inf. Service Extension, Oak Ridge, Tenn.

Cooper, J. B., 1960, Geologic section from Carlsbad Caverns National Park through the Project Gnome site, Eddy and Lea Counties, New Mexico: U.S. Geol. Survey TEI–767.

—— 1961, Test holes drilled in support of ground-water investigations, Project Gnome, Eddy County, New Mexico— Basic data report: U.S. Geol. Survey TEI–786, 116 p., 12 figs. [1962].

—— 1962, Ground-water investigations of the Project Gnome area, Eddy and Lea Counties, New Mexico: U.S. Geol. Survey TEI–802, 67 p., 15 figs. [1962].

Dickey, D. D., 1964, Effects of the GNOME nuclear explosion upon rock salt as measured by acoustical methods, *in* Short papers in the geologic and hydrologic sciences: U.S. Geol. Survey Prof. Paper 501–B, p. B108–B111.

Fenneman, N. M., 1931, Physiography of western United States: New York, McGraw-Hill Book Co., 534 p.

Gard, L. M., 1963, Nuclear explosions—some geologic effects of the Gnome shot: Science, v. 139, no. 3558, p. 911–914.

Gard, L. M., Cooper, J. B., and others, 1962, Hydrologic and geologic studies for Project Gnome: U.S. Geol. Survey Project Gnome Report PNE–130F, 196 p. [Available from U.S. Dept. Commerce, Clearinghouse for Scientific, Federal, and Technical Information, Springfield, Md.]

Goddard, E. N., chm., and others, 1948, Rock-Color Chart: Washington, Natl. Research Council (repub. by Geol. Soc. America, 1951), 6 p.

Hale, W. E., and Clebsch, Alfred, Jr., 1959, Preliminary appraisal of ground-water conditions in southeastern Eddy County and southwestern Lea County, New Mexico: U.S. Geol. Survey TEM–1045, 29 p., 3 figs.

Hoy, R. G., and Foose, R. M., 1962, Earth deformation from a nuclear detonation in salt: Stanford Research Inst., Project Gnome Report PNE–109F, 60 p.

Jones, C. L., 1960, Thickness, character, and structure of upper Permian evaporites in part of Eddy County, New Mexico: U.S. Geol. Survey TEM–1033, 19 p., 2 figs.

King, P. B., 1948, Geology of the southern Guadalupe Mountains, Texas: U.S. Geol. Survey Prof. Paper 215, 183 p.

Kulp, J. L., 1961, Geologic time scale: Science, v. 133, no. 3459, p. 1111.

Moore, G. W., 1958a, Description of core from A.E.C. drill hole no. 1, Project Gnome, Eddy County, New Mexico: U.S. Geol. Survey TEM–927, 27 p., 1 fig. [1959].

—— 1958b, Chemical composition of evaporite deposits: U.S. Geol. Survey TEI–713, 35 p.

Morey, G. W., 1958, The system H_2O-$NaCl$, H_2O-$CaSO_4$, and H_2O-$NaCl$-$CaSO_4$: U.S. Geol. Survey TEI–717, 26 p.

Newell, N. D., Rigby, J. K., Fischer, A. G., Whiteman, A. J., Hickox, A. J., and Bradley, J. S., 1953, The Permian reef complex of the Guadalupe Mountains region, Texas and New Mexico—a study in paleoecology: San Francisco, Calif., W. H. Freeman and Co., 236 p.

Rawson, D. E., 1963, Review and summary of some Project Gnome results: Am. Geophys. Union Trans., v. 44, no. 1, p. 129–135.

Rawson, D. E., Boardman, C., and Jaffe-Chazon, N., 1965, The environment created by a nuclear explosion in salt: Lawrence Radiation Lab., Project Gnome Report PNE–107F, 90 p.

Roller, J. C., Stewart, S. W., Jackson, W. H., Warrick, R. E., and Byerly, P. E., 1959, Seismic measurements by the U.S. Geological Survey during the pre-GNOME high-explosives tests—A preliminary summary: U.S. Geol. Survey TEM–774, 34 p.

Schaller, W. T., and Henderson, E. P., 1932, Mineralogy of drill cores from the potash field of New Mexico and Texas: U.S. Geol. Survey Bull. 833, 124 p.

Stipp, T. F., and Haigler, L. B., 1956, Preliminary structure contour map of a part of southeastern New Mexico showing oil and gas development: U.S. Geol. Survey Oil and Gas Inv. Map OM–177.

U.S. Atomic Energy Commission, 1961, Background information on Project Gnome: U.S. Atomic Energy Comm. AL Pamphlet 3100–1, 38 p.

Vine, J. D., 1960, Recent domal structures in southeastern New Mexico: Am. Assoc. Petroleum Geologists Bull., v. 44, no. 12, p. 1903–1911.

—— 1963, Surface geology of the Nash Draw quadrangle, Eddy County, New Mexico: U.S. Geol. Survey Bull. 1141–B, 46 p.
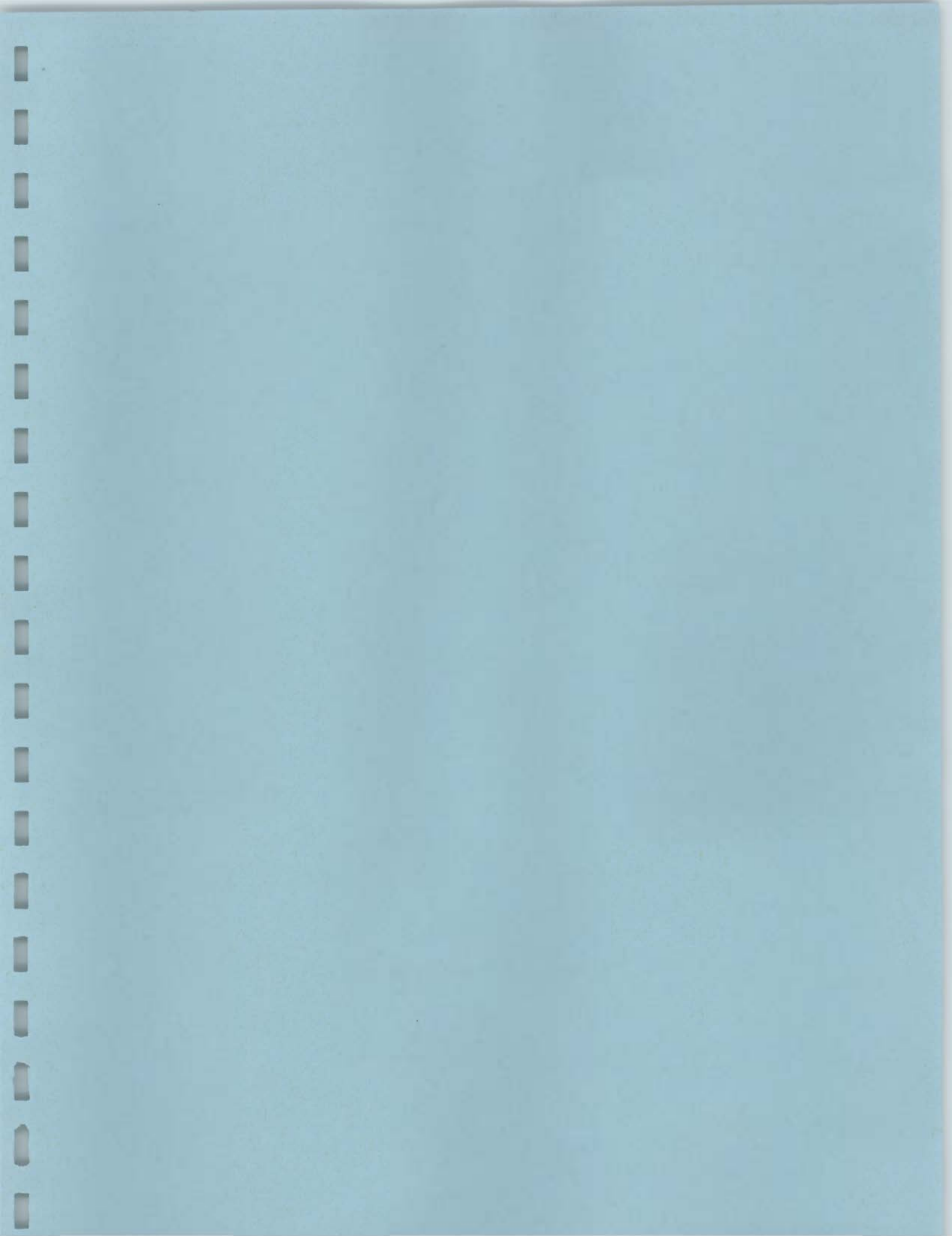
PROJECT GNOME

THE ENVIRONMENT CREATED BY A NUCLEAR

EXPLOSION IN SALT

D. Rawson
C. Boardman
N. Jaffe-Chazan

Lawrence Radiation Laboratory
University of California
Livermore, California

September 1964

CONTENTS

CONTENTS (Continued)

CONTENTS (Continued)

ABSTRACT

The Gnome event, a 3.1 ± 0.5 kiloton nuclear explosion, was conducted at a depth of 361 m in bedded rock salt near Carlsbad, New Mexico. The burst melted approximately 3.2×10^6 kilograms of rock salt and produced a standing cavity with a volume of about 27,200 cubic meters. The cavity has a pronounced bulge at its equator. The development of this asymmetry was controlled by the preshot character of the rock: horizontal weaknesses in the form of bedding planes and clay layers. The molten salt mixed with the condensing radioactive debris and about 11.6×10^6 kg of rock from the cavity walls, to form a radioactive "puddle" of melt and rock breccia at the base of the cavity. This zone is blanketed by about 13.6×10^6 kg of rubble that resulted primarily from ceiling collapse, thus shielding the "puddle" so that when personnel entered the cavity, gamma radiation levels were rarely in excess of 20 mR/hr.

During the dynamic cavity growth period of about 100 msec, radial cracks propagated closely behind the outgoing compressional shock wave. Molten rock had not yet mixed well with vaporized fission products and consequently melt injected into these cracks was not radioactive or only slightly so. The maximum observed extent of these fractures, measured from the center of the explosion, is 40 m laterally, 38 m above and 25 m below.

-5-

Leakage of radioactive gases through the rock is detectable by the presence of radiation damaged salt. Generally, there was no evidence of leakage beyond 40 m and the maximum observed extent at 65.5 m is thought to be associated with fracturing to a natural cavity.

Close-in stemming failed and cavity gases vented dynamically into the emplacement drift. Back-up stemming confined the dynamic venting but allowed the low pressure release of steam and gaseous fission products. The formation of radial cracks and bedding plan partings, coupled with the emplacement configuration to accommodate a neutron-physics experiment, caused the stemming failure.

Asymmetry of rock displacements, fractures observed, and the permanent surface displacements indicate localized uplift of the rock between the cavity and the ground surface. It is interpreted that this uplift was caused by spall of the upper few hundred feet of rock which momentarily decreased the overburden pressure. The cavity pressure then exceeded overburden pressure and the cavity expanded preferentially upwards.

A zone of increased permeability was defined to extend at least 46 m laterally and 105 m above the point of the explosion. The permeability increase was established by complete circulation loss of the drill fluid and is primarily associated with motions and partings along bedding planes – the major preshot weakness in the rock.

ACKNOWLEDGMENTS

CHAPTER 1

INTRODUCTION

1.1 BACKGROUND

Project Gnome was the first scientific experiment with nuclear explosives designed to provide information pertaining to the non-military uses of these explosives. A 3.1 ± 0.5 kt nuclear device was detonated at a depth of 361 m underground in bedded salt on December 10, 1961. The test site for Project Gnome was located about 48 km southeast of Carlsbad, New Mexico.

The Gnome experiment was conducted in the Salado rock formation of Permian age (Fig. 1.1). This formation in the vicinity of the explosion is composed of about 89% halite, or rock salt (NaCl), 7% polyhalite $[Ca_2MgK_2(SO_4)_4 \cdot 2H_2O]$, 1% anhydrite $(CaSO_4)$, and 3% silt and clay. The impurities occur primarily as separate beds interlayered with the salt strata, although they also occur mixed with the salt crystals (Appendix A and B). Overlying the Salado formation are the sedimentary limestones, dolomites, sandstones, claystones, and siltstones of the Rustler and Dewey Lake Formations of Permian age and alluvial deposits of Quaternary age (Reference 1).
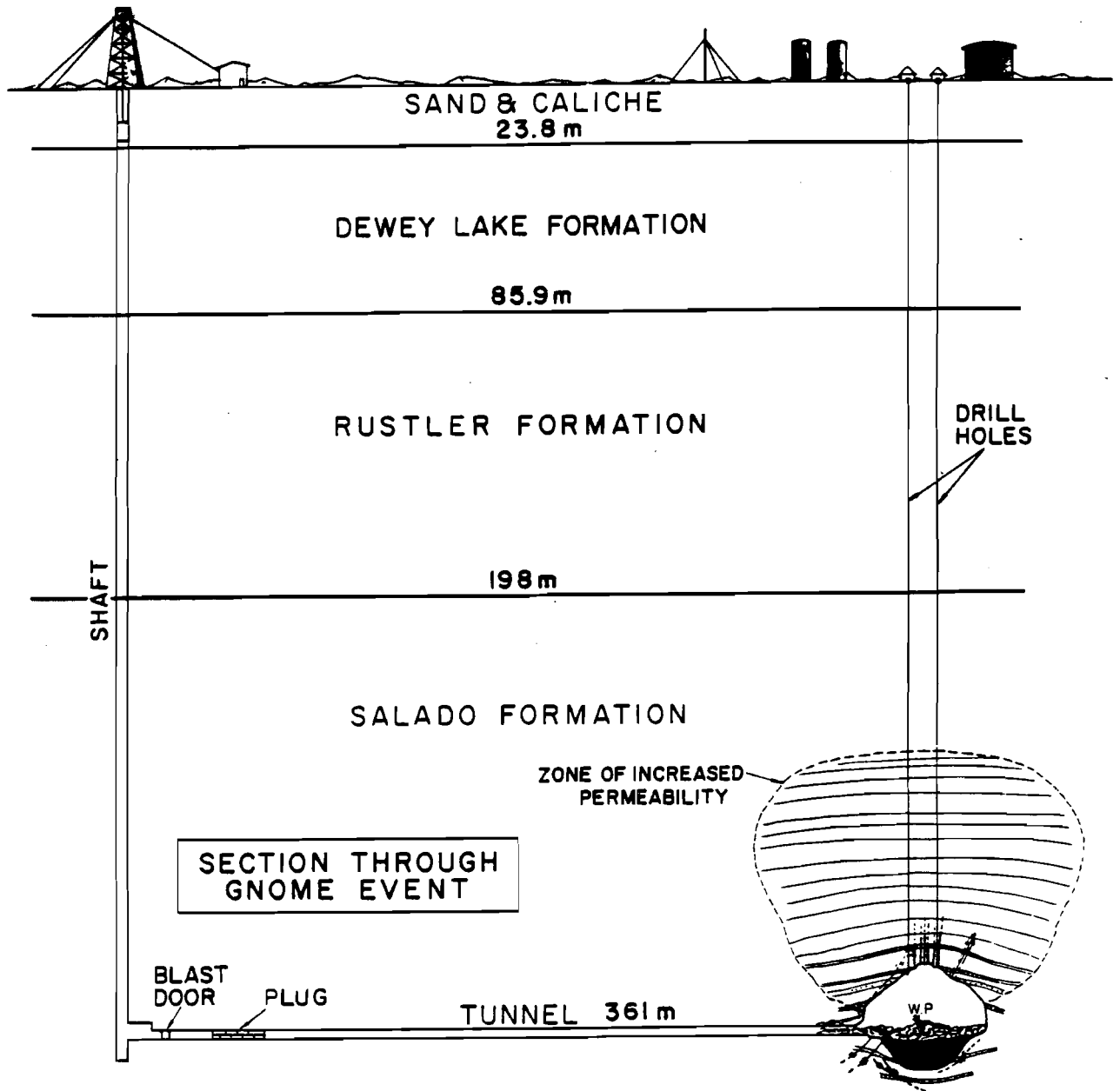
Fig. 1.1 Vertical section through the Gnome postshot environ-
ment,

The Gnome device was emplaced at the end of a buttonhook-shaped drift, a distance of 301 m from the shaft (Fig. 1.2). The first 274 m of the drift were straight along a line between the shaft and the device. The remainder was curved and is referred to as the "buttonhook" portion. The drift was designed so that the buttonhook would close following the detonation and contain the explosion. Requirements for an associated neutron-physics experiment were such that most of the drift had to be line-of-sight to the device. An evacuated pipe (the "neutron pipe") extended from a revolving wheel (the "neutron wheel") through the straight portion of the drift and continued through a drill hole to the device room. Backup stemming was provided in the drift near the shaft to restrict venting if the close-in stemming failed.

1.2 OBJECTIVES

The major objective of the postshot exploration program was to provide a definition of the environment created by the detonation in support of the primary object of Project Gnome: To study the effects of an underground nuclear explosion in salt. Previous experience with volcanic tuff and alluvium at the Nevada Test Site had provided a general understanding of the interaction between nuclear explosions and rock materials. An explosion in salt provided an excellent test of this understanding, since the physical and chemical properties of salt are greatly different from those of tuff and alluvium.
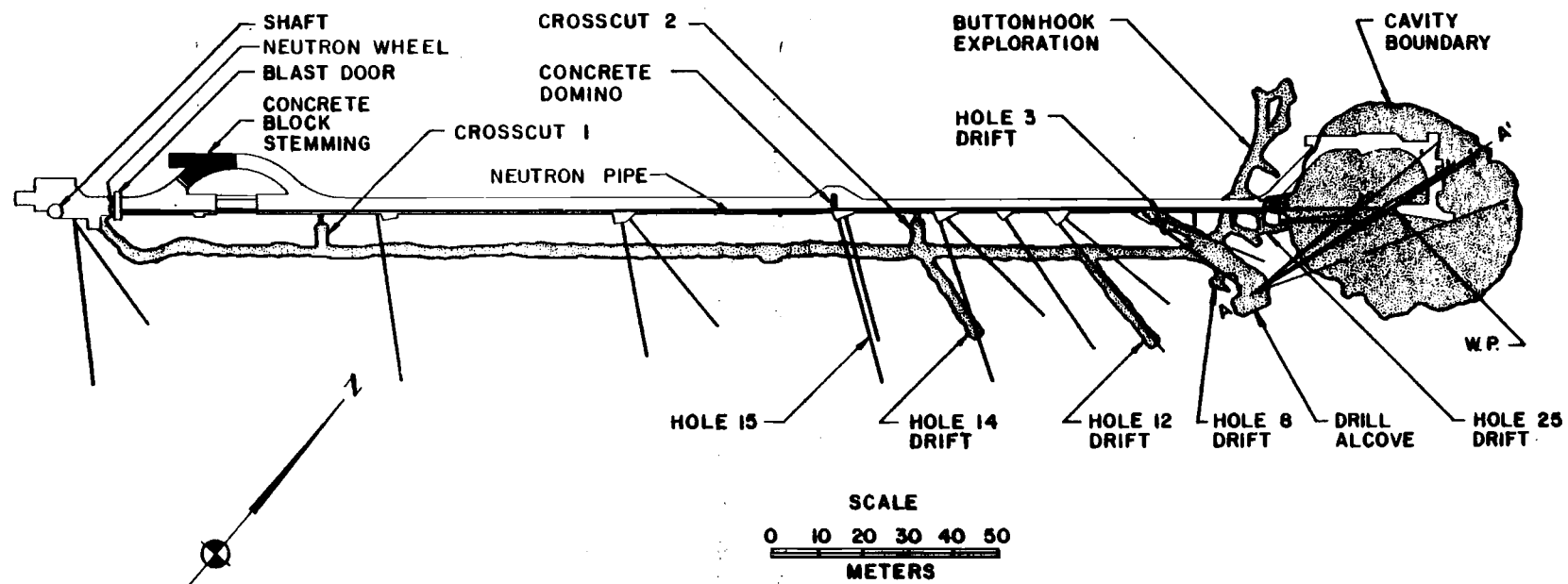
Fig. 1.2 Plan view showing the post-explosion exploration and cavity (shaded) (the fine line drawing indicates the pre-detonation configuration).

-11-

Many data were also obtained pertaining to some of the other objectives of the experiment, specifically:

1.2.1   The Isotopes Program: To determine the feasibility of recovering radioisotopes produced by a nuclear explosion. This method would represent a significant alternative to reactor methods. Although the device used in Gnome was not specifically designed to produce quantities of useful isotopes, the mixed fission products made possible a feasibility study.

1.2.2   The Power Program: To investigate the feasibility of the measurement and extraction of heat deposited by the explosion. It had been suggested that the heat of fusion of the salt melted by the explosion might be extracted and used for electrical power.

1.2.3   Shock Effects Studies: To subject a variety of mineral and organic samples to a range of shock pressures produced by the explosion in order to determine the effects of the explosion (in terms of phase transitions, property changes, etc.) on the samples.

The purpose of re-entry drilling from the surface was to provide radioactive samples for yield determination; to enable measurements concerned with the power feasibility studies; and to provide preliminary definition of the environment created.

-12-

1.3 EXPLORATION PHASES

Post-detonation exploration consisted of: 1) examination of the surface facilities and the ground surface over the working point* (Reference 2); 2) examination of the shaft and the bottom station six days following the detonation (Reference 2); 3) re-entry drilling from the surface into the cavity region during the period from December 11, 1961 to January 18, 1962; 4) underground mining and drilling exploration, including re-entry into the emplacement drift, recovery of shocked samples and instruments, entry into the cavity produced by the explosion and general definition, by direct observation, of the postshot environment. Exploration was complete by the end of September, 1963. This report covers the work accomplished during phases 3 and 4.

1.4 OBSERVATIONS IMMEDIATELY FOLLOWING THE EXPLOSION

Less than one minute following the explosion, radiation was detected at the blast door near the bottom of the shaft (Fig. 1.2) by remote-area radiation monitors. No radiation was detected at the shaft collar until three minutes and forty seconds after the detonation. At approximately seven minutes after zero time, a gray smoke, steam, and associated radioactivity surged from the shaft opening. By eleven minutes following the explosion, copious quantities of steam issued from both shaft and ventilation lines. A large flow continued for

---

*The location of the nuclear device.

about thirty minutes before gradually decreasing. A small flow was still detected through the following day. The radioactive elements that vented through the shaft were volatile and noble gases (Reference 3).

The unexpected venting of steam and associated radioactive gases led to an additional objective for the exploration program — the determination of the cause and nature of venting.

The Gnome event was monitored by geophone arrays from shot time until the shot environment was penetrated by re-entry drilling. The geophone records indicated that noise produced by rock movement lasted for three minutes following the explosion and were very infrequent after that time.

CHAPTER 2

THE CAVITY ENVIRONMENT

2.1 GENERAL

Postshot exploration started first from the surface and then was accomplished by drilling and drift excavation underground (see Fig. 2.1).

On May 17, 1962, only five months after the explosion, excavation along preshot drill hole #25 for the purpose of recovering shocked samples resulted in actual personnel entry into the cavity. This made possible direct observation of the cavity interior, photographic documentation and a minimal triangulation survey to define its size and shape (Fig. 2.1). At that time, the air temperature was 50°C near the cavity entrance, the relative humidity was 60-70%, and the radiation levels varied from place-to-place, but were rarely in excess of 20 mR/hr. One month later a more comprehensive temperature survey indicated a variation between 50 and 57°C within the cavity. It should be noted that for several weeks prior to and following cavity entry, fans located in drill holes from the surface into the cavity had flushed several million cubic meters of air through this environment.
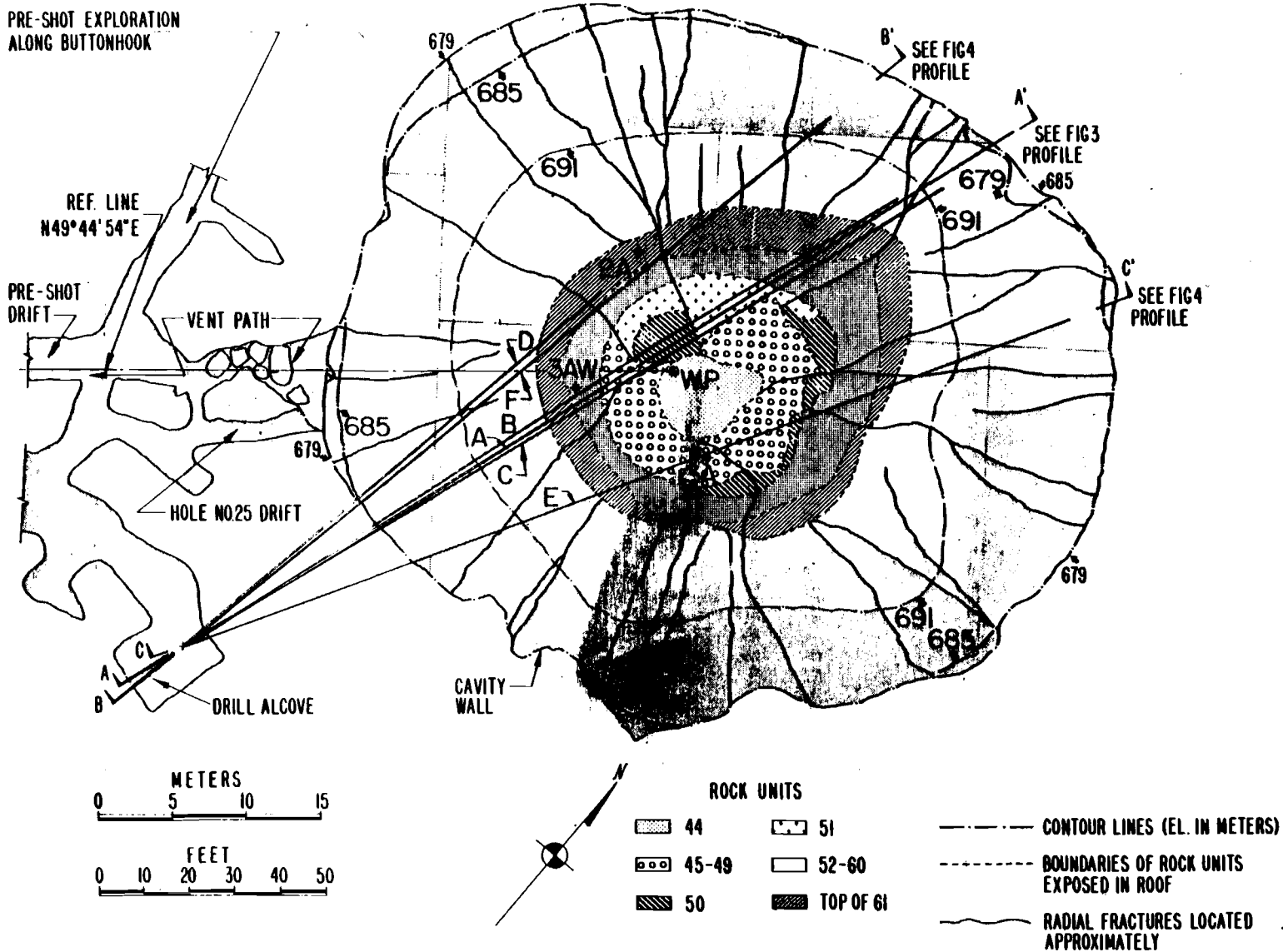
Fig. 2.1 Gnome cavity: reflected ceiling plan.

2.2 CAVITY VOLUME AND SHAPE

An estimate of the total void volume produced by the explosion was made, using a combination of three points from drill holes penetrating the top of the cavity, photographic guides for extrapolation from survey control within the cavity, and underground drill holes which defined the cavity below the working point in 10 places. This volume was calculated to be 27,200 cubic meters (Appendix D) and is in very good agreement with a measurement made by pressurizing the cavity with compressed air. A known volume of air at a known pressure was introduced into the cavity. From these measurements the cavity volume was calculated to be 28,000 ± 2,800 cubic meters (J. Tracy, LRL – verbal communication).

The total void volume of 27,200 cubic meters is equivalent to a sphere with a radius of 18.7 meters. The cavity is asymmetric, however, because of anisotropic resistance to cavity expansion, implosion of the cavity walls, and partial ceiling collapse (see discussion in Chapter 3). The cavity shown in Figs. 2.2 and 2.3 has an average radius of 17.4 m in the lower portion (measured from the working point to the boundary of radioactive melt); an average radius of 24.4 m in the equatorial plane; and an average radius of 22.9 m in the upper portion (measured from the working point to the rock-void interface). The shape of the ceiling of the cavity indicates that the major pre-shot weaknesses in the rock, the bedding planes or horizontal boundaries between

-17-

GNOME CAVITY CROSS SECTION   3 kt

PRESHOT LOCATION OF STRATA

CAVITY VOID

PROJECTED WORKING POINT

WATER LEVEL INTRODUCED BY POST SHOT SURFACE DRILL HOLES

RUBBLE PILE

APPROX. UPPER BOUNDARY OF MELT

MELT DISTRIBUTION, HOLE B

HOLE B

HOLE C

FEET
0   25   50
0   5   10   15
METERS

LEGEND

〜〜〜〜〜 RADIATION DAMAGED SALT ENCOUNTERED IN DRILL HOLES

│ │ │ SLIGHTLY RADIOACTIVE MELT INJECTED INTO FISSURES

═══ FAULT

⋯⋯⋯ BEDDING CONTACTS

≈≈≈ FRACTURE ZONES

GLI-6210-18549A

Fig. 2.2   Cavity profile A-A' (see Fig. 2.1 for plan view).

-18-

CAVITY VOID

RUBBLE PILE

PROJECTED
WORKING POINT

APPROX. UPPER BOUNDARY OF MELT

HOLE 'E'

MELT DISTRIBUTION, HOLE 'E'

PRESHOT LOCATION
OF STRATA

CAVITY PROFILE C-C'

SCALE

0   5   10

METERS

CAVITY VOID

PROJECTED
WORKING POINT

APPROX. UPPER LIMIT OF MELT

HOLE 'F'

HOLE 'D'

MELT DISTRIBUTION, HOLE 'F'

PRESHOT LOCATION
OF STRATA
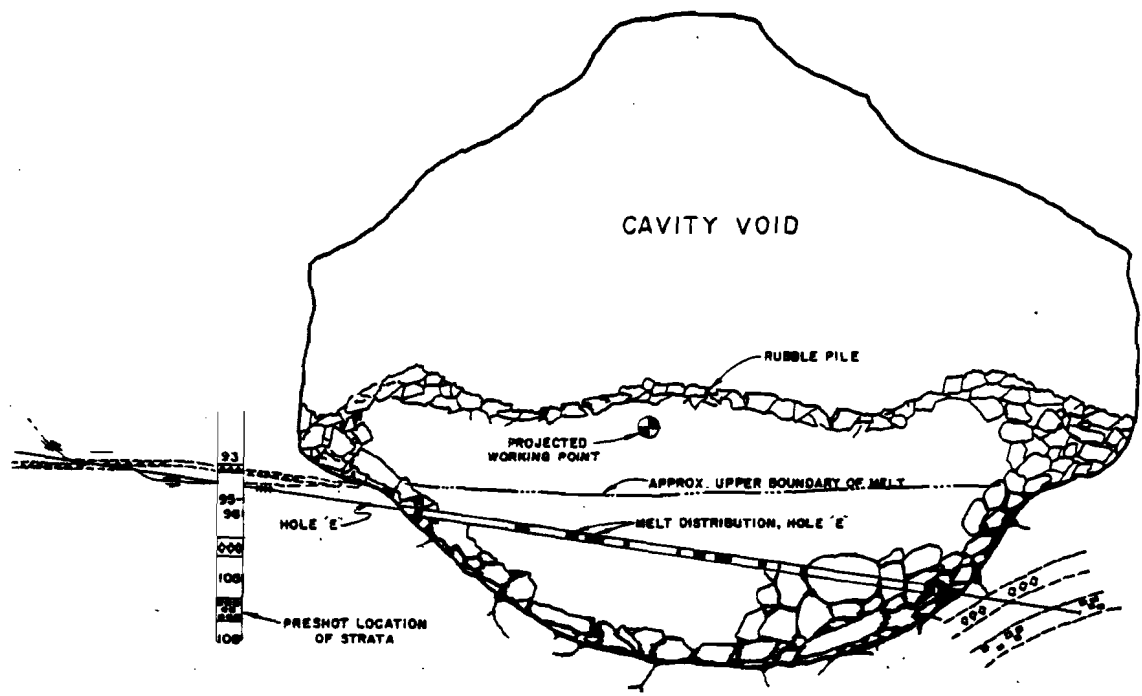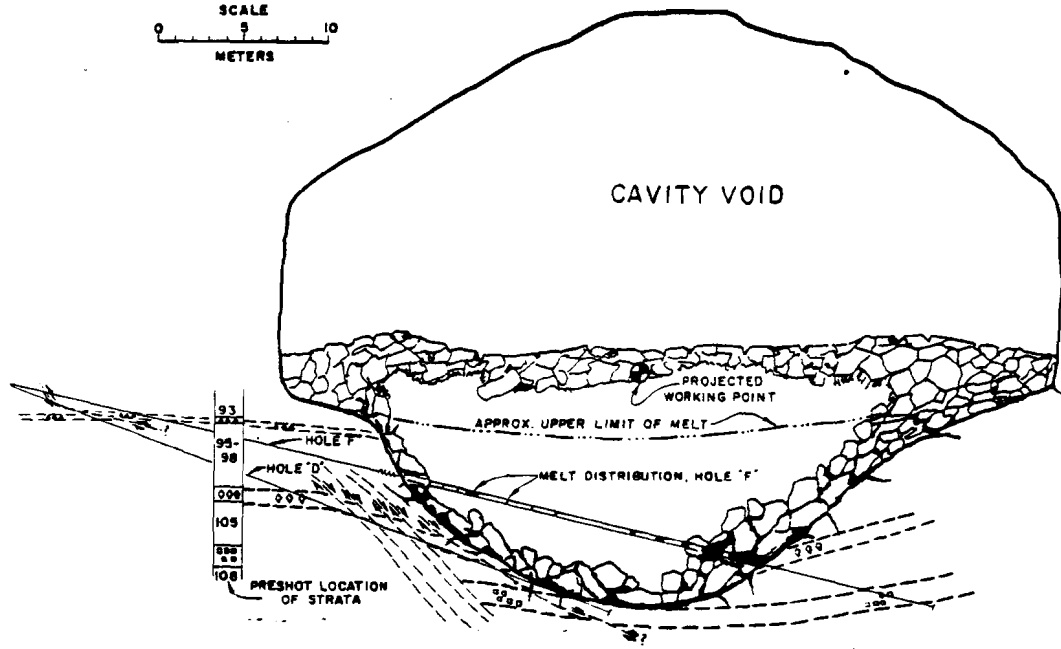
CAVITY PROFILE B-B'

Fig. 2.3 Cavity profiles B-B' and C-C' (see Fig. 2.1 for plan view).

-19-

rock units, somewhat controlled the extent of collapse. It is very likely that less collapse would have occurred if these weaknesses had not existed.

The most significant departure from spherical symmetry is a girdle of rock about 9 m high surrounding the equatorial region of the cavity. This region moved radially further from the working point than rock nearer the base or top of the cavity. The development of this asymmetry was most likely controlled by bedding plane weaknesses and thin horizontal clay strata that separated more competent beds of salt and polyhalite. The explanation of this bulge is discussed further in the sections on permanent displacements and earth deformation. The cavity would be more symmetrical about a vertical axis passing through a point about 4 m northeast of the working point rather than through the working point (the center of the nuclear device). This displacement of the effective center of energy may be due to the shape of the chamber in which the device was detonated, resulting in the initial distribution of the explosion energy as a cylindrical source rather than a spherical one.

2.3 RUBBLE AND ASSOCIATED RADIOACTIVE MELT

The mass of rock melted by the explosion, based on the analysis of ore recovered from drill holes, is estimated to be about 3.2×10^6 kg, equivalent to about 10^6 kg per kiloton of yield.

This mass compares favorably with the expected mass vaporized and melted of about 1.4×10^6 kg per kiloton. This prediction was based on the assumption that 41% of the explosive energy is utilized in melting the rock (Reference 4). The melt became intimately mixed with about 11.6×10^6 kg of rock, much of which was probably imploded, decrepitated, or fell into the cavity early during the first few seconds following the explosion. An estimated 13.6×10^6 kg of rock collapsed later from the upper hemisphere and blanketed the region containing the radioactive melt breccia at the cavity base (Appendix D).

The region denoted as Zone B in Fig. 2.4 can generally be described as a rock-melt breccia in which the melt forms much of the matrix between the larger rock fragments (the range of particle diameters is estimated to be about 15 cm to 3m). The melt itself engulfs smaller rock fragments that range in diameter from a fraction of a centimeter to a few centimeters. The degree of dilution of samples of the melt varies greatly from almost no rock fragments to as much as 30 or 40 percent.

Because much of this zone is typically a mixture of rock fragments cemented together by the melt matrix, it is likely that this material would be self-supporting if actual mining re-entry were necessary. This is especially true near the cavity boundary where the concentration of melt is the highest. Most likely, a liberal amount of rock support would be necessary.

-21-
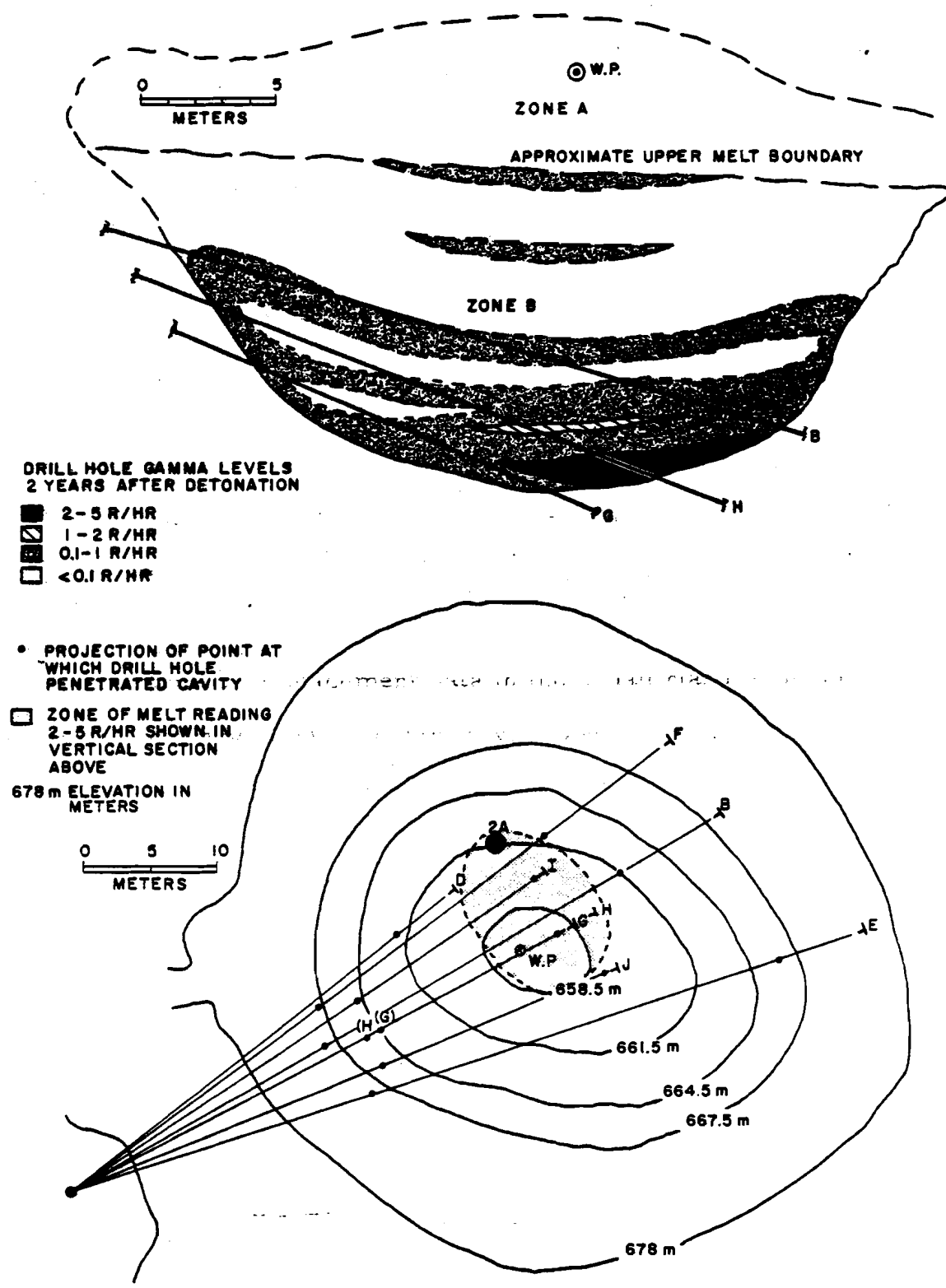
Fig. 2.4 Schematic sections through the Gnome cavity showing approximate distribution of radioactivity two years after the explosion.

This material was sufficiently self-supporting, however, that the drill holes remained open without casing.

The rubble in Zone A, Fig. 2.4, above the zone containing radioactive melt is essentially a loose pile of rock fragments and is not self-supporting. During re-entry drilling the holes caved in this region, causing considerable difficulty. In this zone, the particle-size variation can be approximated with reasonable accuracy by direct observation of the rubble surface exposed at the base of the cavity void. The range in particle size is extremely large, varying from crushed rock fragments less than 1 cm across to large blocks as large as 7 m across the maximum dimension. Blocks exceeding 2 m across account for less than 10 percent of the rubble and the average particle diameter is about 75 cm.

The explosion liberated at least 5×10^4 kg of water from the vaporized and melted rock and an additional 17×10^4 kg or water could have been liberated from the 11.6×10^6 kg of rock that came from the cavity wall and was mixed with the melt. M. Nathans (Reference 5) calculated from the tritium concentration in the vented steam that as much as 4×10^5 kg of water might have been liberated from the rock. Had there not been venting to tap off much of this water, it would have eventually condensed and collected in the voids of the rubble at the base of the cavity. As it was, the water level in the rubble was at an elevation of 673 m, or 2.1 m below the working point. Most of

this water was added during surface re-entry drilling, although some is probably condensed steam that did not escape during cavity venting. A total of about 5×10^5 kg of water entered the cavity and the voids in the rock above the working point as a result of circulation losses during drilling. Water was still dripping very slowly into the cavity one year following the explosion.

As discussed above, the radioactive melt forms a puddle intimately mixed with nonradioactive rock. A schematic cross section through the lower hemisphere of the cavity (Fig. 2.4) shows the approximate gamma radiation distribution based on radiation log data from underground drill holes and hole 2a. This picture is largely conceptual, since it is based on limited data and the logs show a great deal of scatter in radiation levels because of the large amount of nonradioactive rock mixed with the radioactive melt.

This figure shows a zone at the base of the cavity that is highly enriched in radioactivity. In vertical hole 2a a 0.6-m-thick zone had radiation six times levels greater than any other level recorded in this hole. Underground holes, G through J, were drilled in August, 1963, to better define this zone and to obtain additional radioactive samples for the isotopes production study. Data from these holes were used primarily to define the limits of the enriched zone indicated in Fig. 2.4.

-24-

Presently the rubble and melt are being studied in detail in order to determine methods of processing this "ore" for elements that are chemically similar to the actinides. A report by M. Nathans (Reference 5) covers the details of this study. It has been determined that almost all of the fission products (other than the gaseous or volatile ones) remain with the salt impurities when samples are either dissolved in water or remelted to separate the NaCl from the other impurities. Part of the scope of this study is to determine with which chemical species the different radio-elements are associated.

It is interesting to note that the mineral olivine, specifically forsterite (Mg_2SiO_4), makes up a significant portion of the water-insoluble fraction of several samples. This mineral did not occur preshot in the rock. The major source of magnesium was the mineral polyhalite [$Ca_2MgK_2(SO_4)_4 \cdot 2H_2O$]. Magnesium also occurs in the clay minerals and in trace quantities of magnesite ($MgCO_3$). Silica occurs primarily as silt-sized quartz particles and with the clay minerals. Reference 5 also describes a variety of other chemical reactions resulting in several compounds and the radioactivity fractionation associated with these species.

Examples of the solidified salt melt are shown in Fig. 2.5. Sample B-21H is only slightly vesiculated. It was taken from about 2 m from the far cavity boundary in drill hole B (Fig. 2.2), and contains a large amount of rock fragments, presumably blown

-25-
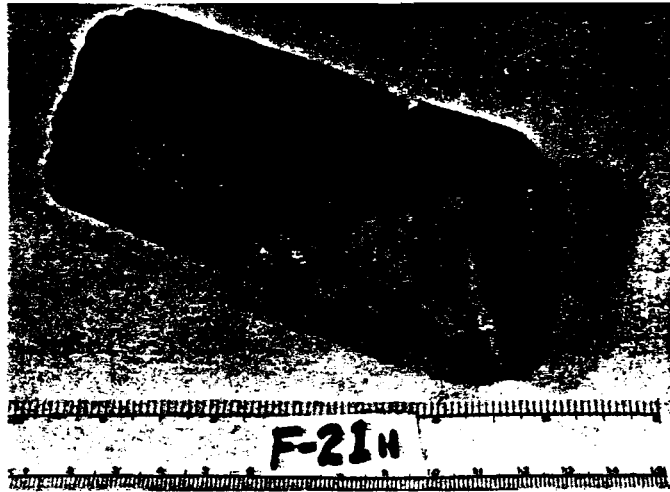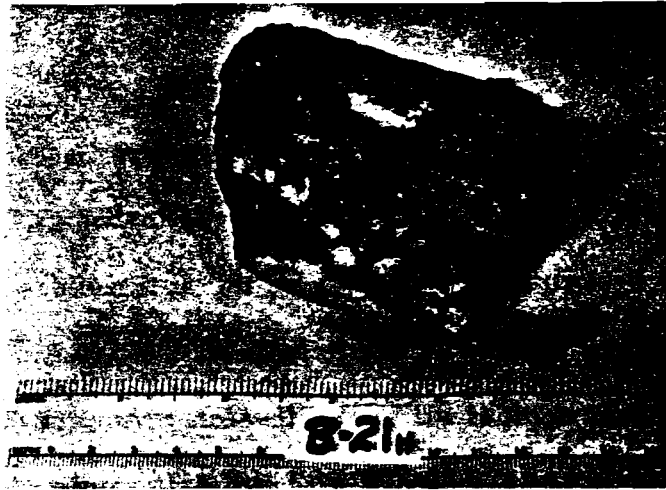
Fig. 2.5   Typical melt samples from underground drill holes.

-26-

off the cavity walls. Some of the fragments underwent fusion because of the superheat of the melt. Sample F-21H is from drill hole F (Fig. 2.3) near the cavity edge. The melt in contact with the unfused salt forms a dense band in contrast with the vesicular melt on the other side of the band. It is interpreted that following cavity growth the rock bounding the cavity broke up and imploded, allowing the salt melt to invade openings that resulted. The newly exposed colder rock quenched the melt, forming unvesiculated melt at the contact. Under normal circumstances, it would be expected that this chilled border would be gradational, but at Gnome it is quite possible that when venting occurred, the cavity pressure dropped rather abruptly, causing violent out-gassing of the melt. This sudden out-gassing, which was closely followed by solidification of the melt, produced vesiculation. Sample E-3H was taken from drill hole E near the central portion of the cavity about 25 ft above the cavity bottom (Fig. 2.3). This melt cooled more slowly than most of the melt observed and developed large crystallites — up to 4 mm in diameter. Most of the melt solidified rapidly and is fine-grained — less than 1 mm.

2.4 ROCK TEMPERATURES

A plot of temperature versus radial distance from the working point is shown in Fig. 2.6. Data points shown were taken from

-27-
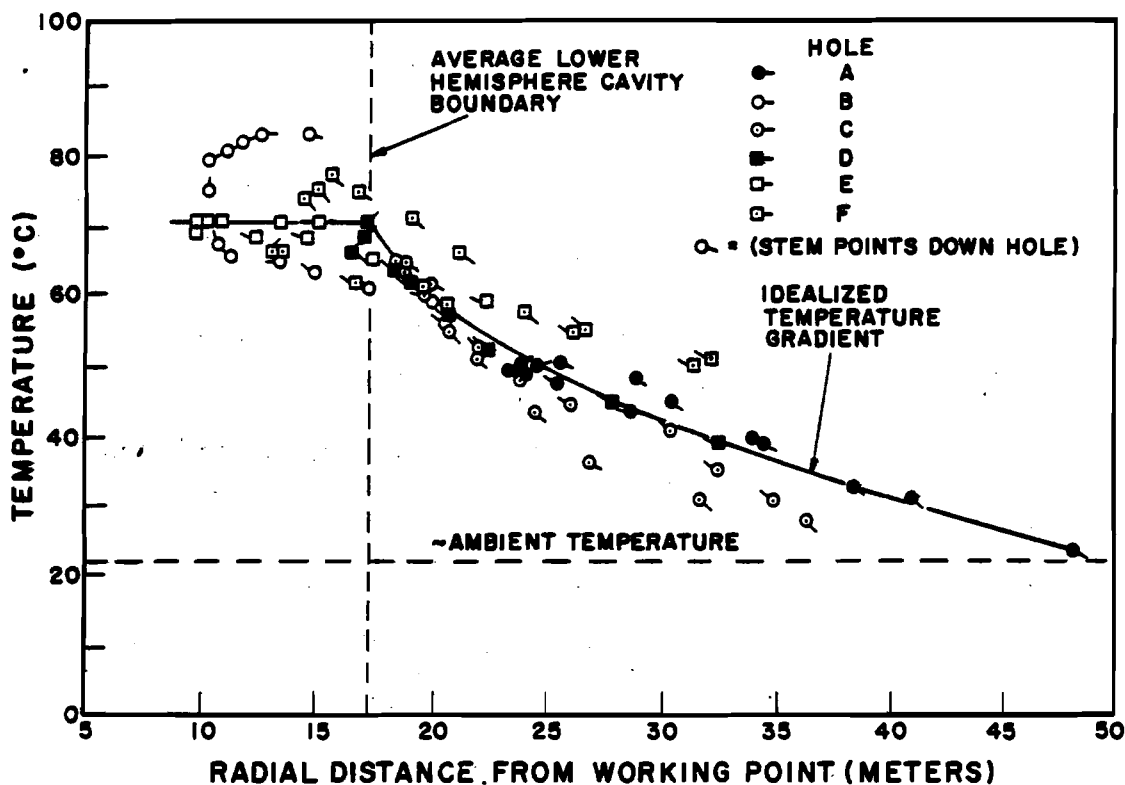
Fig. 2.6   Temperature vs radial distance from working point six months after the detonation.

temperature measurements made about 6 months after detonation, in drill holes A through F.   This plot indicates that the average temperature was 71°C in the rubble-melt zone of the cavity at that time.   Temperatures varied from 63 to 83°C in this region, depending upon the elevation at which the measurement was made. Maximum temperatures were recorded within about 1 m from the lower cavity boundary in each hole that penetrated this zone.

The logs of holes B and C indicate that below the cavity, at equal radial distances from the working point, and at equal angles from the vertical; temperatures are 10-12° higher in a northerly

direction than in the southerly.   This asymmetry is consistent with the asymmetrical position of the zone of highly-radioactive melt described previously.

CHAPTER 3

PERMANENT DISPLACEMENTS

3.1 GENERAL

Displacement of the material surrounding the Gnome explosion has been measured laterally at a distance of 298 m by gages in a drill hole (Reference 6), and the permanent displacement of the surface over the working point is known by surveys (Reference 7). In addition, permanent radial displacements have been determined from preshot and postshot positions of rock strata and other markers such as instrument holes.

Preshot elevations of beds were obtained from the USGS lithologic log (Reference 8) and tunnel map (Reference 1). Postshot positions were determined from geophysical logs of the vertical holes and from core from the underground inclined drill holes. Preshot and postshot positions of beds are generally known within ± 0.3 m. The locations of instrument holes branching off from the main drift were accurately surveyed before and after the detonation.

Figure 3.1 is a plot of the permanent displacement data obtained by postshot underground exploration. R_i – the preshot radial distance of a given point from the working point – is plotted against $1/(R_f - R_i)^2$, where R_f is the corresponding postshot radial distance from the working point. For convenience, a scale showing values for $(R_f - R_i)$ is on the plot and a theoretical curve drawn based on the relationship
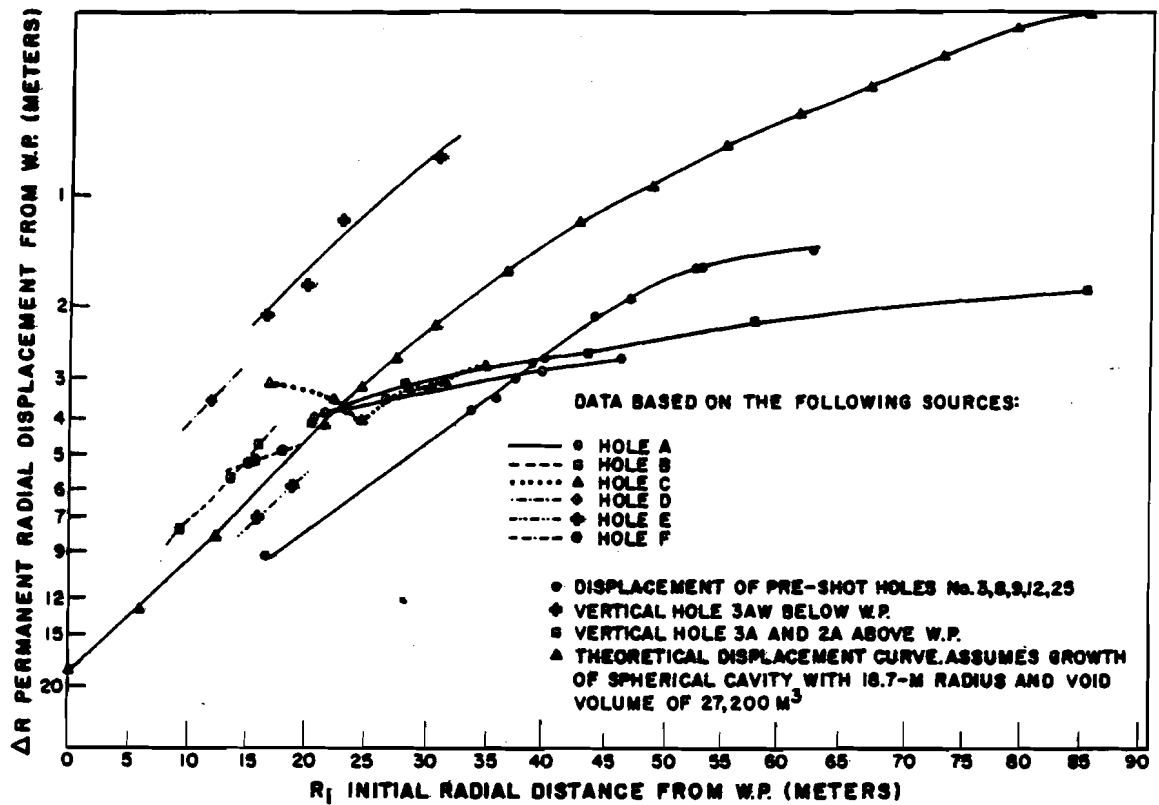
Fig. 3.1   Permanent rock displacement vs distance from working point.

$$R_c = [\, R_f^3 - R_i^3\,]^{1/3}$$ (Appendix C).   In this equation, R_c is a theoretical radius of the void produced by the explosion.   Assuming a void volume of 27,200 m^3 resulting from the growth of a spherical cavity, R_c is equal to 18.7 m.   The systematic departures of the data from the theoretical curve are discussed below.

3.2   DISPLACEMENTS SURROUNDING THE CAVITY

Permanent displacements of rock strata were obtained from the records of holes drilled below the working point (drill holes B, C, D, E, F, and 3AW).   These displacements generally plot above the theoretical curve for given R_i values, indicating R_c is less than

-31-

18.7 m in this region. The average value for R_c calculated from these data is 16.3 m. Permanent radial displacements of instrument holes #3, 8, 9, 12, and 25 fall below the theoretical curve, thus indicating that R_c in the equatorial region is greater than 18.7 m. The average value for R_c calculated from these data is 22.9 m. The displacement at 298 m was about 3.5 cm at 0.5 sec after the explosion, measured by gages in a drill hole at the elevation of the working point (Reference 6). The R_c of 21 m calculated from this displacement compares favorably with the average R_c calculated from instrument-hole data.

Permanent-displacement data in the equatorial region and below the working point generally have nearly constant R_c values, and the slopes of these curves usually parallel the theoretical curve (Fig. 3.1). Variations of R_c can generally be explained by differential motions of rock along fault planes revealed in the mining and drilling exploration.

Applying the theoretical equation to the displacement data obtained above the working point (drill holes A, 2A, and 3A), it is found that R_c increases with radial distance from the working point and the slopes of the curves do not parallel the theoretical curve, but are less steeply inclined.

These data indicate an asymmetrical distribution of rock displacement surrounding the cavity, implying different phenomena above the cavity relative to the equatorial region and below the cavity. This is further discussed in Section 3.3.

-32-

3.3 IMPLICATIONS OF LOCALIZED UPLIFT BETWEEN THE CAVITY AND THE GROUND SURFACE

The asymmetry of the rock displacement associated with cavity growth and subsequent rock motions may be explained in the following manner:

A reasonable assumption is that the force resisting cavity growth is about equal to the weight of the overlying rock. In Gnome, the observed asymmetry in the equatorial region indicates that this force was nonuniformly distributed. The growing cavity met less resistance horizontally, in the direction of the inherent weakness in the rock; i.e., bedding planes between various rock strata. Thin clay seams between halite and polyhalite strata are most conspicuous in that they form both structurally weak planes and lubricated glide surfaces.

Immediately following an underground nuclear explosion, a shock wave is produced by the impact of the expanding hot gases with the confining rock medium. This shock wave travels to the surface, where it is reflected back toward the cavity region. As the rarefaction wave returns from the surface, the upper several hundred feet of rock is spalled (goes into free fall) which also momentarily decreases the overburden pressure. At that time the compressed rock can adjust and much of the cavity volume is transferred from compressed rock into upward unloading and permanent surface doming. Local cavity growth can also occur, since the gas

-33-

pressure within it may well exceed the overburden pressure while the upper few hundred feet of rock is spalling.

From the elevation about 105 m above the working point down to the cavity, the rock was found to be significantly more porous and permeable than it was preshot. This phenomenon resulted in circulation losses while drilling from the surface and was observed by comparing preshot and postshot sonic geophysical logs. The permeability is primarily associated with bedding plane partings and extends at least 46 m laterally from the working point as evidenced by circulation losses in USGS drill hole #6 (Reference 9). At the far end of drill hole A, Fig. 2.1, faulting above the cavity was encountered in which the rock over the working point was dropped downward relative to the rock lateral to the working point. These data suggest that there was an inward sag or down-drop towards the cavity of rock strata above the working point. The backdropping of strata occurred for a distance of about 105 m vertically above the working point. This movement is superimposed upon a general uplift of the rock between the cavity and the surface. Both of these motions are in addition to the rock motion associated with cavity growth that took place primarily during the first 75 to 100 msec following the explosion.

Near the top of this permeable zone, at 85 m above the working point, where backdropping of strata is minimal, the difference between the $\triangle R$ (i.e., $R_f - R_i$) on the theoretical curve (Fig. 3.1)

-34-

and the $\triangle R$ shown on the curve from drill hole 2A and 3A data,
is almost 2 m. From the existing data, a minimum of 2m is the
best estimate of the magnitude of the uplift of the rock up to 85 m
above the cavity that is additional to the upward deformation
associated with cavity growth during the first 100 msec.
Uplift is probably a little greater in the rock immediately above
the cavity since gross permeability and associated porosity increases
were observed as high as 105 m above the working point. This
amount of uplift assumes a maximum initial cavity radius R_c of 18.7
m prior to uplift (see Section 3.4).

Doming at the surface was spread over an area about 360 m
in radius (Reference 2), and had a maximum permanent vertical
displacement of 0.6 m. The uplift of rock near the ceiling of the
cavity represents only a small volume increase relative to the total
cavity volume or the volume represented by permanent surface
uplift. Further evidence supporting the hypothesis that an uplifted
plug is formed is given in Section 4.1.

The cone-shaped uplifted zone shown in Fig. 3.2 indicates
that a possible effect of backdropping of some of the rock is to
tighten up the arch over the cavity, rather than weaken it. This
process may have been important in producing cavity stability.
The lack of a significant number of open fractures above the cavity
to interconnect the preshot structural weaknesses in the rock is
very important from a radiation-safety point of view. The radial
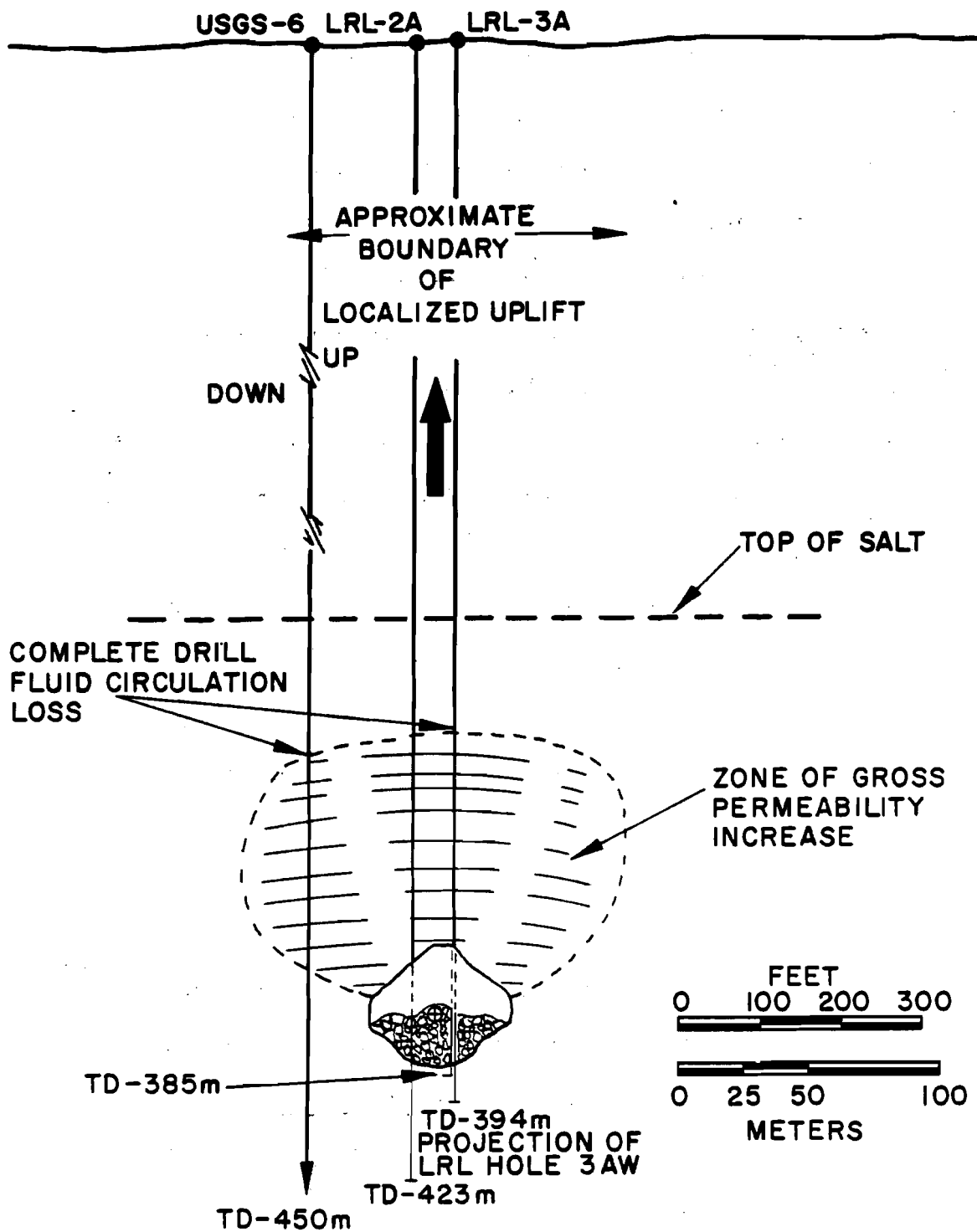
Fig. 3.2 Vertical section showing configuration of localized uplift.

fractures that were produced by the explosion were filled with melt, sealing in the gases.

3.4 SUMMARY OF CAVITY RADII AND IMPLICATIONS ABOUT "BLOW-OFF" OF THE CAVITY WALLS

As pointed out in Section 3.1, R_c is the radius of the theoretical cavity void. The void produced by the explosion is equivalent to an 18.7-m-radius sphere; and the average value of R_c below the working point is 16.2 m, contrasted to an average of 22.9 m in the equatorial region of the cavity. R_c above the working point cannot be greater than about 18.7 m and be consistent with the measured cavity volume. Table 3.1 summarizes values of R_c, and compares these with the final cavity radii defined on p. 17.

TABLE 3.1   THEORETICAL AND FINAL CAVITY RADII COMPARISON

	R_c, Radius of Theoretical Cavity Void (m)		Final Cavity Radius (m)	
	Range	Average	Range	Average
Below the working point	12.5-21.9[a]	16.2	14.9-19.8[c]	17.4
Equatorial region	21.0-26.2[b]	22.9	19.5-30.2[d]	24.4
Above the working point	Maximum of	18.7	20.4-27.1[e]	22.9

[a]20 data points   [c]10 data points   [e]15 data points
[b]11 data points   [d]25 data points

Much of the variation in both R_c and final cavity radii shown by the range values in the table can be explained by observed differential movement of rock along fault planes discussed in Section 4.3 on rock deformation.

In the region below the working point and in the equatorial region, the difference between the average radius of the cavity void (R_c) and the final cavity radii is about 1.2 m. It seems probable that this thickness represents an annular shell of the cavity wall that breaks up, decrepitates, spalls, or is imploded into the cavity. Thus openings develop in the rock bounding the lower hemisphere of the cavity and the fluid, radioactive salt melt invades these openings. The extent of the melt defines the final cavity boundary. This annular zone is called the "blow-off" zone; it produces the rock that blows into the cavity where it mixes with and cools the melt. Assuming that the average thickness of this zone is 1.2 m surrounding an 18.7-m-radius sphere, then about 5.6×10^3 m^3 of rock mixed with about 3.2×10^6 kg of melt in the rubble is "blow-off" material from the cavity walls. The difference between 5.6×10^3 m^3 and the estimated total rubble volume is 11.46×10^3 m^3, which would roughly, be the amount added by ceiling collapse into the cavity. Figure 6.1b is a schematic drawing illustrating the "blow-off" phenomena and the various dimensions discussed above. Appendix E is a further discussion of the rubble distribution.

-38-

CHAPTER 4

FRACTURING AND DIFFERENTIAL ROCK MOTIONS

4.1 LOCAL UPLIFT OF STRATA OVER THE SHOT POINT

The existence of an uplifted region over the shot point was
inferred on the basis of permanent displacement data and a mech-
anism for its formation was discussed in Section 3.3. Additional
evidence pointing to its existence and crudely defining its shape is
discussed in this section. Figure 4.1 is a map of the ground-surface
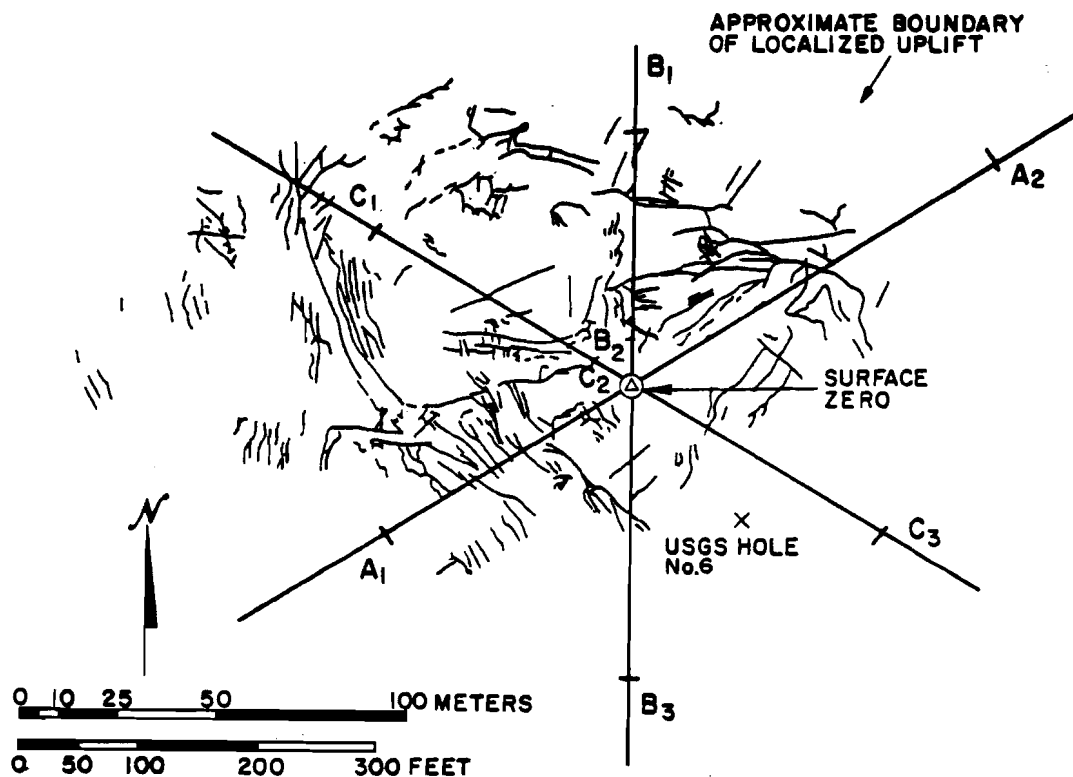
Fig. 4.1 Map of Gnome ground surface showing fractures and
approximate boundary of uplifted region (modified after Fig. 4.2 of
Reference 2).

fracture pattern produced by the explosion as mapped by Hoy and Foose (Reference 2). Figure 4.2 shows permanent-displacement profiles of the ground surface along Section A_1-A_2, B_1-B_3, and C_1-C_3 located in Fig. 4.1. As these profiles show, the surface
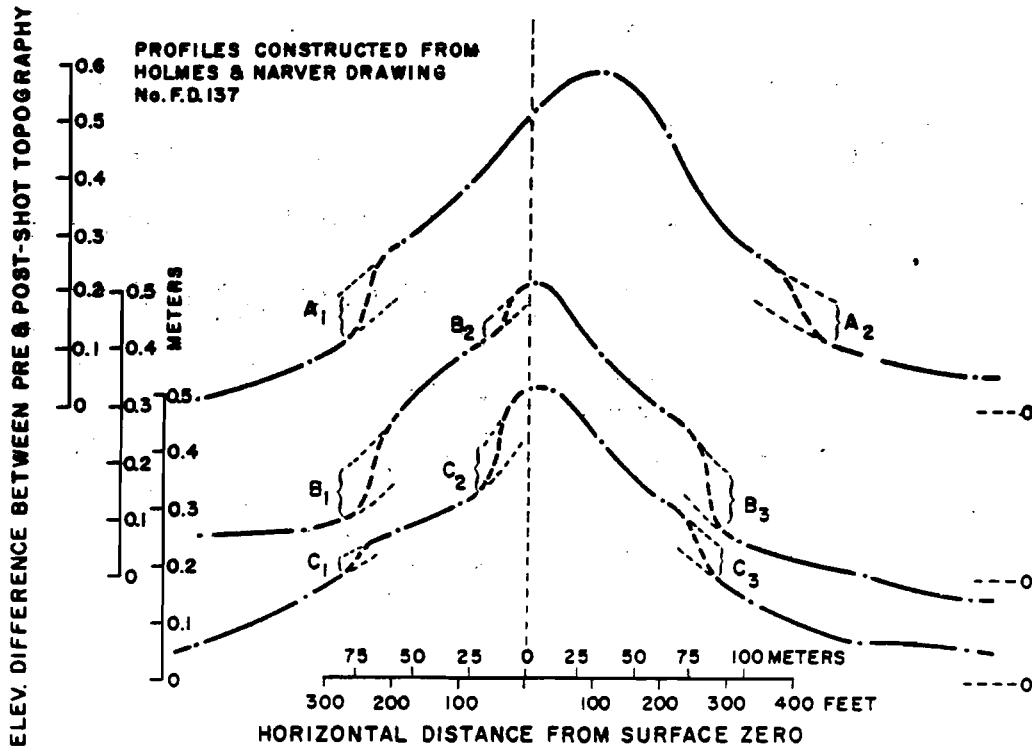
Fig. 4.2 Profiles of the Gnome ground-surface permanent displacements showing the uplifted region configuration (see Fig. 4.1 for plan view).

doming is not a smooth arch, but there are locations of abnormally large uplift or differential rock motion within fairly restricted zones (A_1, B_1, A_2, B_2, etc.). It is suggested that these zones may be the locations of the boundary of the uplifted region. Figure 4.1 shows the trace of these boundary zones based on the survey data and there

is a parallelism between this trace and the trace of observed surface fractures.

The USGS drilled vertical hole #6 at a distance of 46 m from surface ground zero. This hole encountered fractures at depths of 122 and 183 m from the surface (Reference 9). This fracturing may be associated with the boundary of the uplifted region. This boundary is probably broad and diffuse consisting of slightly folded strata and some shear fracturing. There is no evidence indicating that uplift though localized permitted leakage of radioactivity from the immediate cavity environment.

4.2 MELT AND GAS INJECTED FROM THE CAVITY INTO FRACTURES

Irradiation of rock salt results in distinctive yellow, blue, and purple coloration. For this reason, areas where radioactive gases were able to permeate are detectable even though radiation levels in some instances were near background at the time of exploration. Molten salt injected into cracks from the cavity characteristically is black and contains varying amounts of radioactivity. Using these color criteria, it was observed that above the working point, both gases and slightly radioactive melt permeated a distance of 38 m from the working point. This is rather surprising since a zone of greatly increased permeability extends vertically to a distance of about 105 m. Because of the infrequency of melt injections

-41-

LEGEND - Fig. 4.3

A. Echelon tension fractures resulting from movement on major thrust fault.   Probably extend full length of "buttonhook drift."

B. Voids encountered at this location.

C. Major thrust fault associated with closure of the "buttonhook drift."

D. Abrupt termination of radiation damage at tension fracture.

E. Approximate postshot boundary of left rib of "buttonhook" indicated by extent of melt and rock breccia.

F. Approximate extent of major tunnel closure.

G. Encountered water leakage from polyhalite #94 from this point to end of drift.

H. Location of accelerometer that failed at 16 msec.

I. Major overthrust fault with maximum observed displacement of 3 m (see Fig. 4.6a).

J. Postshot location of sand bags in hole #25 alcove.

K. Sheet of radioactive melt injected along a parting of clay beds.

L. Preshot location of hole #25 alcove.

M. Preshot location of "buttonhook drift."

NOTE: DATA SHOWN NORTH OF REFERENCE
LINE ARE PLOTTED AT ELEV. 676 METERS;
DATA SOUTH OF THE LINE PLOTTED AT
ELEV. 675 METERS.

BUTTONHOOK EXPLORATION
DRIFT

PRE-SHOT EMPLACEMENT DRIFT

MAIN POST-SHOT
EXPLORATORY DRIFT

VENTING PATH
REFERENCE LINE

W.P.

CAVITY WALL

LEGEND

RADIATION DAMAGED SALT

MELT &/OR MELT-ROCK BRECCIA

FAULT DIPPING 60°S E

HOLE NO. 25 DRIFT

HOLE NO. 12
DRIFT

HOLE NO. 3 DRIFT

HOLE NO. 8 ALCOVE

EXPLORATORY
DRILLING ALCOVE

SCALE

0 10 20 30 40 50
FEET

0   5   10   15
METERS

N
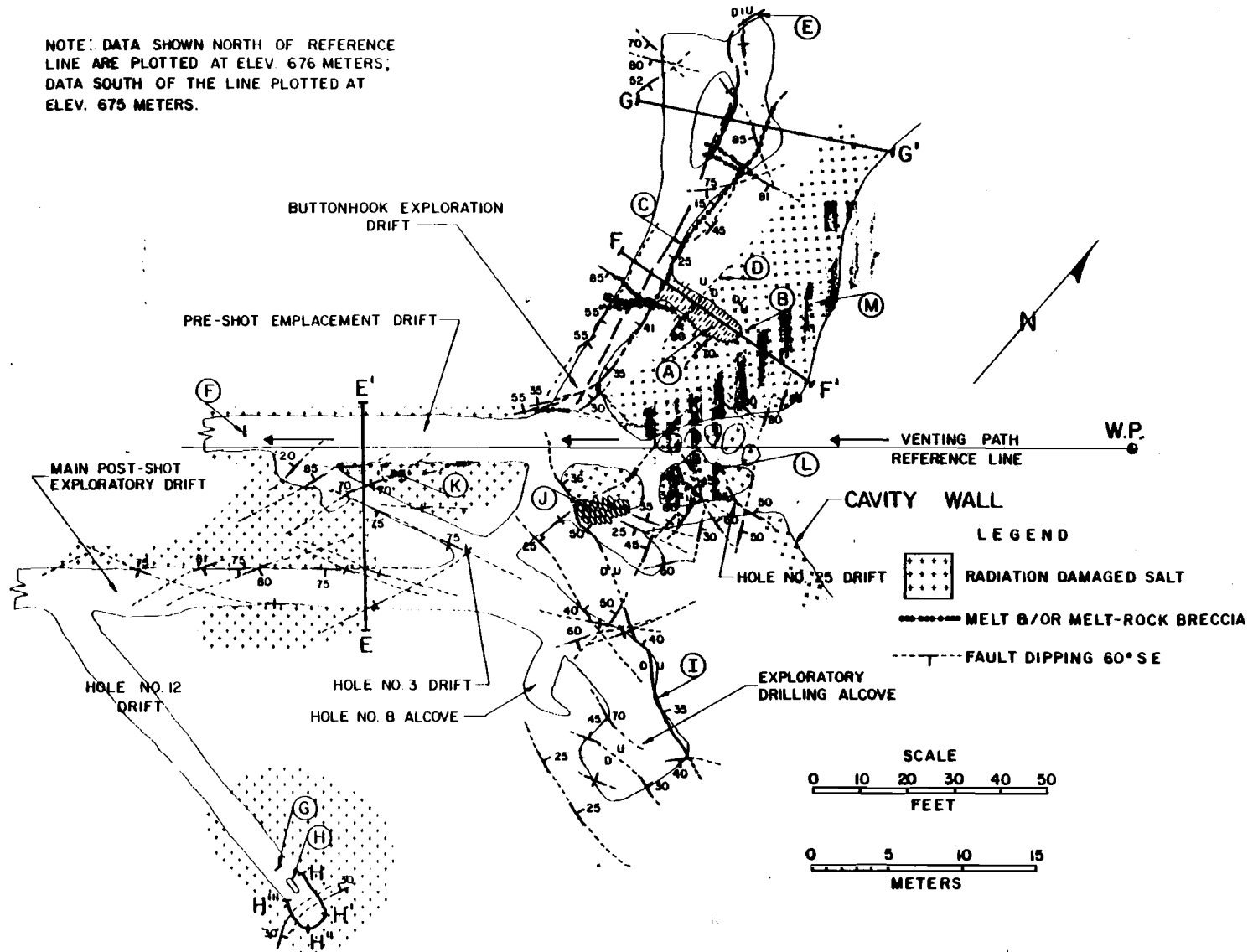
Fig. 4.3   Rock deformation revealed by postshot mining — plan view.

and radiation-damaged salt encountered in exploration of this region, the relatively short vertical extent of these injections above the working point, and since the amount of radioactivity in the injected melt is much lower than melt encountered within the cavity; it is concluded that the open fractures communicating with the cavity developed early during the dynamic growth period. Injection at this time (10-100 msec) is likely because good physical mixing between the molten rock and the vaporized fission products would not yet have occurred.

In the equatorial region beyond the cavity, melt was observed as far as 40 m from the working point, and evidence of gaseous injection was observed as far out as 65.5 m. These distances refer to melt and gas injections that are believed to be unrelated to the vent path down the line-of-sight emplacement drift. Melt was injected into a clay parting along the line-of-sight emplacement drift to a distance of 58 m from the working point, and melt was also in the drift as far away as the concrete block stemming (Fig. 1.2). Cracks from this drift were also permeable to gases. Figure 4.3 shows the fracturing and the distribution of radiation-damaged salt and melt injection in this equatorial region.

Preshot hole #12 was explored to recover an instrument that failed at 16 msec (Reference 6) following the explosion. It was found to have been located in a region of anomalously large rock deformation with accompanying radiation damage in the salt and water leakage (Fig. 4.3) indicating permeable communication with the cavity. The

early failure of the instrument, coupled with the intense local deformation and its associated permeability communicating with the cavity, indicates that the fracturing started at about 16 msec, or immediately following the passage of the compressional shock wave. The cross section H-H''' (Fig. 4.4) located in plan in Fig. 4.3 is a detailed map of the deformation at the end of the hole #12 drift.

SCALE

0   0.5   1.0   1.5 METERS

LIMIT OF RADIATION DAMAGE

INSTRUMENT HOLE No.12
ELEVATION: 672.6m

LEGEND

- POLYHALITE MARKER BED No.94 AND BASAL CLAY
- RADIATION DAMAGED HALITE ROCK
- PLASTICALLY DEFORMED HALITE ROCK
- SHEAR PLANES INTERTWINED ROUGHLY PARALLEL TO BEDDING. (THESE PLANES WERE PERMEABLE TO RADIOACTIVE GASES)
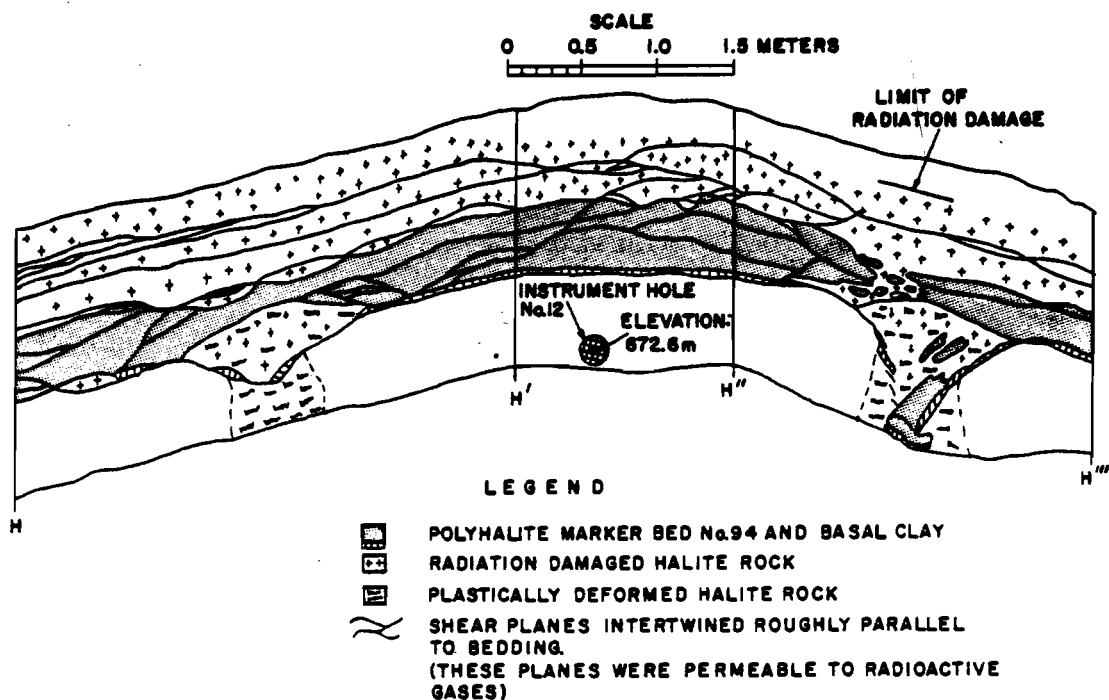
Fig. 4.4   Vertical section H-H''' showing deformation at end of hole #12 drift (see Fig. 4.3 for plan view).

Note the local downward motion of rock unit #93 through and mixed with that of the lower rock unit #94. This is very intense deformation at a distance of 65 m and compares with the intensity of deformation associated with closure of the "buttonhook" drift at a distance of about 30 m from the working point. The possible existence of a

-45-

natural cavity in the salt near the instrument location that was col-
lapsed by the shock wave could be the explanation of this deformation.
Such cavities are known to occur in the Salado formation (C. Jones,
verbal communication) and are generally brine-filled. Figure 4.5
also shows the anomalously large radial displacements in that region.
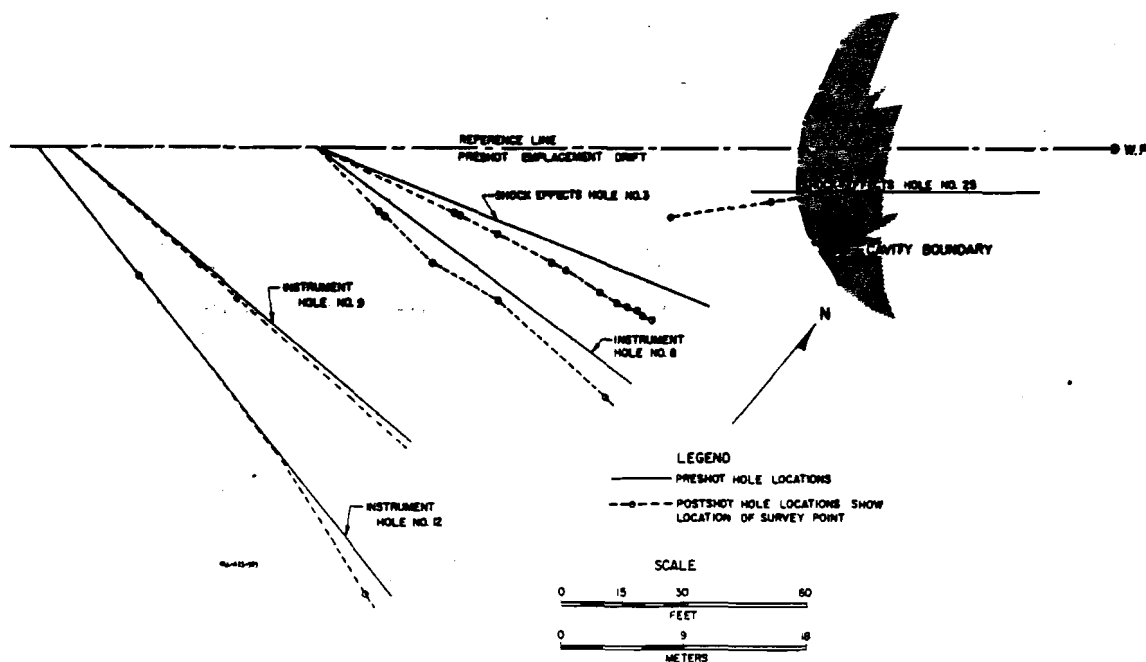
Fig. 4.5 Displacement of underground instrument and shock-study
sample holes — plan view.

Exploration along the postshot location of the "buttonhook" drift,
Fig. 4.3, encountered nonradioactive melt that was injected into the
open drift and was then caught up in the rock motions associated with
the drift closure. This relationship again supports the thesis that
melt and possibly some radioactive gases escaped from the cavity

primarily during dynamic cavity growth. An exception, of course, is melt and gases that vented into the emplacement drift.

Below the shot point, neither melt samples, radiation-damaged salt, nor radiation levels above background, were noted further than 25 m from the working point or 6 m beyond the cavity edge.

4.3 DEFORMATION SURROUNDING THE CAVITY

Fractures resulting from the expanding cavity produced by the explosion and subsequent fracture development associated with unloading of the compressed rock can be grouped into the following four general categories:

(1) Radial tension cracks emanating from the cavity;

(2) Peripheral faults with planes that generally parallel the cavity boundary;

(3) Bedding plane faults;

(4) Near vertical joints primarily in the vicinity of preshot emplacement drifts.

Figure 4.3 shows the projection of the traces of major faults, and joints at the elevations of 674.8 and 675.7 m that were revealed during mining exploration. Figure 2.1 is a reflected ceiling plan of the interior of the cavity showing the traces of major radial cracks. These cracks (type 1) occur with a frequency of about one every 4 or 5 m at the equator of the cavity and extend to a distance laterally and above the cavity of about 38 m. These are the cracks containing

-47-

injected melt (see Fig. 4.3 in the region of the "buttonhook drift" and the vertical section Fig. 2.2).

Also shown in these two figures are the curved peripheral faults. Below the shot point in drill holes B and C, the peripheral faults (type 2) are inferred from the attitude of fault planes in the core relative to the orientation of bedding planes. In the vicinity of the drill alcove (Fig. 4.3), this type of faulting grades into overthrust faults that further grade into horizontal bedding-plane slips along clay seams. Figures 4.6a and b shows examples of this kind of faulting. The throw or differential motion between blocks was measured to be 2.5 to 3.0 m across the fault marked (I) in Fig. 4.3. This was the largest fault observed; most differential motions are on the order of 0.5 m or less. This peripheral type of faulting does not contain melt injections and is probably formed after cavity growth when unloading or rebound adjustments to the stressed rock are likely to take place. Associated with these curved faults emanating from the region below the cavity is a gentle upwarping of the strata in the equatorial region. Marker bed #94 which was located a few meters below shot point became uplifted from its preshot elevation out to a distance of about 64 m. Beyond that point, the vertical displacement is not measurable. In the drill alcove polyhalite marker bed #94 was uplifted from 0.3 to 0.6 m instead of being depressed. This bed was located below the working point elevation prior to the explosion (see Fig. 2.1).

-48-

(a)
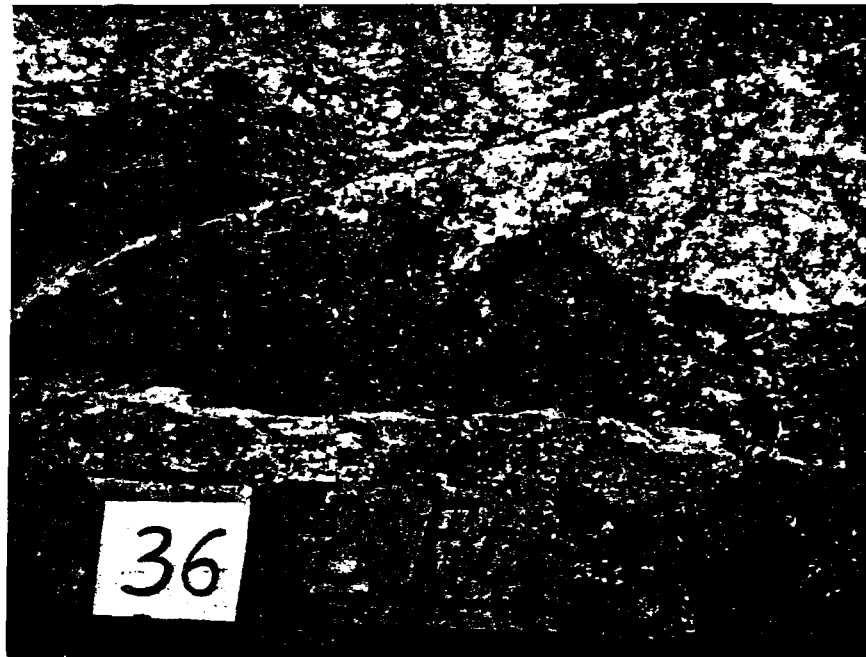
(b)

Fig. 4.6 Typical faults produced by the explosion:

The near-vertical joints are primarily associated with deformation in the rock near the line-of-sight portion of the emplacement drift. These joints form two distinct sets that intersect each other in a criss-crossed or trellis pattern. At a distance of 60 m from the shot point, the joints intersect the line of the drift at an angle of about 20°. Close to the cavity edge this angle has increased to 75°. Figure 4.3 shows some of the major joints mapped and Fig. 4.7 is a schematic drawing illustrating the trellis pattern of the joints and fractures associated with the line-of-sight drift. If this idealized
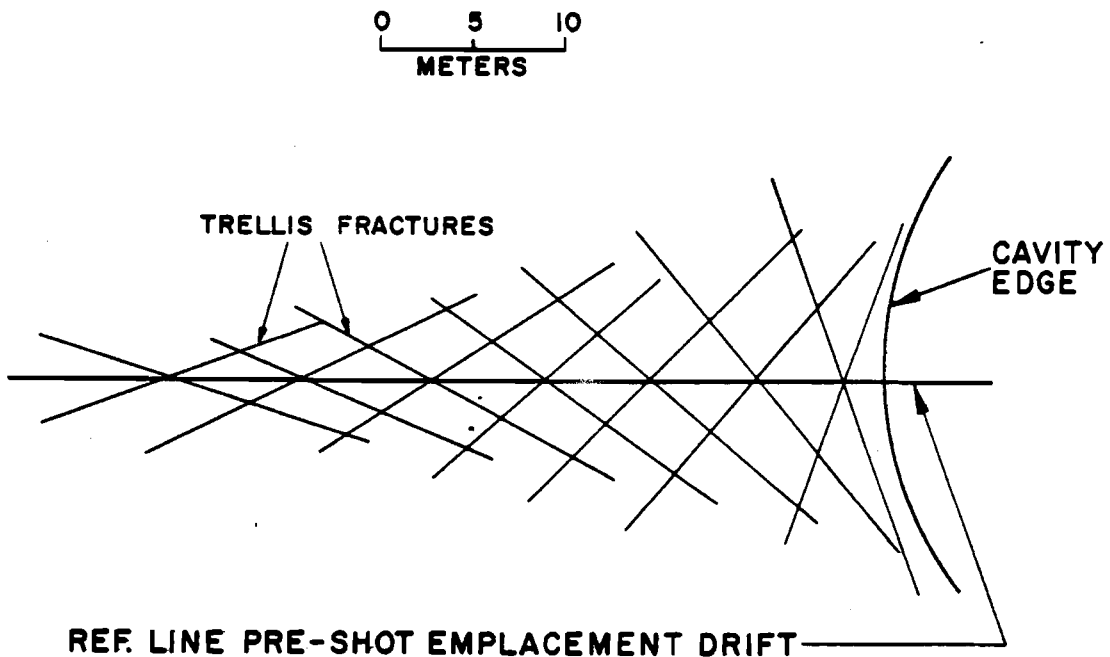
Fig. 4.7 Plan schematic of trellis fracture pattern associated with deformation along the line-of-sight emplacement drift.

interpretation is correct, it indicates that the rock bounding the drift failed in shear as the compressional wave passed and subsequent cavity growth distorted these weak zones.

4.4   DEFORMATION OF THE PRESHOT EMPLACEMENT DRIFT

In addition to the trellis pattern of fractures associated with the deformation of the line-of-sight portion of the emplacement drift, the drift was noticeably constricted by plastic deformation.   Cross section E-E' (Fig. 4.8) located in plan on Fig. 4.3 shows the approximate size of the postshot emplacement drift at 53.3 m from the working point compared to its preshot cross section.   At this distance, the drift apparently squeezed nearly shut prior to venting and was
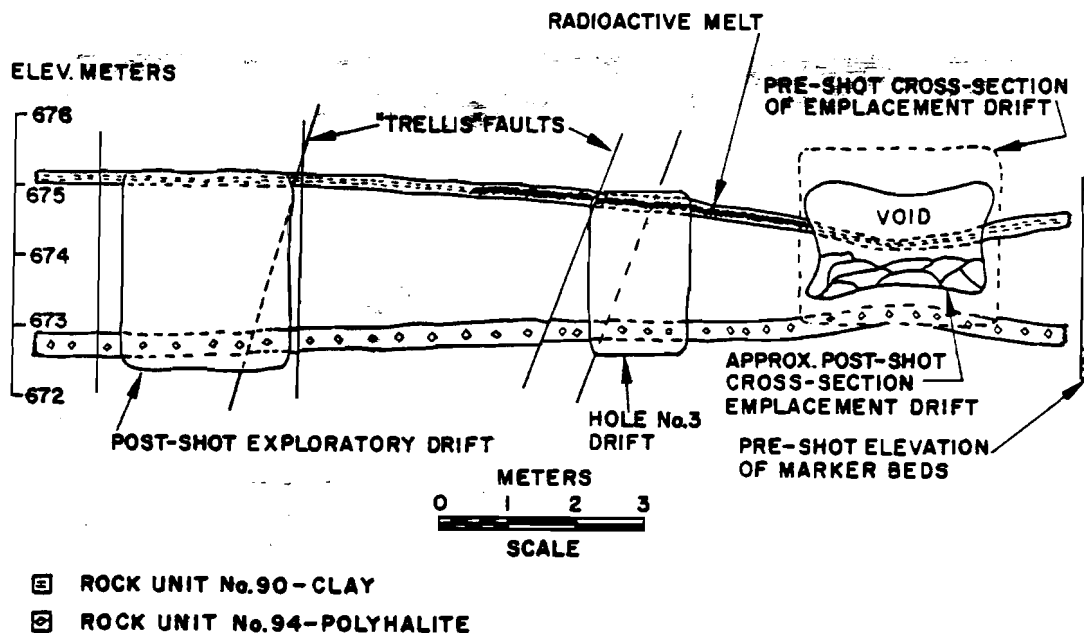
Fig. 4.8   Vertical section E-E' showing partial closure of preshot emplacement drift (see Fig. 4.3 for plan view).

-51-

then blown open to its final shape when venting occurred (see discussion on Venting — Chapter 5).

The curved or "buttonhook" portion of the emplacement drift sealed effectively and was not involved in the cavity venting process. The explored portion of this drift was tangential to the shot point rather than radial (as was the emplacement drift in the previous discussion), and the nature of tunnel closure was quite different. In the line-of-sight drift, ineffective closure was accomplished by plastic flow and slippage along the trellis fractures. In the "buttonhook" portion of the drift, the radial component of the outward moving, compressional shock wave met the drift at a right angle and virtually slammed one wall into the other. More precisely, the closure was accomplished by the movement of a wedge-shaped block into the open drift. The boundaries of this major block are partly controlled by clay seams in the rock that appear to have lubricated the movement of the major block. Figure 4.9 shows two cross sections illustrating the detailed structure of the deformation; their locations in plan view are marked in Fig. 4.3.

In the vicinity of Section G-G', radial cracks following the compressional shock wave opened up, allowing superheated melt to enter the drift prior to its closure. Here, the melt was mixed and trapped with the rock moving to seal off the drift and it formed the matrix of a melt-rock breccia. As it was injected into the drift, the melt encountered lead bricks and wood in an instrument alcove

CAVITY WALL

MELT & SOOT-COATED BLOCKS

MELT & SOOT-COATED VOIDS

CONTAINING MANY ROCK FRAGMENTS OF No.91-92 & A FEW OF No.82-89

MELT OF U

EXPLORATORY DRIFTS

ELEV. (m)
678
677
676
675
674
673

G

CAVITY WALL

PRE-SHOT LOCATION OF ROCK UNITS

No.81

CLAY

No.90

82-89

91-92

CLAY

PRE-SHOT LOCATION OF BUTTONHOOK DRIFT

RADIATION-DAM ARROW TO CAVITY WITH NUMEROUS JOINTS.

EN ECHELON

METERS

0   1

EXPLORATORY DRIFT

MELT BRECCIA MARKING POST-SHOT BOUNDARY OF BUTTONHOOK DRIFTS.

ELEV (m)
678
677
676
675
674
673

F

G'

F'

Fig. 4.9 Vertical sections F-F' and G-G' showing closure of "buttonhook drift" (see Fig. 4.3 for plan view).

off the drift. The lead melted and the wood burned mixing with the salt-melt breccia. Analyses of the melt breccia shown in Fig. 4.10a, b, and c, indicate that lead combined with sulfur and chlorine from the melt to form galena (PbS) and laurionite ($Pb[OH]_2 \cdot Pb[Cl]_2$) (Reference 10). The laurionite was probably formed by the reaction of water dissolved in the salt melt with $PbCl_2$. The sulfur necessary to combine with the lead was probably released by a reduction of sulfates associated with the molten salt. Hydrocarbons from the burning wood created a reducing atmosphere. An alternative explanation of the formation of the melt breccia is that it was produced locally in the drift by extremely high pressures and temperatures developed from the dynamic conditions of closure. The hypothesis of melt injection from the cavity (even though it is nonradioactive) is most consistent with the relationships observed. Some of these relationships are as follows:

1. Voids in the same region are coated with a mixture of soot, lead, and fused salt (see Section G-G' of Fig. 4.9);

2. In the breccia, insulation was still on wires and shock-produced Neumann bands[*] were not found in recovered steel samples that had been intimately mixed with the melt, indicating not nearly high enough pressures developed for melting;

---

[*]Neumann bands are characteristic deformation features in steel caused by intense shock or impact loading.
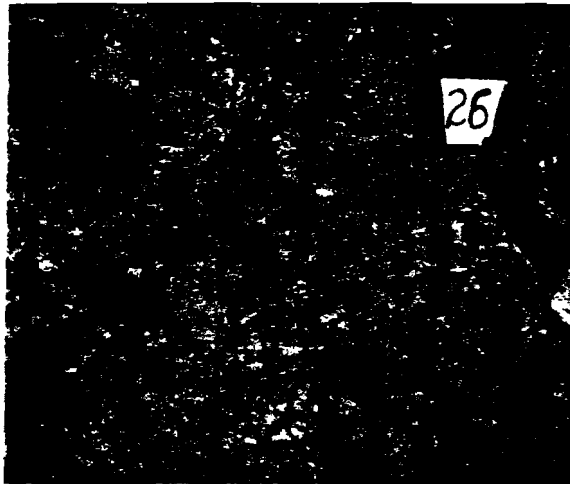
(a)

(b)

(c)

Fig. 4.10   Intrusive melt breccia.

3. The percentage of melt, lead, and carbon in the breccia decreases from that located in the vicinity of cross section G-G' until absent from the breccia in the vicinity of cross section F-F'. Most of the matrix of the breccia is clay at that location.

4. As shown in Fig. 4.2, the preshot size of the drift was large where the alcove is located compared to the rest of the drift. This portion of the drift is also nearest the shot point and thus a logical place for cracks to open to melt injection from the growing cavity. If the melt was injected from the cavity into the cracks ⟨illegible⟩ to follow imme⟨illegible⟩d ⟨illegible⟩ ⟨illegible⟩ to the drift prio⟨illegible⟩ This ⟨illegible⟩ occu⟨illegible⟩ in the dynamic cavity growth per⟨illegible⟩ the cavity was small and the thickness of ⟨illegible⟩ melted by the shock waves was relatively large (see Fig. 6.1a). Under these conditions poor mixing of the thick melt zone with the vaporized fission products would be likely and then explain the nonradioactive melt found in the drift.

CHAPTER 5

VENTING

5.1 THE VENTING PROCESS

Before developing a generalized interpretation of the venting processes a few pertinent facts and comments should be made:

1. As shown in Fig. 1.2, the neutron pipe was an open pipe that extended from the line-of-sight portion of the emplacement drift to the working point, thus introducing an inherent weakness in that region.

2. As shown in Fig. 4.9, the strata at the elevation of the emplacement drift were characterized by several clay seams of unusually low tensile strength. The clay is also very plastic, thus introducing another weakness.

3. In Section 4.4, it was mentioned that the squeezing action to close off the line-of-sight drift was ineffective compared to the tight closure of the drift where its walls were oriented tangentially, and not radially, to the shot point.

4. The block motion associated with the closure of the "button-hook" portion of the drift must result in the development of a boundary weak zone in the vicinity of the neutron pipe since south of this pipe (Fig. 1.2) there is no drift and radial rock movement would be less.

5. As shown in Figs. 4.3 and 4.8, radioactive melt was injected from the partly closed emplacement drift as a sheet into a parted clay

seam. Here the melt quenched and was not vesiculated indicating that it solidified under high pressure and, therefore, before the pressure drop that resulted from venting.

6. Venting occurred within 1 minute after the explosion (Section 1.4).

Between about 100 msec and one minute following the explosion, melt and gases were able to penetrate from the cavity into the closed but apparently permeable line-of-sight portion of the emplacement drift. This zone was especially weak for reasons 1 through 4, listed above.

The compressional wave produced by the explosion was reflected at the ground surface and returned to the cavity region as a rarefaction wave at about 320 msec. The intensity of this wave may have been great enough to put the rock into tension and cause parting of the clay seam (5 above). The permeability in this region would then be momentarily increased so that melt could be injected from the cavity into the parting and probably then into the more permeable or open drift beyond. When this occurred there was no longer much resistance to the cavity pressure and dynamic venting occurred. Melt, rock, neutron pipe, vent line, and most of what was in the drift were blown down the drift. Much debris piled up at the cement domino (Fig. 1.2). Radioactive melt was encountered as far as the concrete block stemming (Fig. 1.2). This stemming effectively throttled the dynamic venting and converted it to a leak. The drift

from the stemming into the cavity was probably near the overburden pressure of 1,200 psi. From the porous plug to the blast door, the pressure built up about 55 psi – sufficient to break one of two rupture disks in the blast door. From there, the blow-out continued up the shaft, through a filter and out into the open. The concrete block stemming performed as it was designed, to hold overburden pressure, but it was not gas-tight. Particulate radioactivity and violent venting were contained underground while steam and gaseous fission products escaped.

As was pointed out by E. Teller (Reference 11), the knowledge of how to control venting could be very important in recovering gaseous redioelements from a specially designed nuclear device. By accident, Gnome venting contributed greatly to this knowledge.

5.2 THE VENT PATH ENVIRONMENT

Following is a pictorial trip down the vent path from the shaft station down the emplacement drift and into the cavity:

Re-entry down the shaft 6 days following the explosion revealed very little damage. Hairline cracks were observed in several places in the concrete lining of the shaft between the surface and the top of salt. In general, these cracks correlate with the location of bedding planes between differing rock strata. Several below a depth of 146 m were seeping water. Others developed at joints in the cement. In the salt, there is an indication of slight parting at several places.

These were invariably associated with the bedding plane boundaries of clay seams and stringers of polyhalite and anhydrite – planes of essentially no tensile strength. In general, very little rock spalled from the shaft walls. At a depth of 326.1 to 327.4 m, about 2.5 m^3 of material spalled from a very friable siltstone. The cage was lowered to within a few meters of the bottom station or drift level where the displacement of a metal safety railing stopped it. Fig. 5.1 shows the descent from the cage to the drift level and damage at the bottom station. Note the sag of the ceiling where spall occurred to a clay layer located 1 m above. Spall is the major damage in this region and most likely would not have occurred if that clay seam had been immediately above the drift. A 4.6-m-deep sump at the bottom of the shaft was full of water and the drift floor had up to 25 cm of standing water. Most of the water condensed from vented steam; however, some also seeped from the above-mentioned cracks. The salt exposed in these underground workings was colored due to the high radiation fields developed as a result of venting.

Figure 5.1b shows the "I" beam wall buttressing the concrete block stemming through which leakage occurred. It was determined that leakage was restricted to this region by pressurizing the Gnome cavity with air and surveying the vent path leakage.

Figures 5.1c and d show a comparison of the preshot and post-shot condition of a portion of the drift between the concrete block stemming and the blast door, a distance about 270 m from the shot

(a)
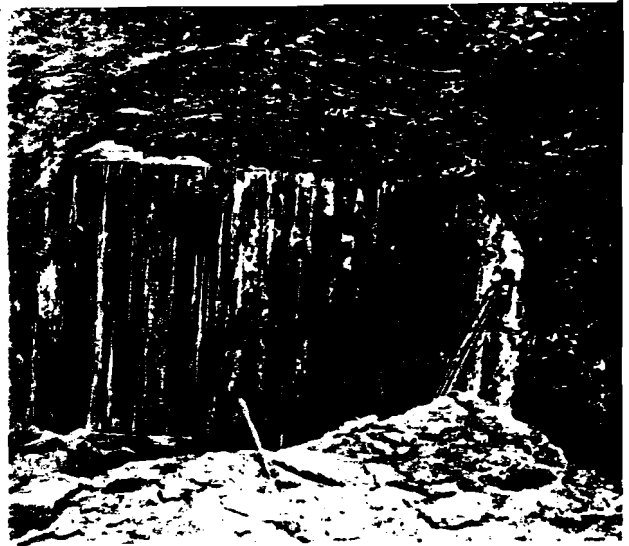
(b)
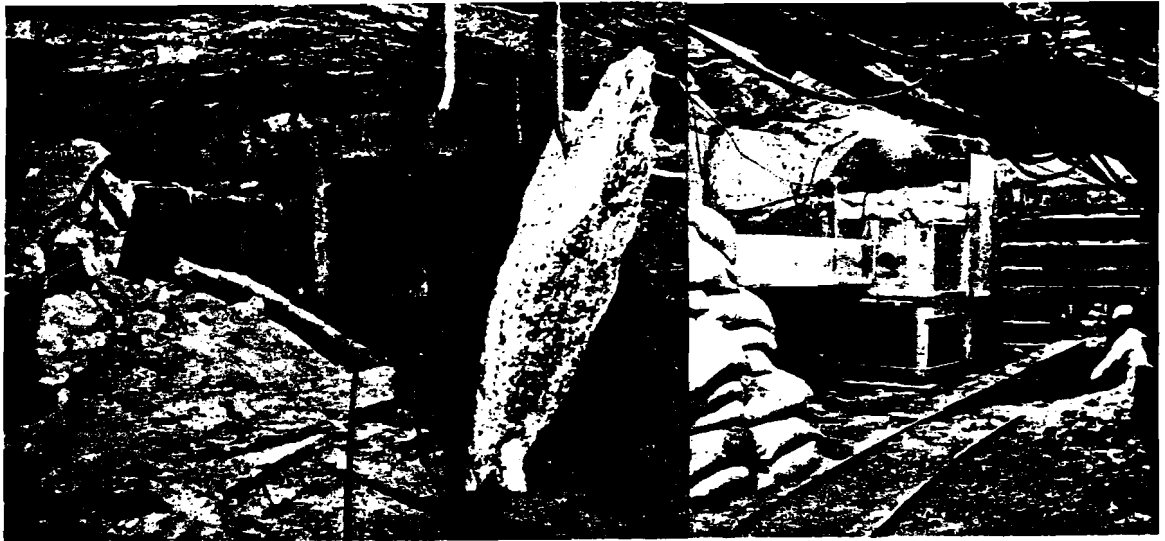
(c)

(d)

Fig. 5.1 Deformation of emplacement drift near shaft.

point. Again, most of the damage resulted from spall of the back to the clay seam.

Figure 5.2a shows the drift on the side of the concrete block stemming that experienced dynamic venting. Here, in addition to spall, there is evidence that material had been transported down the drift and had been subject to high pressure.

Figure 5.2b shows the collapsed neutron pipe in this region. Radioactive melt was also found that was ejected from the cavity. Radiation field levels were 1 to 3 R/hr (gamma radiation) six months following the explosion and the levels varied greatly, but generally decreased toward the cavity. Readings were generally between 1 R/hr and 100 mR/hr in the drift.

Figure 5.2c shows the drift in the vicinity of crosscut 1 (Fig. 1.2) approximately 105 m from the shot point. Note the curved distortion of the back and the bent bars and straps. Also, considerable scour of the walls was observed testifying to the violent movement of debris down the drift.

Figure 5.2d shows the boundary of a shear zone that was encountered while excavating crosscut 2 (Fig. 1.2). In this zone shearing in a horizontal direction occurred along vertical planes striking parallel to the emplacement drift. It extends from the right rib of the drift into the wall rock about 3 m and is associated with the failure of a drill alcove excavated on the right rib of the emplacement drift. The drill alcove was a departure from the line-of-sight drift,
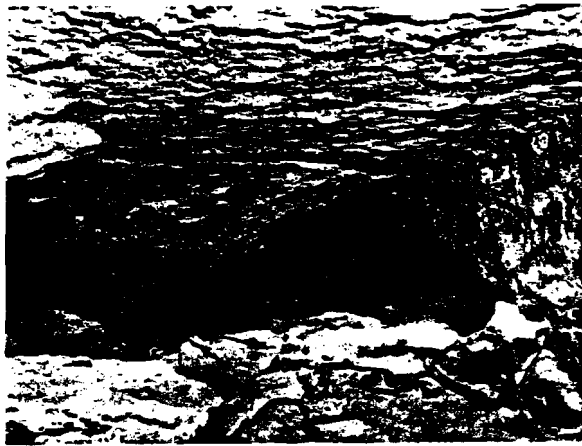
(a)

(b)

(c)

(d)

Fig. 5.2   Deformation of emplacement drift between shaft and cavity.

-63-

in that the walls were no longer line-of-sight to the shot point in the
alcove. This apparently was a significant perturbation on the stress
distribution associated with the compressional shock wave causing
the rock beyond the alcove and adjacent to the emplacement drift
to fail in shear.

Figure 5.3a shows the drift at a distance of about 41 m from
the shot point near the end of the postshot location of the line-of-
sight portion of the emplacement drift. Here the salt is pock-marked
with many large etch pits caused by steam erosion. The smooth
dark patch in the center of the picture is a pond of water that con-
densed from the vented steam and the white crust is re-crystallized
salt left by evaporation of brine.

Figure 5.3b is a picture of a small portion of the breakthrough
region between the cavity and the line-of-sight drift. It is possible
to crawl from the cavity through to the drift.

Figure 5.3c is a view from inside the Gnome cavity looking
toward the portal to the vent path at the cavity wall.

Figure 5.4 is a view of the cavity interior; the arrow points
to a man for scale. The stalactites resulted from the evaporation
of brine introduced during re-entry drilling.

(a)

(b)
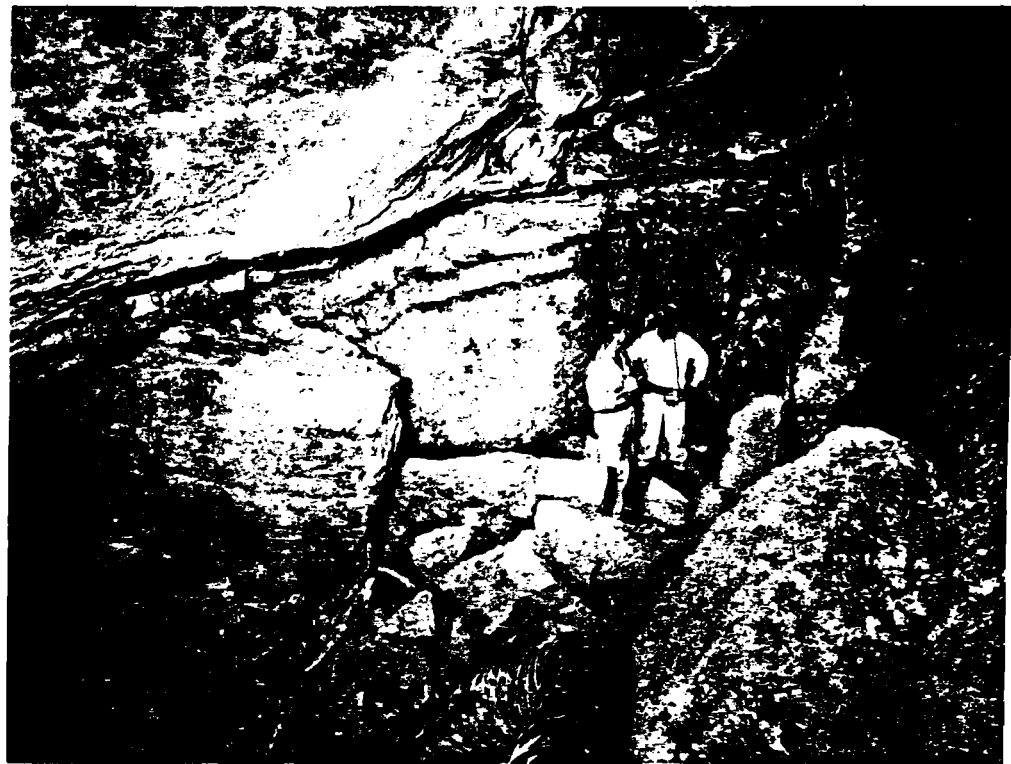
(c)

Fig. 5.3 Vent path.

Fig. 5.4 View of interior of the Gnome cavity. Note size of man.

CHAPTER 6

AN INTERPRETATION OF THE EXPLOSION DYNAMICS

The description of the environment created by the Gnome event and the interpretations of processes leading to the observed results have been rather arbitrarily compartmentalized for the purposes of presenting the data. Actually, the period of cavity growth is about 100 msec, the accumulation of the melt and rubble at the base of the cavity was completed after a few minutes, and venting was complete in about 24 hours. Thus, the environment described resulted from very dynamic conditions and the observed effects are greatly inter-related. In order to convey some feeling for the development of the environment observed, a sequence of schematic illustrations have been prepared re-constructing the growth of the cavity as a function of time (Fig. 6.1). The illustrations are, of course, idealized; guidance for the temperature and pressure of the cavity gas was obtained from calculations made by Fred Seidl and Arturo Maimoni of LRL. These are order-of-magnitude approximations.

Figure 6.1a shows the cavity at about 3 msec and Fig. 6.1b at about 30 msec. When the nuclear device explodes, it creates an expanding plasma of extremely high temperature and pressure on the order of a few million degrees Celsius and several million bars. The plasma expands and slams into the confining rock, creating a supersonic compressional shock wave intense enough to vaporize

-67-

1   Working Point — center of the nuclear explosive device.

2   Vaporized and ionized rock and device material.

3   Rock fused by supersonic compressional shock wave.

4   Location of rock strata.

5   Outgoing compressional shock wave.

6   Radial cracking and melt injection.

7   Rarefaction wave returning from ground surface.

8   Zone of rock that breaks up and "blows off" cavity surface.

9   Rock from 8 mixes with melt 3 and begins to accumulate a "puddle" at cavity base.

10   Return of rarefaction wave 7 leads to slight cavity growth and uplift of ceiling.

11   Fractures associated with uplift of cavity ceiling.

12   Extension of radial fractures and further melt injection.

13   Bedding plane partings in rock strata.

14   Probable time of venting from cavity into emplacement drift.

15   Melt and rock breccia — "puddle."

16   Rubble from ceiling collapse.

Figure	A	B	C	D	E	F
Time	~3 msec	~25 msec	~300 msec	~1 sec	~1 min	~5 min
Cavity Temperature (°C)	~100,000	~20,000	~4,000	~2,000	~1,000	~500
Cavity Pressure (bars)	~400,000	~300	~80	~40	~20	~5
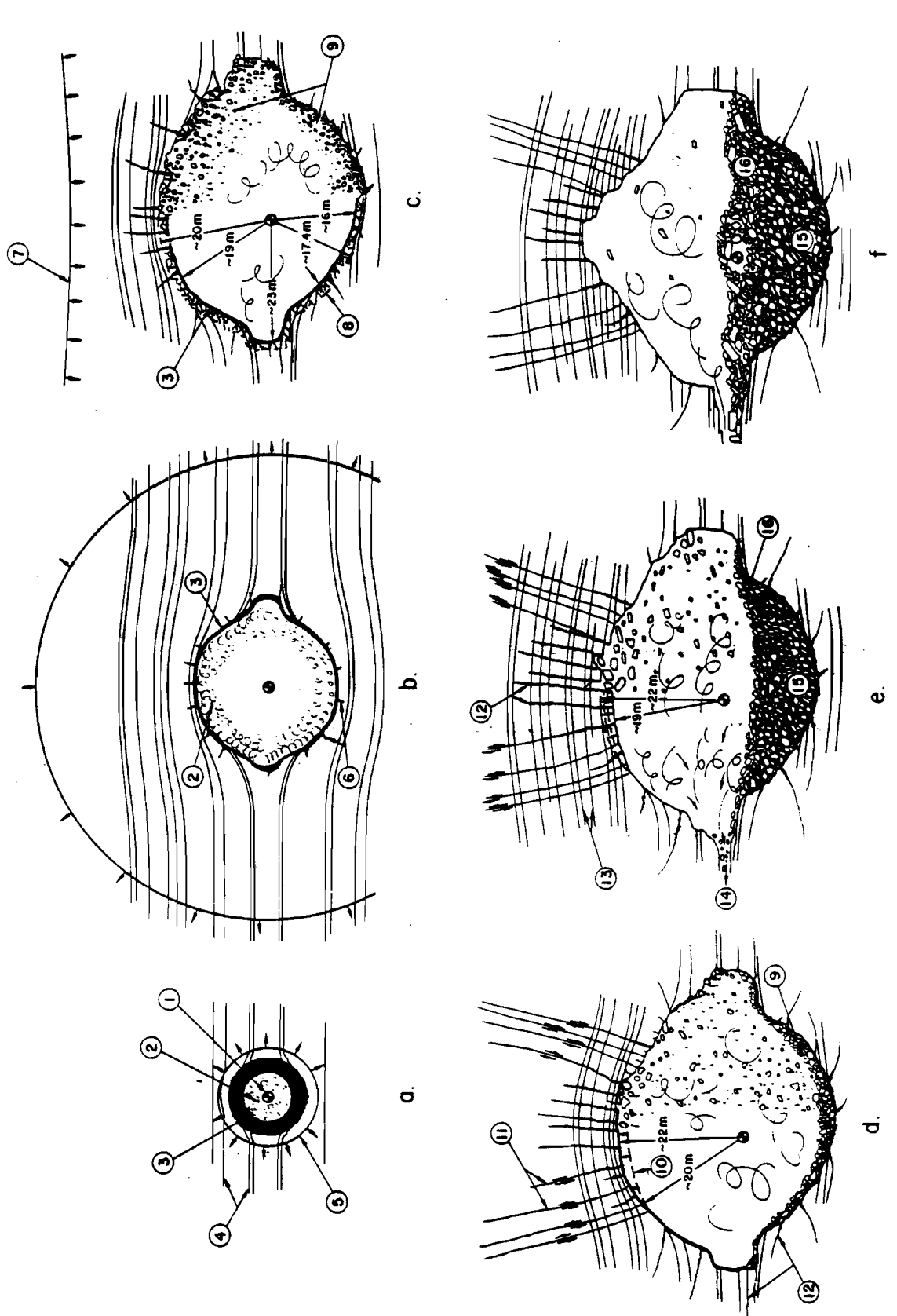
Fig. 6.1 Schematic vertical sections showing cavity development.

-69-

rock for some distance and then melt it for a further distance (about 7 m in the case of Gnome). The shock wave moves out, compressing the rock and decreasing in intensity with distance. It soon becomes a wave moving at the sonic velocity of the rock. The growth of the cavity follows behind the compressional wave and expands because of the driving force of the gas until the internal pressure is balanced by the resisting overburden pressure. At about 100 msec the expansion of the cavity is complete and the compressional shock wave has travelled a distance of about 475 m horizontally and about 300 m vertically (Reference 6). In the case of Gnome, it appears that the force resisting cavity growth in the direction parallel to the bedding planes in the rock was less than in the direction normal to these planes; this led to the development of the bulge in the equatorial region of the cavity. During this time period, radial tensional cracks opened up permitting the injection of melt and possibly some gas from the cavity. Generally, the injected melt contains little or no radioactivity because of poor mixing with the vaporized fission products.

As the expanding cavity comes to rest, the lining of fused rock flows and rains under the influence of gravity. This brings the melt into intimate contact with the condensing radioactive vapor and traps much of the fission debris. Near the end of cavity growth (Fig. 6.1c), "blow-off" of the cavity wall rock occurs resulting in rather intimate mixing of cooler rock and rapidly dropping temperatures inside the cavity. Since molten salt is about as fluid as water,

-70-

it fills most of the pore spaces in the lower hemisphere that developed
as the wall rock breaks up and is quenched where in contact with the
cooler rock. The rain of rock and melt creates a "puddle" at the
base of the cavity where the nongaseous fission products are trapped
(Fig. 6.1d and e).

While the puddle is forming another important event occurs —
the arrival of the rarefaction wave from the ground surface. This
wave tends to put the rock into tension, or at least decompression,
and provides one mechanism for relief of the compressed and
stressed rock and also slight further expansion of the cavity if its
pressure then exceeds the resisting pressure of the confining rock
(Fig. 6.1d). While the rarefaction wave travels from the ground
surface back to the cavity region, the upper few hundred feet of
rock spalls, and at Gnome the free-flight period for the ground sur-
face lasted from 157 msec to a little over 1 second following the
explosion (Reference 6). This allowed time for the rarefaction wave
to return to the cavity and localized uplift to develop in the rock
overlying the cavity, while the overburden weight decreased because
of spall of the upper rock layers. Also at this time, compressed
rock surrounding the cavity was unloaded and adjustments were
made — most notably the upward arching of the rock surrounding
the cavity. A most probable time for venting would be at this time,
when the rarefaction wave arrives, tending to part the rock strata
and provide an escape path from the cavity to the open drift. The

rarefaction wave would also shake the cavity which might disrupt its stability and initiate some roof collapse.

Figure 6.1e shows the cavity after venting. Melt and rubble are still accumulating in the base of the cavity. The uplifted rock sags or partly drops back toward the cavity, leaving partings along the bedding planes between rock strata, and the ceiling of the cavity collapses.

In Fig. 6.1f, the "smoke is clearing," and the envisioned picture is very similar to that observed on re-entry exploration.

REFERENCES

1. Hydrologic and Geologic Studies, Project Gnome Report PNE-130F, U. S. Geologic Survey, September 25, 1962.

2. Hoy, R. B. and R. M. Foose, "Earth Deformation from a Nuclear Detonation in Salt," PNE-109P, Stanford Research Institute, March, 1962.

3. Randolph, P. and G. Higgins, "Various Papers Giving Some Early Gnome Results," Lawrence Radiation Laboratory (Livermore, California) Rept. UCID-4423, January 19, 1962.

4. Higgins, G. H., D. E. Rawson, and W. Z. Wade,"Chemical Reactions Induced by Underground Nuclear Explosions," Lawrence Radiation Laboratory (Livermore, California) Rept. UCRL-5882 Rev., 1961.

5. Nathans, M. W., "Isotope Program," PNE-102F (to be published).

6. Weart, W. D., "Particle Motion Near a Nuclear Detonation in Halite," PNE-108P, 1961.

7. Holmes and Narver, Field Drawing #F-01371, December 27, 1961.

8. Gard, L. M., "Lithologic Log of the Recover-Hole Core, Project Gnome," U. S. Geol. Surv. Tech. Letter, Gnome 1, November, 1961.

REFERENCES (Continued)

9. Sterrett, T. S., "Summary of Drilling Data for USGS Hole 6 and 7, Project Gnome," U. S. Geol. Surv. Tech. Letter, Gnome 14, September, 1962.

10. Gard, L. M., "Some Geologic Effects of the Gnome Nuclear Explosion," U. S. Geol. Surv. Tech. Letter, Gnome 15, October, 1962.

11. Teller, E., "Plowshare," Nuclear News, Vol. 6, No. 3, March, 1963.

APPENDIX A

DESCRIPTION OF ROCK STRATA SURROUNDING
THE GNOME EVENT

The rock units described below indicate the variability of strata in the vicinity of the Gnome event, and Figs. 2.1, 2.2, 2.3, 4.4, 4.8, and 4.9 are maps showing the relations of certain of these units to other features produced by the explosion. The descriptions are condensed from the USGS Lithologic Log of the AEC Recovery Hole (Tech. Letter: Gnome-1). The unit numbers were derived by assigning number 1 to the first unit described in this log, at a depth of 304.8 m, and then continuing consecutively through the last unit described, No. 135, which ends at 396.2 m. In the listing below, units which are referred to in this report are grouped together for purposes of simplicity and clarity.

Unit Nos.	Preshot depth (m)	Description
14 - 17	311.7 - 314.9	Clear halite rock with minor clay and polyhalite
18 - 20	314.9 - 316.1	Halite rock, clayey at top, 40% polyhalite in middle
21 - 26	316.1 - 317.3	Clear halite rock with considerable polyhalite and red clay near bottom
27	317.3 - 317.7	Polyhalite rock
28	317.7 - 320.3	Orange halite rock with minor poly- halite

Unit Nos.	Preshot depth (m)	Description
29 - 31	320.3 - 322.4	Halite rock, with several clay layers
32 - 34	322.4 - 323.9	Orange halite rock with thin polyhalite layer
35 - 37	323.9 - 325.4	Claystone and clayey halite rock
38	325.4 - 328.4	Orange halite rock with minor polyhalite and silt
39	328.4 - 328.9	Clayey halite rock
40 - 41	328.9 - 331.1	Reddish halite rock with minor clay and polyhalite
42	331.1 - 332.9	Polyhalite rock, with halite and clay layers
43	332.9 - 336.5	Halite rock with minor polyhalite
44	336.5 - 337.2	Clayey halite rock
45 - 51	337.2 - 339.5	Halite rock with minor silt and polyhalite
52 - 60	339.5 - 343.1	Polyhalite, halite, anhydrite and clay layers
61	343.1 - 344.3	Silty halite rock
62 - 64	344.3 - 345.9	Halite rock with clay and polyhalite
65	345.9 - 350.8	Halite rock with many thin layers of anhydrite
66 - 77	350.8 - 352.4	Halite rock with clay and polyhalite layers
78 - 80	352.4 - 357.2	Halite rock with considerable polyhalite and clay
81	357.2 - 357.7	Polyhalite rock (Marker Bed #120)
82 - 93	357.7 - 361.9	Halite rock with clay and polyhalite

Unit Nos.	Preshot depth (m)	Description
94	361.9 - 362.3	Polyhalite rock (Marker Bed #121)
95 - 98	362.3 - 366.1	Orange halite rock with minor poly-halite and clay
99 - 104	366.1 - 366.9	Halite, polyhalite and clay layers
105	366.9 - 369.6	Orange halite rock with minor poly-halite and clay
106 - 107	369.6 - 370.9	Halite rock with minor polyhalite
108	370.9 - 374.7	Pinkish-gray halite rock with 30% clay
109 - 110	374.7 - 376.4	Clayey halite rock
111 - 114	376.4 - 381.6	Union anhydrite bordered on top and bottom by polyhalite
115 - 120	381.6 - 385.5	Clayey halite rock with gray clay seams
121 - 123	385.5 - 389.2	Orange halite rock with minor poly-halite
124 - 126	389.2 - 390.8	Claystone and halite rock
127 - 133	390.8 - 393.8	Gray to orange halite rock with 1-2% polyhalite and 5-10% clay

APPENDIX B

APPROXIMATE PRESHOT CHEMICAL COMPOSITION

OF THE ROCK FUSED AND VAPORIZED BY

THE GNOME EVENT

The following percentages represent average values obtained from chemical analyses of preshot drill-hole core samples weighted to represent the zone of fused and vaporized rock. Composite samples were analyzed representing a sphere of rock surrounding the explosion center of 8.5 m radius.

Si	0.185%	K	1.43%
Cl	55.4%	Fe	0.04%
Ca	1.40%	Al	0.071%
Mg	0.65%	Na	35.0%
SO_4	6.38%	C	0.094%
		H_2O	~ 1.5%

APPENDIX C

ASSUMPTIONS INHERENT IN THE TREATMENT

OF THE PERMANENT DISPLACEMENT DATA

The equation used to analyze the permanent displacement data is: $R_c = \left(R_f^3 - R_i^3\right)^{1/3}$. This equation is based on the relationship:

$$\frac{4}{3}\pi R_c^3 = \frac{4}{3}\pi R_f^3 - \frac{4}{3}\pi R_i^3$$

where:

R_c = Radius of theoretical cavity void,

R_f = Postshot radial distance of point p from working point, and

R_i = Preshot radial distance of point p from working point.

It assumes that the displacement of material is radial from the working point and that neither density changes nor faulting occur in the rock as it yields to the force of the expanding cavity. These assumptions are not true, however. Faulting was observed, and probably some permanent compaction of the rock, especially the clay units, did occur. Thus, cavity radii calculated by means of the foregoing equation are only approximations.

APPENDIX D

CAVITY VOID, RUBBLE, AND MELT VOLUME

CALCULATIONS

D.1 EXISTING CAVITY VOID VOLUME

The average planimetered area of three vertical sections of the existing cavity void is 795 m^2. Assuming this void to be roughly hemispherical, the following relationship exists:

$$\frac{\pi}{2} R^2 = 795 \text{ m}^2 \quad \text{or} \quad R = 22.6 \text{ m,}$$

where R is the radius of the hemisphere. The volume of the existing cavity is therefore:

$$\frac{2}{3} \pi (22.6)^3 = 24,180 \text{ m}^3$$

D.2 TOTAL VOLUME OF RUBBLE, MELT AND INTERSTITIAL VOID IN THE LOWER HEMISPHERE OF THE CAVITY

D.2.1 Volume of Rubble and Interstitial Void Above the "Approximate Upper Boundary of Melt" (Fig. 2.2). The average height and radius of this zone are 5.2 m and 22.9 m respectively. Assuming a cylindrical shape, its volume is

$$\pi (22.9)^2 (5.2) = 8,560 \text{ m}^3$$

D.2.2 Volume of Melt, Rubble, and Interstitial Void Below the "Approximate Upper Boundary of Melt." This zone is approximately a spherical segment with an average height of 12.2 m and

average radius at the upper melt boundary of 18.3 m. Its volume can be expressed as follows, using the formula for volume of a spherical segment.

$$V = \frac{\pi}{6} \, 12.2 \, [3(18.3)^2 + (12.2)^2] = 7,360 \text{ m}^3$$

Total volume of cavity rubble, melt, and interstitial void is therefore the sum of A and B or 15,920 m^3.

D.3 VOLUME AND MASS OF MELT

The average percentage of melt encountered by the underground drill holes is 27%. Using this percentage to represent the melt content of the spherical segment in D.2.2, the resulting melt volume is 1,980 m^3. The average bulk density of this melt is 1.6 g/cc. Therefore, its mass is:

$$(1,600 \text{ kg/m}^3)(1,980 \text{ m}^3) = 3.2 \times 10^6 \text{ kg}$$

D.4 TOTAL VOID VOLUME CREATED BY THE DETONATION

D.4.1 Void Volume Represented by the Porosity of the Melt. The porosity of the melt is approximately 27% (bulk density = 1.6, natural state density = 2.2) and the total volume of the melt is 1,980 m^3. Therefore its vesicular void volume is:

$$(0.27)(1,980 \text{ m}^3) = 540 \text{ m}^3$$

D.4.2 Void Volume Representing the Interstitial Pore Space in the Rubble. Assuming a porosity of 28% for the rubble (excluding the melt which fills up a large amount of that space) the total void

-81-

volume of the rubble pile is:

$$(0.28)(15,920 \text{ m}^3) = 4,460 \text{ m}^3$$

A porosity of 28% was chosen because the Hardhat event in granite produced a rubble-filled chimney with this porosity. Subtracting the volume of the melt (1,980 m^3), the resulting volume of rubble pore space is 2,480 m^3.

Total void volume created by the detonation is therefore the sum of the following volumes:

Cavity	24,180 m^3
Melt pore volume	540 m^3
Rubble pore volume	2,480 m^3
	27,200 m^3

D.5   TOTAL VOLUME AND MASS OF RUBBLE

The volume of the rubble, obtained by subtracting the pore volume of the rubble (2,480 m^3) and melt, including pore space, (1,980 m^3) from the total volume of the rubble pile (15,920 m^3) is 11,460 m^3.

Assuming a natural state bulk density of 2.2 g/cc, the rubble mass is:

$$(2200 \text{ kg/m}^3)(11,460 \text{ m}^3) = 25.2 \times 10^6 \text{ kg}$$

APPENDIX E

RUBBLE DISTRIBUTION

The total volume of rubble, exclusive of interstitial void, is roughly 11,460 m^3. Of this volume, approximately 5,300 m^3 is intimately associated with the melt in the lower hemisphere of the cavity. The remaining 6,160 m^3 blankets this region and contains very little melt.

The average theoretical cavity radius of the lower hemisphere, defined by permanent rock displacements, is approximately 16.2 m, and that defined by the extent of melt is 17.4 m. The difference of 1.2 m in these radii may represent the thickness of the shell of rock "blown off" the cavity walls at early times. Assuming this thickness to be roughly uniform around the cavity and assuming a cavity radius prior to "blow-off" of 18.7 m (the radius of a sphere of approximately 27,200 m^3 volume), the volume of the shell of blown-off rock is 5,600 m^3. Since this volume is very close to that of the rubble associated with melt, it is suggested that the bulk of the rubble in this region was blown off the cavity walls.

The average radius of the upper hemisphere of the cavity is approximately 22.9 m. A maximum early-time cavity radius of 18.7 m in this region is assumed. The 4.2-m difference in these radii represents the thickness of both collapsed and blown-off rock. Assuming a thickness of 1.2 m was blown off (as determined previously), a 3-m-thick shell of rock collapsed from the roof of the cavity. Cavity

-83-

profiles suggest this shell extended to an elevation of approximately 682 m or 7.9 m above the working point. The volume of this shell of collapsed rock can be approximated by the difference in volume of spherical segments with respective heights of 13.7 m (21.6 less 7.9 m) and 10.8 m (18.7 less 7.9 m), and basal radii of 25 m (scaled from Figs. 2.1 and 2.2) and 22.1 m. This results in a collapsed rock volume of 5,850 m^3, which compares favorably with the volume of rock overlying the melt zone.

TECHNICAL REPORTS SCHEDULED FOR ISSUANCE
BY AGENCIES PARTICIPATING IN PROJECT GNOME

AEC REPORTS

AGENCY	REPORT NO.	SUBJECT OR TITLE
LRL	PNE-101	Power Studies
LRL	102	Isotopes Program
ORNL	103	Design of Sequenced Gas Sampling Apparatus
LRL	104	Close-In Shock Studies
LRL	105	Stress Measurements with Piezoelectric Crystals
LRL	106	Post-Shot Temperature and Radiation Studies
LRL	107	Geologic Studies of the Tunnel and Shaft
SC	108	Particle Motion near a Nuclear Detonation in Halite
SRI	109	Earth Deformation from a Nuclear Detonation in Salt
USC&GS	110	Seismic Measurements from a Nuclear Detonation in Halite
SRI	111	Intermediate-Range Earth Motion Measurements
LRL	112	An Investigation of Possible Chemical Reactions and Phase Transitions Caused by a Nuclear Explosive Shock Wave
LRL	113	Resonance Neutron Activation Measurements
LASL	114	Symmetry of Fission in U^{235} at Individual Resonances
EG&G	115	Timing and Firing
WES	116	Design, Test and Field Pumping of Grout Mixtures
USWB	126	Preliminary Report of Weather and Surface Radiation Prediction Activities for Project Gnome; Final Analysis of Weather and Radiation Data
H&N, INC	127	Pre-Shot and Post-Shot Structure Survey

AGENCY	REPORT NO.	SUBJECT OR TITLE
RFB, INC	PNE-128	Summary of Predictions and Comparison with Observed Effects of Gnome on Public Safety
SC	129	Monitoring Vibrations at the US Borax and Chemical Company Potash Refinery
USGS	130	Hydrologic and Geologic Studies
FAA	131	Federal Aviation Agency Airspace Closure
USPHS	132	Off-Site Radiological Safety Report
REE Co	133	On-Site Radiological Safety Report
USBM	134	Pre and Post-Shot Mine Examination

DOD REPORTS

AGENCY	SUBJECT OR TITLE
EG&G	Technical Photography of Surface Motion
STL	Shock Spectrum Measurements - Reed Gage
SC	Microbarographic Measurements
USGS	Study of Electric and Magnetic Effects
SC	Electromagnetic Waves from Underground Detonations
EG&G	Subsurface Electromagnetic Waves
SGC	Earth Currents from Underground Detonations
ERDL	Reflectance Studies of Vegetation Damage
SRI	Visual and Photographic On-Site Inspection
SRI	Seismic Noise Monitoring
ERDL	Soil Density Studies
TI	Geochemical and Radiation Surveys
USGS	Solid State Changes in Rock
EG&G	Radon Studies
C&GS	Intermediate Range Seismic Measurements
GeoTech	Long Range Seismic Measurements
USGS	Aeromagnetic and Aeroradiometric Surveys
ARA	On-Site Resistivity and Self Potential Measurements

ABBREVIATIONS FOR TECHNICAL AGENCIES

ARA	Allied Research Associates Inc., Boston
EG&G	Edgerton, Germeshausen, and Grier, Inc., Boston, Las Vegas, and Santa Barbara
ERDL	USA C of E Engineer Research and Development Laboratories, Ft. Belvoir
GeoTech	The Geotechnical Corporation, Garland
LASL	Los Alamos Scientific Laboratories, Los Alamos
LRL	Lawrence Radiation Laboratory, Livermore
SC	Sandia Corporation, Albuquerque
SGC	Space-General Corporation, Glendale
SRI	Stanford Research Institute, Menlo Park
STL	Space Technology Laboratories, Inc., Redondo Beach
TI	Texas Instruments, Inc., Dallas
USC&GS	Coast and Geodetic Survey, Washington, D. C. and Las Vegas
USGS	Geological Survey, Denver
WES	USA C of E Waterways Experiment Station, Jackson
FAA	Federal Aviation Agency, Salt Lake City
H&N, Inc.	Holmes and Narver, Inc., Los Angeles
RFB, Inc.	R. F. Beers, Inc., Alexandria
REECo	Reynolds Electrical and Engineering Co., Las Vegas
USBM	U. S. Bureau of Mines, Washington, D. C.
USPHS	U. S. Public Health Service, Las Vegas
USWB	U. S. Weather Bureau, Las Vegas

DISTRIBUTION LIST — PROJECT GNOME

AGENCY	NO.COPIES	AGENCY	NO.COPIES
Oak Ridge National Laboratory Union Carbide Nuclear Company P. O. Box X Oak Ridge, Tennessee		Chief Air Force Technical Applications Center Washington 25, D. C.	6
ATTN: J. W. Landry	1	Chief Defense Atomic Support Agency Washington 25, D. C.	6
Sandia Corporation Sandia Base P. O. Box 5800 Albuquerque, New Mexico		Commander Field Command, Defense Atomic Support Agency Sandia Base, Albuquerque, New Mexico	
ATTN: W. R. Weart	1	ATTN: FCWT ATTN: FCTG5	8 2
Stanford Research Institute P. O. Box 725 Menlo Park, California		Armed Services Technical Information Agency (ASTIA) Arlington Hall, Virginia	2
ATTN: R. B. Hoy	1	Sandia Corporation Sandia Base, Albuquerque, New Mexico	
Stanford Research Institute P. O. Box 725 Menlo Park, California		ATTN: Section 7290, Mr. A. D. Thornbrough	2
ATTN: L. M. Swift	1	Space Technology Laboratories, Inc. Ramo-Wooldridge Corporation P. O. Box 95001 Los Angeles 45, California	
U. S. Coast and Geodetic Survey Washington 25, D. C.			
ATTN: Mr. W. V. Mickey	1	ATTN: Mr. James F. Halsey	1
U. S. Coast and Geodetic Survey Washington 25, D. C.		U. S. Geological Survey Federal Center Denver 25, Colorado	
ATTN: Dr. Dean S. Carder	1	ATTN: Dr. George Keller and Mr. Karl Roach	2
U. S. Coast and Geodetic Survey Washington 25, D. C.		Edgerton, Germeshausen & Grier, Inc. 300 Wall St., P. O. Box 1912 Las Vegas, Nevada	
ATTN: Mr. L. M. Murphy	1	ATTN: Mr. R. A. Lusk	2
Los Alamos Scientific Laboratory P. O. Box 1663 Los Alamos, New Mexico		Director Mine Detection Branch Engineer Research & Development Laboratories Fort Belvoir, Virginia	
ATTN: G. A. Cowan	1	ATTN: Mr. S. E. Dwornik	2
Edgerton, Germeshausen & Grier, Inc. 160 Brookline Avenue Boston 15, Massachusetts		Texas Instruments, Inc. Geosciences Division P. O. Box 35084, Airlawn Station Dallas 35, Texas	
ATTN: Mr. F. I. Strabala	2	ATTN: Mr. Hubert M. Rackets	2
U. S. Army Engineer Waterways Experiment Station Corps of Engineers Jackson Installation, Concrete Division P. O. Drawer 2131 Jackson, Mississippi		The Geotechnical Corporation P. O. Box 28277 Dallas 28, Texas	
ATTN: J. M. Polatty	3	ATTN: Mr. Ernest Stevens	2
Shell Development Co. 3737 Bellaire Blvd. Houston, Texas		U. S. Coast & Geodetic Survey Department of Commerce P. O. Box 267 Mercury, Nevada	
ATTN: Dr. Aaron J. Seriff	1	ATTN: Mr. Thomas H. Pearce	2
University of California Lawrence Radiation Laboratory Livermore, California		U. S. Coast & Geodetic Survey Department of Commerce Washington 25, D. C.	
ATTN: Technical Information Division	25	ATTN: Chief, Division of Geophysics	2
Assistant to the Secretary of Defense for Atomic Energy Department of Defense Washington 25, D. C.	1	Allied Research Associates, Inc. 43 Leon Street Boston 15, Mass.	
Chief Advanced Research Projects Agency Washington 25, D. C.	6	ATTN: Dr. Arnold H. Glaser	1

9	ABERDEEN PROVING GROUND
1	AEROJET-GENERAL CORPORATION
1	AIR FORCE INSTITUTE OF TECHNOLOGY
1	AIR FORCE WEAPONS LABORATORY
1	ALBUQUERQUE OPERATIONS OFFICE
1	ARGONNE NATIONAL LABORATORY
3	ARMY ENGINEER NUCLEAR CRATERING GROUP
1	ARMY ENGINEER RESEARCH AND DEVELOP- MENT LABORATORIES
6	ARMY ENGINEER WATERWAYS EXPERIMENT STATION
1	ARMY MATERIALS RESEARCH AGENCY
2	ARMY MATERIEL COMMAND (DN-RE)
1	ARMY MATERIEL COMMAND (NA)
1	ARMY MATERIEL COMMAND (RP)
1	ARMY NATICK LABORATORIES
2	ARMY NUCLEAR DEFENSE LABORATORY
1	ATOMIC ENERGY COMMISSION, BETHESDA
1	AEC SCIENTIFIC REPRESENTATIVE, ARGENTINA
1	AEC SCIENTIFIC REPRESENTATIVE, BELGIUM
1	AEC SCIENTIFIC REPRESENTATIVE, ENGLAND
1	AEC SCIENTIFIC REPRESENTATIVE, FRANCE
1	AEC SCIENTIFIC REPRESENTATIVE, JAPAN
3	ATOMIC ENERGY COMMISSION, WASHINGTON
2	ATOMICS INTERNATIONAL
1	AVCO CORPORATION
2	BATTELLE MEMORIAL INSTITUTE
1	BATTELLE-NORTHWEST
12	BEERS (ROLAND F.), INC.
1	BEERS (ROLAND F.), INC., LAS VEGAS
1	BLUME (JOHN A.) AND ASSOCIATES
1	BROOKHAVEN NATIONAL LABORATORY
1	BUREAU OF MINES, BARTLESVILLE
1	BUREAU OF MINES, COLLEGE PARK
1	BUREAU OF MINES, LARAMIE
1	BUREAU OF MINES, WASHINGTON
1	BUREAU OF NAVAL WEAPONS
1	BUREAU OF SHIPS (CODE 1500)
1	DEFENSE ATOMIC SUPPORT AGENCY, LIVERMORE
1	DEFENSE ATOMIC SUPPORT AGENCY, SANDIA
1	DEFENSE ATOMIC SUPPORT AGENCY, WASHINGTON
25	DIVISION OF PEACEFUL NUCLEAR EXPLOSIVES. WASHINGTON
1	DU PONT COMPANY, AIKEN
1	DU PONT COMPANY, WILMINGTON
1	EDGERTON, GERMESHAUSEN, AND GRIER, INC., LAS VEGAS
1	FUNDAMENTAL METHODS ASSOCIATION
1	GENERAL ATOMIC DIVISION
1	GENERAL ELECTRIC COMPANY, CINCINNATI
1	GENERAL ELECTRIC COMPANY, SAN JOSE
3	HAZLETON NUCLEAR SCIENCE CORPORATION
2	HOLMES AND NARVER, INC.
2	LOS ALAMOS SCIENTIFIC LABORATORY
1	LOVELACE FOUNDATION FOR MEDICAL EDUCATION AND RESEARCH
1	MOUND LABORATORY

1	MUESER, RUTLEDGE, WENTWORTH AND JOHNSTON
1	NASA MANNED SPACECRAFT CENTER
2	NASA SCIENTIFIC AND TECHNICAL INFORMATION FACILITY
1	NATIONAL AGRICULTURAL LIBRARY
1	NATIONAL REACTOR TESTING STATION (PPCO)
1	NAVAL RADIOLOGICAL DEFENSE LABORATORY
5	NEVADA OPERATIONS OFFICE
1	NEW YORK OPERATIONS OFFICE
1	NRA, INC.
1	OAK RIDGE OPERATIONS OFFICE
1	OFFICE OF ASSISTANT GENERAL COUNSEL FOR PATENTS (AEC)
1	OFFICE OF NAVAL RESEARCH (CODE 422)
7	OFFICE OF THE CHIEF OF ENGINEERS
1	OHIO STATE UNIVERSITY
1	PETROLEUM CONSULTANTS
1	PHYSICS INTERNATIONAL COMPANY
1	PICATINNY ARSENAL
1	POWER REACTOR DEVELOPMENT COMPANY
1	PUBLIC HEALTH SERVICE
5	PUBLIC HEALTH SERVICE, LAS VEGAS
1	PURDUE UNIVERSITY
1	RADIOPTICS, INC.
1	RAND CORPORATION
1	RESEARCH ANALYSIS CORPORATION
2	REYNOLDS ELECTRICAL AND ENGINEERING COMPANY, INC.
5	SAN FRANCISCO OPERATIONS OFFICE
4	SANDIA CORPORATION, ALBUQUERQUE
1	SANDIA CORPORATION, LIVERMORE
1	SAVANNAH RIVER OPERATIONS OFFICE
1	SCHOOL OF AEROSPACE MEDICINE
1	SOUTHWEST RESEARCH INSTITUTE
1	STANFORD RESEARCH INSTITUTE
1	STRATEGIC AIR COMMAND
1	TENNESSEE VALLEY AUTHORITY
1	UNION CARBIDE CORPORATION (ORGDP)
4	UNION CARBIDE CORPORATION (ORNL)
1	USAF HEADQUARTERS (AFTAC)
1	U. S. COAST AND GEODETIC SURVEY, SAN FRANCISCO
1	U. S. GEOLOGICAL SURVEY, ALBUQUERQUE
3	U. S. GEOLOGICAL SURVEY, DENVER
2	U. S. GEOLOGICAL SURVEY, MENLO PARK
1	U. S. GEOLOGICAL SURVEY (NOLAN)
1	U. S. GEOLOGICAL SURVEY, WASHINGTON
1	U. S. MISSION TO THE INTERNATIONAL ATOMIC ENERGY AGENCY
2	U. S. WEATHER BUREAU, LAS VEGAS
1	U. S. WEATHER BUREAU, WASHINGTON
2	UNIVERSITY OF CALIFORNIA, BERKELEY
4	UNIVERSITY OF CALIFORNIA, LIVERMORE
1	UNIVERSITY OF CALIFORNIA, LOS ANGELES
1	UNIVERSITY OF TENNESSEE (UTA)
1	WHITE SANDS MISSILE RANGE
285	DIVISION OF TECHNICAL INFORMATION EXTENSION
75	CLEARINGHOUSE FOR FEDERAL SCIENTIFIC AND TECHNICAL INFORMATION